



ČESKÉ VYSOKÉ UČENÍ TECHNICKÉ V PRAZE

FAKULTA STROJNÍ

U12120

DEPT., OF AUTOMOBILES, COMBUSTION ENGINES AND RAIL VEHICLES

IMPROVEMENT OF THE EXISTING TEST STANDS

(Modernizace laboratorních stanovišť)

Diplomová práce

Study program - MAE (Master of Automotive Engineering)

Thesis supervisor - Doc. Dr. Ing. Gabriela Achtenová

Raghavendar Balaji

Prague 2019



Acknowledgement

First and foremost, I would like to thank the almighty I believe in, for giving me such supportive parents as I am greatly indebted to their love and support; without them I could not have been the person I am today and for providing such a valuable opportunity to work under Prof. Achtenova, one of the most knowledgeable, yet humble and helpful teachers I have ever come across in my life. I extend my heartfelt gratitude to Mr. Lukas Kazda, who tirelessly helped me with my work besides his extensive schedule, Mr. Emrich for his profound guidance in LabVIEW and Mr. Zoul for the sincere efforts taken to discuss and help me solve my project issues. I would like to thank my colleagues Ms. Shakthi Senthilprathaban and Mr. Nishanth Nithyanandham, who supported me emotionally and motivated me to push beyond my limits, which has been a critical factor for the completion of this thesis.



Summary

Topics of the master thesis –	1. Angle acquisition and measurement of moment of inertia 2. Measurement of gearbox transmission error 3. Proposal for variable pressure actuation of disk brake test bench
Master student –	Raghavendar Balaji
Thesis coordinator –	Doc. Dr. Ing. Gabriela Achtenová

The goal of this master thesis is divided into three parts – One is to familiarize with the measurement of moment of inertia of an object with the existing test bench in the laboratory of Automotive Department at Juliska. This task consists of determining the angle of inclination of the suspended object with a sensor, compute a formula to calculate moment of inertia of any proposed object and program it with LabVIEW for automatic results. Also, a procedure process to measure has been created and explained.

The second part consists of measuring the transmission error of a given gearbox using two incremental rotary encoders. The program has been written in LabVIEW which uses the reference input RPM to determine the fluctuation of movement in the gears. The resultant difference, i.e., the transmission error is then found out after processing the data in NI DIAdem. The experiment has been carried out as a prototype without the loading of gear. The resultant transmission error is computed and documented.

The third part consists of proposing a suggestion of a mechanism to actuate the hydraulic force variedly according to parameters provided by the user.

Keywords

Moment of inertia, angle acquisition with dual axes sensor, torsional pendulum method, LabVIEW programming, angle of inclination, transmission error, incremental rotary encoder, DIAdem, counter input, period of revolution, synchronized averaging in time domain, comb filtration, linear actuator, hydraulic aggregate, brake actuation.



Statement of declaration –

I hereby declare that my works of master thesis “Angle acquisition and measurement of moment of inertia”, “Measurement of gearbox transmission error”, “Proposal for implementation of variable pressure actuation of disk brake on test bench” have been completed by me separately and under the guidance of the supervisor and consultants.

Raghavendar Balaji

In Prague, on **11 – 01 – 2019**

Signature



Contents

A.	MOMENT OF INERTIA MEASUREMENT	- 8 -
1.	Introduction	- 8 -
2.	Theoretical methods to calculate moment of inertia	- 8 -
2.1	With Routh's and Lee's rule.....	- 8 -
2.2	By integral method.....	- 9 -
3.	Determination of <i>COG</i>	- 10 -
4.	Concepts of calculation for complex 3D bodies	- 12 -
4.1	Inertia Matrix.....	- 12 -
4.2	Ellipsoid of inertia.....	- 14 -
4.3	Parallel axis theorem	- 14 -
4.4	Rotation transformation.....	- 16 -
4.5	Measurement of moment of inertia.....	- 16 -
5.	Practical measurement of moment of inertia	- 17 -
5.1	Predefined methodology implemented	- 17 -
5.2	Components for experimentation	- 18 -
5.3	Period of oscillation determination	- 20 -
5.4	Sensors for angle of inclination	- 21 -
5.5	Connection of sensors with old and new customized PCBs	- 26 -
5.6	LabVIEW programming for angle acquisition	- 29 -
5.7	Example check of moment of inertia result with modelling software	- 31 -
6.	Conclusion for sub-topic.....	- 35 -
7.	Prospects and future work	- 35 -
B.	MEASUREMENT OF GEARBOX TRANSMISSION ERROR	- 36 -
1.	Introduction	- 36 -
2.	Literature review and previous works	- 36 -
3.	Concepts related to transmission error.....	- 37 -
3.1	Root Mean Square (RMS) or Standard Deviation of a signal	- 38 -
3.2	Nyquist- Shannon Sampling theorem.....	- 38 -
3.3	Aliasing	- 38 -
3.4	Fourier Transformation	- 39 -
3.5	Comb Filter	- 41 -



4.	Experimental setup for measurement.....	- 42 -
4.1	Asynchronous electric motor	- 43 -
4.2	Gearbox on test stand	- 44 -
4.3	Incremental Rotary Encoders LARM IRC 305/6000 PA	- 45 -
4.4	Advantech ADAM terminal board	- 46 -
4.5	NI 9401 DAQ module.....	- 46 -
4.6	CompactDAQ chassis cDAQ-9174.....	- 47 -
5.	Data acquisition from LabVIEW 14	- 47 -
6.	Processing obtained data with NI DIAdem	- 48 -
6.1	Data preparation for analysis	- 49 -
6.2	Transmission Error measurement of RPM signal.....	- 49 -
7.	Inference and conclusion	- 61 -
8.	Future work and prospects	- 61 -
C.	ACTUATION OF DISC BRAKE ON TEST BENCH.....	- 62 -
1.	Introduction	- 62 -
2.	Current experimental setup	- 62 -
2.1	Hydraulic pusher	- 63 -
2.2	Actuating lever	- 63 -
2.3	Pressure feedback sensor.....	- 64 -
3.	Proposed solution for actuation	- 64 -
4.	Alternate solution proposal for actuation	- 66 -
4.1	Hydraulic aggregate.....	- 67 -
5.	Conclusion	- 68 -
D.	LIST OF FIGURES	- 69 -
E.	LIST OF TABLES	- 72 -
F.	LIST OF ANNEXURES	- 73 -
	Annex 1 – Instruction to connect the sensors with DAQCard 6062E and PCBs.....	- 74 -
	Annex 2 – Instruction for moment of inertia calculation and obtained results.....	- 77 -
	Annex 3 – Instruction to create the task for Counter Input in NI MAX application.	- 82 -
	Annex 4 – Instruction manual for analysis in NI DIAdem.....	- 84 -
G.	ATTACHMENTS.....	- 87 -
1.	Moment of Inertia measurement.....	- 87 -
2.	Measurement of gearbox transmission error.....	- 91 -



Attachments for experimental setup	- 91 -
Attachments for LabVIEW programming.....	- 94 -
Attachments for post-processing in DIAdem.....	- 99 -
3. Actuation of disc brake.....	- 110 -
H. REFERENCES AND LITERATURE WORKS.....	- 114 -
I. LIST OF SYMBOLS AND ABBREVIATIONS.....	- 118 -
J. LIST OF CONTENTS IN DVD	- 119 -



A. MOMENT OF INERTIA MEASUREMENT

1. Introduction

Moment of inertia is primarily defined as the opposition exerted by a body to the angular acceleration along the axis of rotation. The term was coined by Leonhard Euler in his book *Theoria motus corporum solidorum seu rigidorum* in 1765 and it is an integral part of Euler's second law ^[1]. Mathematically, moment of inertia I is the ratio of the net angular momentum L of a system to the angular velocity ω around a principal axis ^{[2][3]}, i.e.,

$$I = \frac{L}{\omega} \quad (1.1)$$

For a rigid composite system, the moment of inertia is the sum of the moments of inertia of its subsystems about the same axis. It is generally given by,

$$I = \int_M r^2 dm. \quad (1.2)$$

Where “ r ” is the distance from the centre of rotation and “ M ” is the entire mass of the body.

2. Theoretical methods to calculate moment of inertia

There are quite a few ways to determine the moment of inertia of a standard object. The simplest would be to look up in a predefined table for regular objects. For more complex bodies, the methodology becomes more complicated and different measures are used to get the values.

2.1 With Routh's and Lee's rule

Routh's rule states that the moment of inertia of a rigid object is unchanged when the object is stretched parallel to an axis of rotation that is a principal axis, provided that the distribution of mass remains unchanged except in the direction parallel to the axis ^[4]. This theorem is usually used in accordance with the parallel and perpendicular axes theorem for different shapes.

$$I = \frac{M \times S}{3}, \text{ for rectangular lamina or square shaped bodies} \quad (1.3)$$

$$I = \frac{M \times S}{4}, \text{ for circular or rectangular lamina} \quad (1.4)$$

$$I = \frac{M \times S}{5}, \text{ for spherical bodies} \quad (1.5)$$

Where, M = Mass of the body

S = Sum of the squares of the perpendicular axes.

Lee's rule for a symmetrical solid defines moment of inertia “ I ” as ^[5] –

$$I = M \left(\frac{a^2}{(3+k_1)} + \frac{b^2}{(3+k_2)} \right). \quad (1.6)$$



Where, a and b are the lengths of the semi-axes perpendicular to the rotation axis.

k_1 and k_2 are the maximum and minimum value of the curvature respectively.

- (i) For flat surfaces, k_1 and $k_2 = 0$.
- (ii) For cylindrical surfaces, k_1 and $k_2 = 1$.
- (iii) For spherical surfaces, k_1 and $k_2 = 2$.

But this method only provides instructions for standard shaped bodies such as rectangular, cylindrical and spherical. Hence, in real life it can be used only for primitive structured bodies.

2.2 By integral method

When a body is of complex structure, we implement the integral method. Considering that a body has a mass ‘ m ’, when an infinitesimally small elemental area is taken, it has a mass of ‘ dm ’ and an area of ‘ dA ’. Taking the perpendicular distance of the body from the axis of rotation through the centre of gravity (COG) as r , the moment of inertia is given by

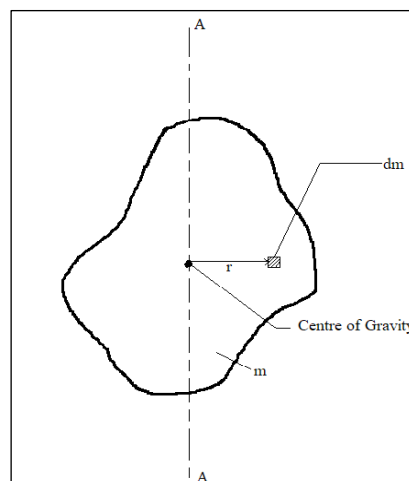


Figure 1 Irregular body with COG

$$I = \int_M r^2 dm \text{ (or) } I = \int_A r^2 dA. \quad (1.7)$$

The first formula is usually used for a 3D object whereas the second formula is used for a body with negligible thickness or 2D object. The general form of a 3D object can be derived from the kinetic energy of the body.

$$\text{Kinetic energy denoted by K.E,} \quad = \quad \frac{1}{2}mv^2. \quad (1.8)$$

The relation between linear velocity ‘ v ’ and angular velocity ‘ ω ’ is –

$$v = r \times \omega \quad (1.9)$$



Hence K.E becomes,

$$\text{K.E} = \frac{1}{2}mv^2 = \frac{1}{2}m(r \times \omega)^2 = \frac{1}{2}mr^2\omega^2 = \frac{1}{2}I\omega^2. \quad (1.10)$$

Where $I = mr^2$.

But in real scenario, the perpendicular distance 'r' and continuous mass distribution 'm' varies at each point inside the body, hence the formula can be rewritten as –

$$\text{K.E} = \frac{1}{2} \int_M (\omega^2 r^2) dm. \quad (1.11)$$

Since the angular velocity 'ω' is constant,

$$\text{K.E} = \frac{1}{2} \omega^2 \int_M r^2 dm. \quad (1.12)$$

Thus, we get the original equation,

$$I = \int_M r^2 dm. \quad (1.13)$$

3. Determination of COG

As seen above, to determine the moment of inertia of a body, we need the perpendicular distance from COG of the body and we primarily determine the COG by the moments method. In our case, we take the example of a wheel for the body and determine its COG. In the below diagram, we take the moments about points G and B.

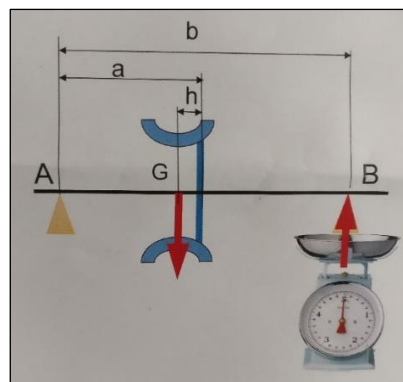


Figure 2 COG through moments method

Here, point A is the reference and we calculate the moments with the distances from it. The body is mounted on a rod or beam at a distance of 'a' from point A, and a resulting measure on scale is m_{tot} with the COG of body a little offset from the mounting position, by a distance 'h'. The other end of rod is placed on a weighing scale to measure the weight and the force acting on point B. The mass of the rim is taken as m_{rim} and the measure on scale only for the rod is taken as m_{rod} . Hence, the offset distance from the axial centre of the rim to the COG is derived as below –

$$m_{rim} \times (a - h) - (m_{tot} - m_{rod}) \times b = 0$$



$$h = \frac{m_{rim} \times a - (m_{tot} - m_{rod}) \times b}{m_{rim}} \quad (1.14)$$

Another method would be, to determine the moment due to the offset of *COG* from the central axis, by mounting the body horizontally on a pivot about a predefined axis. With a similar moment formula and procedure mentioned above, one co-ordinate can be obtained i.e., the distance from the mounting point. But the exact position of the *COG* can lie along any point on the plane (Plane 1 in Figure 3) at that distance perpendicular to the ground. To reduce the position to a more specific set of points, we mount the body vertically or rotate by 90° and adopt the similar method. By determining the moment, we get the distance of *COG* from the mounting point and determine the vertical plane (Plane 2) in the same manner. By the intersection of these planes, we now get two points (*a*) and (*b*) in figure below and a line through these planes. Now, mount the body in such a way that the line obtained is in a horizontal position and between the endpoints of the weighing scale and pivot. We will now get the third point for the *COG* through the intersection of the plane by the point obtained with moment method and the horizontal line which is already pre-defined.

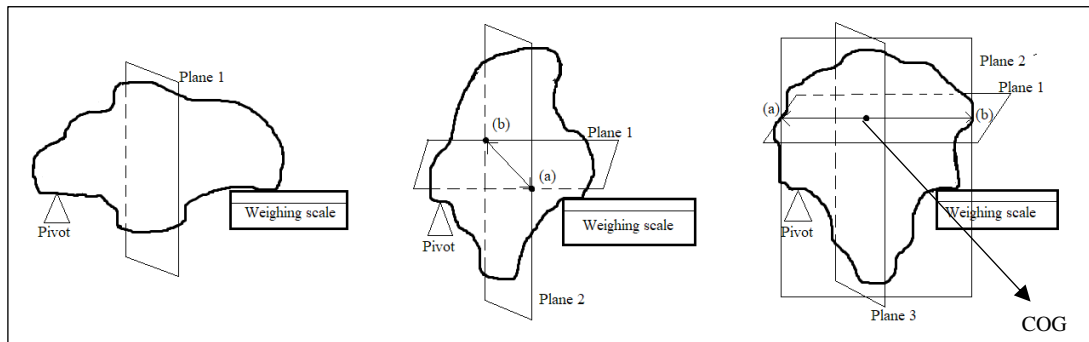


Figure 3 *COG of a 3D object*

One such almost similar method example to measure *COG* is followed in the case of a car where it is found through the moment on wheelbase, trackwidth and finally by mounting the car at an inclination to the ground. With this, we would can determine the exact location of the *COG*. Firstly, the car is mounted on the scale horizontally. By this, the forces acting on wheels can be obtained. Also, we already know the mass of the vehicle.

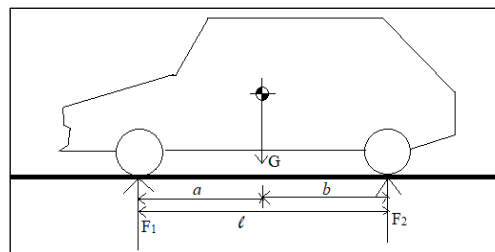


Figure 4 *Computing longitudinal COG position for a car*

The distance between the front axle of the vehicle and the *COG* is taken as '*a*' and correspondingly with the rear as '*b*', with the total wheelbase of the vehicle as '*l*'. Taking the moment about one of the ends, we get



$$b = l \times \left(\frac{F_1}{G}\right) \tag{1.15}$$

We know that,

$$l = a + b$$

which gives,

$$a = l - b.$$

Hence, from the above calculation, we can find ‘a’, which is the distance from the *COG* to the front axle of the vehicle. Similar method can be adopted with the trackwidth of the vehicle too. For the height of the *COG*, we tilt the object through a definite angle and calculating the moment about a pivoted point as shown below.

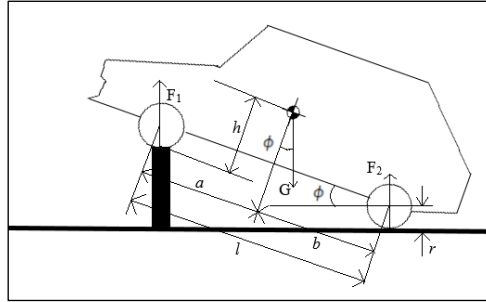


Figure 5 Computing the height of *COG* of a car

The height component of the *COG* can be calculated from the moment about the rear wheel contact on the ground.

$$h = \left[b - l \times \left(\frac{F_1}{G}\right) \right] \times \cot(\phi) + r. \tag{1.16}$$

4. Concepts of calculation for complex 3D bodies

4.1 Inertia Matrix

The inertia matrix can be derived from the formula of angular momentum of a body as follows ^[7] –

$$\text{We know that the angular momentum of a body, } L = I \times \omega$$

For a composite body with continuous distribution of mass, the previous equation can be re-written as,

$$L = \int_M (r \times v) dm. \tag{1.17}$$

For a rigid body, the distance between a particle in it and the centre of mass will remain constant, with its velocity given by

$$v = \omega \times r$$

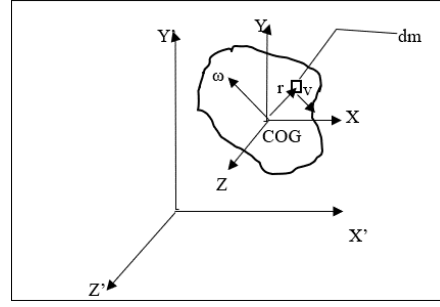


Figure 6 Co-ordinate system on a 3D plane

Hence, the angular momentum becomes, $L = \int_M (\mathbf{r} \times (\boldsymbol{\omega} \times \mathbf{r})) dm$

We know $\mathbf{A} \times (\mathbf{B} \times \mathbf{C}) = (\mathbf{A} \cdot \mathbf{C})\mathbf{B} - (\mathbf{A} \cdot \mathbf{B})\mathbf{C}$,

Hence $= \int_M [(\mathbf{r} \cdot \mathbf{r})\boldsymbol{\omega} - (\mathbf{r} \cdot \boldsymbol{\omega})\mathbf{r}] dm. \quad (1.19)$

According to cartesian coordinates, $\mathbf{r} = x\mathbf{i} + y\mathbf{j} + z\mathbf{k}$ and $\boldsymbol{\omega} = \omega_x\mathbf{i} + \omega_y\mathbf{j} + \omega_z\mathbf{k}$. So, the above equation is written as,

$$\begin{aligned} L = & (\omega_x \int_M (x^2 + y^2 + z^2) dm - \int_M ((\omega_x x + \omega_y y + \omega_z z) x') dm) \mathbf{i} \\ & + (\omega_y \int_M (x^2 + y^2 + z^2) dm - \int_M ((\omega_x x + \omega_y y + \omega_z z) y') dm) \mathbf{j} \\ & + (\omega_z \int_M (x^2 + y^2 + z^2) dm - \int_M ((\omega_x x + \omega_y y + \omega_z z) z') dm) \mathbf{k} \end{aligned} \quad (1.18)$$

Simplifying,

$$= (I_{x'x'}\omega_x - I_{x'y'}\omega_y - I_{x'z'}\omega_z) \mathbf{i} + (-I_{y'x'}\omega_x + I_{y'y'}\omega_y - I_{y'z'}\omega_z) \mathbf{j} + (-I_{z'x'}\omega_x - I_{z'y'}\omega_y + I_{z'z'}\omega_z) \mathbf{k}$$

$I_{x'x'}$, $I_{y'y'}$, $I_{z'z'}$ are the moments of inertia with respect to x' , y' and z' axes respectively, written as

$$I_{x'x'} = \int_M (y'^2 + z'^2) dm, I_{y'y'} = \int_M (x'^2 + z'^2) dm, I_{z'z'} = \int_M (x'^2 + y'^2) dm. \quad (1.19)$$

The remaining terms I_{xy} , I_{yz} , I_{xz} , I_{yx} , I_{zx} and I_{zy} are called as *products of inertia*, which can either be positive or negative since,

$$I_{x'y'} = I_{y'x'} = \int_M x'y' dm, I_{x'z'} = I_{z'x'} = \int_M x'z' dm \text{ and } I_{y'z'} = I_{z'y'} = \int_M y'z' dm. \quad (1.20)$$

Writing in the matrix form, it yields

$$\begin{bmatrix} L_{Gx} \\ L_{Gy} \\ L_{Gz} \end{bmatrix} = \begin{bmatrix} I_{x'x'} & -I_{x'y'} & -I_{x'z'} \\ -I_{y'x'} & I_{y'y'} & -I_{y'z'} \\ -I_{z'x'} & -I_{z'y'} & I_{z'z'} \end{bmatrix} \begin{bmatrix} \omega_x \\ \omega_y \\ \omega_z \end{bmatrix}. \quad (1.21)$$

In generalized terms, the above equation can be written as,

$$L_G = [I_G]\boldsymbol{\omega}$$

Where $[I_G]$ is the inertia matrix tensor with respect to the $x'y'z'$ axes and the COG, G .



4.2 Ellipsoid of inertia

The equations obtained above define the moment of inertia of a body about a local reference frame. But the moment of inertia also depends on the orientation of the axis of rotation, i.e., α , β , γ . When the axis of rotation changes, so does the moment of inertia. Hence, after calculation, we will get the final general equation as –

$$I_x x^2 + I_y y^2 + I_z z^2 + 2I_{xy}xy + 2I_{yz}yz + 2I_{xz}xz = 1. \quad (1.22)$$

The above equation is termed as the “*ellipsoid of inertia*” since it describes the moment of inertia of a body as a function of orientation of axis of rotation. If the product of inertia terms is zero, we would get –

$$I_1 x_1^2 + I_2 y_1^2 + I_3 z_1^2 = 1.$$

From the above equation, the length of the principal semi – axes of the ellipsoid of inertia are

$$l_1 = \frac{1}{\sqrt{I_1}},$$

$$l_2 = \frac{1}{\sqrt{I_2}}$$

$$l_3 = \frac{1}{\sqrt{I_3}}$$

Thus, the moment of inertia of the body with the axes passing through *COG* of the body would be

$$I_o = I_1 \cdot \cos(\alpha) + I_2 \cdot \cos(\beta) + I_3 \cdot \cos(\gamma). \quad (1.23)$$

Where α , β , and γ are the rotation angles of x , y and z axes respectively.

4.3 Parallel axis theorem

The parallel axis theorem, also known as Steiner’s theorem^[8], is used to determine the mass moment of inertia or second moment of area of a rigid body about any axis, provided the body’s moment of inertia through a parallel axis through the object’s *COG* and the perpendicular distance between the axes.

Consider a body of mass m , has a mass moment of inertia of I_o about its *COG*. Then the moment of inertia about any axis at a distance d , parallel to the one passing through the *COG* is given by

$$I = I_o + (m \times d^2). \quad (1.24)$$

In a 3D plane, when the centre of mass of a body is translated to a new set of axes at x' , y' , z' from the initial frame or co-ordinate system as shown in the figure below, the moment of inertia is given as follows^[6] –

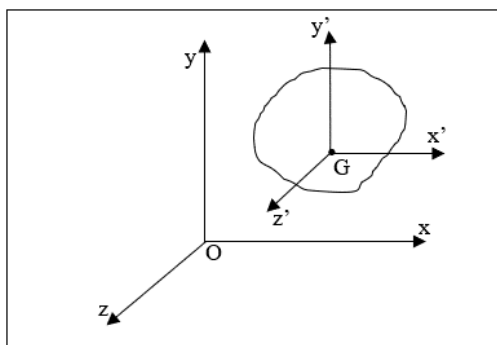


Figure 7 Translation of axes to a new co-ordinate system

$$(I_{xx})_O = \int_m (y^2 + z^2) dm = \int_m ((y_G + y')^2 + (z_G + z')^2) dm$$

On simplification, we get $(I_{xx})_O = (I_{xx})_G + m(y_G^2 + z_G^2)$

The terms y' and z' are the co-ordinates respective to the centre of mass of the body and hence their integrals become zero if mounted at the centre of mass itself. Similarly, for the other two axes we can write as follows –

$$(I_{yy})_O = (I_{yy})_G + m(x_G^2 + z_G^2) \quad \& \quad (I_{zz})_O = (I_{zz})_G + m(x_G^2 + y_G^2)$$

The product of inertia, if any would be given by –

$$(I_{xy})_O = (I_{yx})_O = I_{xy} + mx_G y_G, \quad (I_{yz})_O = (I_{zy})_O = I_{yz} + my_G z_G$$

$$\& \quad (I_{xz})_O = (I_{zx})_O = I_{xz} + mx_G z_G$$

In case of symmetrical objects about the three planes, the product of inertia terms would be zero and we would be left with the principal moments of inertia.

The entire inertia matrix is given by, $I = I_o + m \times R$

Where,
$$I_o = \begin{bmatrix} I_{xx} & I_{xy} & I_{xz} \\ I_{yx} & I_{yy} & I_{yz} \\ I_{zx} & I_{zy} & I_{zz} \end{bmatrix} \text{ and}$$

$$R = \begin{bmatrix} y_G^2 + z_G^2 & x_G y_G & x_G z_G \\ x_G y_G & x_G^2 + z_G^2 & y_G z_G \\ x_G z_G & y_G z_G & x_G^2 + y_G^2 \end{bmatrix}$$

$$\text{So, } I = \begin{bmatrix} (I_{xx})_G + m(y_G^2 + z_G^2) & I_{xy} + mx_G y_G & I_{xz} + mx_G z_G \\ I_{yx} + mx_G y_G & (I_{yy})_G + m(x_G^2 + z_G^2) & I_{yz} + my_G z_G \\ I_{zx} + mx_G z_G & I_{zy} + my_G z_G & (I_{zz})_G + m(x_G^2 + y_G^2) \end{bmatrix} \quad (1.25)$$

In case of just principal moments, the only terms remaining would be the diagonal ones and others would be zero, as discussed above.



4.4 Rotation transformation

To obtain the entire generalized formula for the moment of inertia about an entirely new set of co-ordinates, only translation will not be sufficient. Hence, we use rotation transformation of the axes too about all the three x , y and z axes at angles α , β and γ respectively.

We know that for transformation about the axes, the rotation matrix is given by –

$$T_x = \begin{bmatrix} 1 & 0 & 0 \\ 0 & \cos \alpha & -\sin \alpha \\ 0 & \sin \alpha & \cos \alpha \end{bmatrix}, T_y = \begin{bmatrix} \cos \beta & 0 & \sin \beta \\ 0 & 1 & 0 \\ -\sin \beta & 0 & \cos \beta \end{bmatrix}, T_z = \begin{bmatrix} \cos \gamma & -\sin \gamma & 0 \\ \sin \gamma & \cos \gamma & 0 \\ 0 & 0 & 1 \end{bmatrix}$$

Where T_x , T_y and T_z are the transformation matrices. The inertia tensor matrix is –

$$I = \begin{bmatrix} (I_{xx})_G + m(y_G^2 + z_G^2) & I_{xy} + mx_G y_G & I_{xz} + mx_G z_G \\ I_{yx} + mx_G y_G & (I_{yy})_G + m(x_G^2 + z_G^2) & I_{yz} + my_G z_G \\ I_{zx} + mx_G z_G & I_{zy} + my_G z_G & (I_{zz})_G + m(x_G^2 + y_G^2) \end{bmatrix}$$

We take the above mentioned general matrix just in case the body is translated to a new set of co-ordinates. If not, then the distances x_G , y_G and z_G would become zero and we just have the principal inertia matrix.

The resultant moment of inertia can be calculated with the following relation –

$$I_F = [T_z]^T [T_y]^T [T_x]^T [I] [T_x] [T_y] [T_z]. \quad (1.26)$$

Where $[T_x]^T$, $[T_y]^T$ and $[T_z]^T$ are the transpose matrices of the original transformation matrices.

4.5 Measurement of moment of inertia

One of the most prominent methods to determine the moment of inertia of an object is through a torsional pendulum where the object is suspended from the ceiling through a wire of stiffness k , length l and diameter d . It is then twisted through a small angle of ϕ about the vertical axis through the base of the body. The equation of motion of the setup is written as –

$$\frac{d^2 \phi}{dt^2} = -\frac{k}{I} \phi, \quad (1.27)$$

which is derived from the torque equations according to Hooke's law and for twist, ϕ as –

$$\tau = -k\phi \quad (1.28)$$

Hence,

$$\tau = I \frac{d^2 \phi}{dt^2}. \quad (1.29)$$

Solving the second order differential equation, we get



$$\omega = \sqrt{\frac{k}{I}} \quad (1.30)$$

which results in the oscillation period T of

$$T = 2\pi \sqrt{\frac{I}{k}} \quad (1.31)$$

And the half period of oscillation τ of

$$\tau = \frac{T}{2} = \pi \sqrt{\frac{I}{k}}$$

The stiffness of the spring k is calculated with the formula,

$$k = \frac{Gd^4\pi}{32 \times l} \quad (1.32)$$

The above-mentioned formula can be used when the shear modulus of the wire G and the radius of the wire are known. Alternatively, the stiffness can be found out using half period formula for a known object of inertia I_o and determining the period through any means available.

5. Practical measurement of moment of inertia

5.1 Predefined methodology implemented

In the laboratory of CVUT at Juliska, we determine the moment of inertia of a wheel which is suspended from the ceiling through a string and hinged at both, the top and bottom with a Cardan joint and a bolt and nut assembly. Since the wheel has a hole at the centre, it can't be mounted at that point. Hence, we mount at an offset distance from the centre of the wheel on the rim and the moment of inertia is found at this position.



Figure 8 Experimental setup for wheel moment of inertia



We determine the moment of inertia of the wheel through the fore mentioned torsional pendulum method. To determine the period of oscillation, a small piece of paper or cardboard is attached to the bottom end of the wheel with part of it sticking out to interrupt the light signal (which in turn changes the voltage) emitted by the photo gates that are placed vertically in the circular path of motion (or) sway of the body. The figure below shows the given setup.



Figure 9 *Experimental setup for light sensing*

Since the wheel or any other object mounted might have a non-uniform mass distribution or density, it can have its inclination from the horizontal in two planes. Hence, we implement the U – joint to incline in both directions. To acquire this angle of tilt from the horizontal, a protractor is currently used manually which might lead to parallax errors even though it might seem accurate to measure. The work assigned to me, is to implement a sensor to determine this angle and program it with LabVIEW to get more accurate results. This angle would be later used to determine the actual moment of inertia of the body.

For an irregular and complex object, the mounting gets difficult. In such cases, we use a base or a platform of known geometry on which the object is placed. Initially, the moment of inertia of the platform is found out and then along with the body, and the difference would give us the moment of inertia of the body ^[9].

5.2 Components for experimentation

5.2.1 DAQ Card 6062E

The data acquisition device of E series by National Instruments(NI) is shown below, which has 16 analog inputs and 2 analog outputs of 12 bit resolution. It also has 8 digital I/O lines and two 24 bit counters, but which we utilize to acquire analog signals and transmit them to the computer. The main specification of the card useful for this experiment are given in “[Attachment 1.1](#)”.

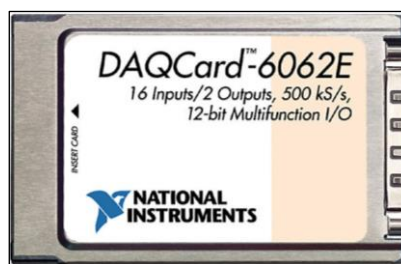


Figure 10 DAQ Card 6062E

5.2.2 Terminal board junction, NI CB-68LP

The connection from the sensors to the NI Data Acquisition devices is done through a terminal board, through a shielded 68 pin SCSI cable, SHC68-68-EP. The terminal board has 68 pin connections, with each corresponding to a terminal in the DAQ device. It is a Printed Circuit Board (PCB) with two layers etched with copper element. The specification is given in the table below –

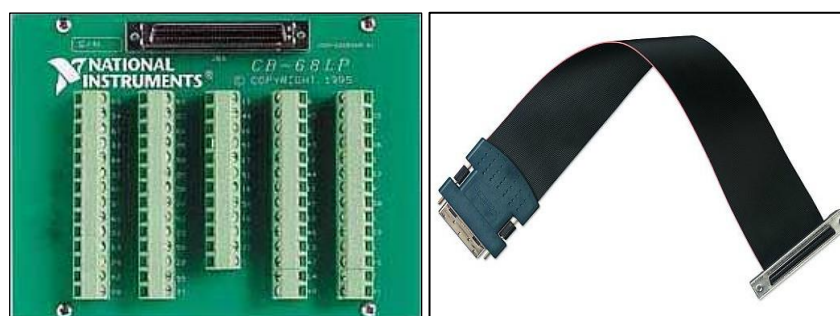


Figure 11 NI CB - 68LP (left) and SHC68-68-EP (right)

Table A-1 Specification of NI CB - 68LP

SPECIFICATIONS	
Overload voltage	60 VDC
Operating temperature	0 to 70°C
Maximum altitude	2000 m

Two electrical Printed Circuit Board (PCB) connections exist for the measurement of inertia testbench. The one which already exists, consists of a conventional NI screw terminal board which has 68 pins corresponding to the same number of pins of used data acquisition card - DAQCard 6062E. Since we need to screw every wire of every sensor into the slots for the experiment each time, new alternative needs to be found to keep the connections as simple as possible - to just plug in a connector and acquire the required data and then plug out at our convenience without interference of many separate wires.

For this purpose, a new PCB has been designed to plug the DAQ Card on one side and the connectors for angle measurement and photogate on the other side. The description of components and the electrical scheme of existing and new PCB



connections are given in the following sub-chapters. The entire connection scheme with installation instructions for both old and new PCBs are written in “[Annex 1](#)” of this document, and also in the following chapters for general description.

5.3 Period of oscillation determination

The work done to determine the period was by implementing a DAQ Card 6062-E in association with an NI CB – 68LP, which is a 68-pin board to get the voltage signals from the light gate of the setup. The DAQ Card implemented is an Analog input card which is connected to the board through a communicator wire which transmits the signal to the computer. The light gate has a laser beam passing from the top, which is the emitter to the receptor at the bottom. When the wheel rotates, the paper obstructs the path of light which produces a voltage change in the circuit. This is sent to the computer through the DAQ Card as Analog signal and is processed further by the program in LabVIEW. An 82kΩ resistor is connected in parallel to the connection ^[10].



Figure 12 Photo gate with emitter and receiver

The parameters of the given LED diode and the phototransistor are as below –

Table A-2 Parameters of Photo gate used

Object	Voltage [V]	Current [mA]	Wavelength [nm]	Size [mm]
LED	2.1	20	625	5
Phototransistor	32	50	560-950	5

The schematic focusing only on the connection for oscillation period through light detection with NI terminal board, is given below. The entire electrical connection schematic with angle measurement equipment used is given in the following chapters.

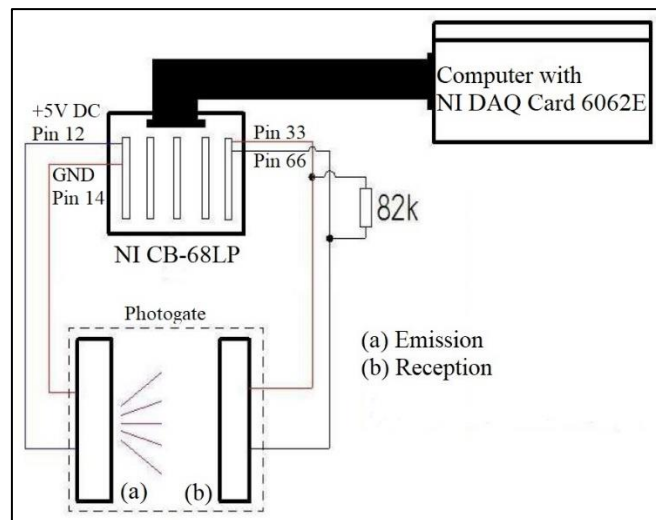


Figure 13 Schematic of the light sensing connection with old PCB ^[10]

LabVIEW was used to program the obtained signals accordingly and adapt them to determine the half period of oscillation and consequently calculate the moment of inertia of the body.

5.4 Sensors for angle of inclination

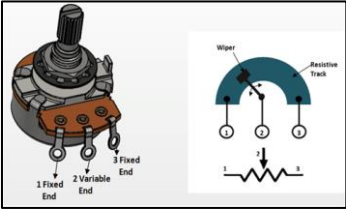
As suggested in previous chapters, to avoid parallax error during measurement, my task is to implement a sensor which can accurately provide the angle of inclination. This can be done in several ways (or) with diverse types of sensors, but the advantages and disadvantages are to be discussed before selecting the right one.

5.4.1 Results of comparison of sensors

The working and various other aspects of sensors should be compared to finalize it, to fit the need and usage. The table of comparison between different types of sensors are given in the following page.



Table A-3 Comparison of advantages and disadvantages between sensors

Potentiometer	Hall – effect angle sensor	MEMS inclinometer
Advantages -		
 <p>Figure 14 Potentiometer diagram and circuit connection ^[11]</p>	 <p>Figure 15 Hall Effect angular sensor IC from Allegro Microsystems ^[12]</p>	 <p>Figure 16 Two axes inclinometer IC from Murata ^[13]</p>
Exact potential difference between 2 points in a circuit.	Non – contact magnetic measurement and wear free lifelong sensors.	Measure w.r.t gravitational force.
No current from cell at null point.	High sensitivity and speed operation is supported.	Easy to install and integrate to an application.
Amplification of output usually not required.	Insensitive to dust, humidity and vibrations.	Dust and humidity resistant.
Potentiometer efficiency is high.	Less conductivity and high voltage.	Accurate usage in static and mobile application.
Inexpensive, around 5 Euros.	Moderate pricing around 25 Euros ^[16]	Analog and digital output variants are available.
Low input of 2 to 5V is sufficient.	4 – 20VDC supply voltage is sufficient.	10 – 15VDC supply voltage is sufficient.
	12 to 16-bit cca resolutions are available.	12 to 24-bit resolutions for higher resolutions.

Disadvantages -		
Existence of drag torque or inertial loading.	Need strong magnets to measure beyond 10 cm gap.	Slightly expensive, at around 100 Euros.
Limited bandwidth and low 8 to 10-bit resolution.	Affected by external magnetic field.	More than 30VDC for few applications.
Wear and tear due to large force to move wipers.	Significant drift, requires compensation.	Accuracy compensation for hot temperatures.
Dead zones in sensor ends.		
Controlled environment usage.		



So, based on the above-mentioned factors the sensor is bought according to the needs of experimentation. The sensors shortlisted are FCP50A – 1 -Turn Potentiometer^[17], Allegro A1332 Hall Effect Angle Sensor^[18] and SITALL STS – 003 – 2 MEMS Inclinometer Sensor with Analog Output^[19]. For the rating, I have given it from 0 to +5, with 0 being the least favourable and +5, the most favourable.

Table A-4 Final criteria for selection of sensor

Parameters	FCP50A	A1332	SITALL
Space required	Compact (+4)	Additional space for sensor mount (+2)	Compact (+5)
Measurement direction	1 – axis (0)	1 – axis (0)	2 – axes (+4)
Angular resolution (deg)	1° approx. (+1)	0.03° to 0.1° (+3)	0.1° (+3)
Response time (ms)	Instantaneous (+5)	1 to 10 ms (+2)	0.1 to 10 ms (+4)
Temperature range (°C)	-55° to 125°C (0)	-40° to 125°C (0)	-40° to 80°C (0)
Supply voltage (V)	5V DC (+4)	4 to 20V DC (+3)	6 to 15V DC (+4)
Output voltage (V)	2 to 5V (+4)	0.5 to 5.5V (+4)	0.3 to 4.7V (+4)
Output type	Analog (+3)	Programmable (+5)	Analog (+5)
Wear	Wears after certain period (0)	No wear, but drift occurs (+3)	No wear (+5)
Working environment	Clean environment (0)	Any condition (+5)	Any condition (+5)
Price (€)	5€ (+5)	20€ (+3)	80 to 100€ (+1)
TOTAL	+26	+31	+40

5.4.2 SITALL STS-003-2-180-U MEMS Inclinometer Sensor

The sensor which I have chosen for this test bench is the SITALL STS-003-2-180-U MEMS Sensor from SITALL Sensors, which is a dual axis inclinometer. While there are several versions of this sensor according to angle measurement range, with an increment of 5°, which are $\pm 5^\circ$, $\pm 10^\circ$ etc., until $\pm 90^\circ$ on both sides of both axes, it would be better to implement the sensor with $\pm 90^\circ$ as it can be used for other purposes also. Since the output is Analog type, it is easier to implement and program despite the small noise it produces. With 100 Hz refresh rate and a sinusoidal output characteristic, we can obtain optimum results.



Figure 17 *Mounting of sensor with wheel*

Also, the housing of this sensor is compact, resistant to oil, grease and fuel, can be mounted anywhere and can withstand temperatures up to 80°C. The specification of the sensor in experimental setup is given below.

Table A-5 *Specification of selected inclinometer from Sitall*

SPECIFICATION – STS-003-2-U-180	
Input Voltage [V]	6 - 15V DC
Output Voltage [V]	0.3 - 4.7V DC
Current required [mA]	< 60
Number of outputs	2 (X and Y axes)
Measurement angle [°]	± 90° each
Weight [gm]	90gm

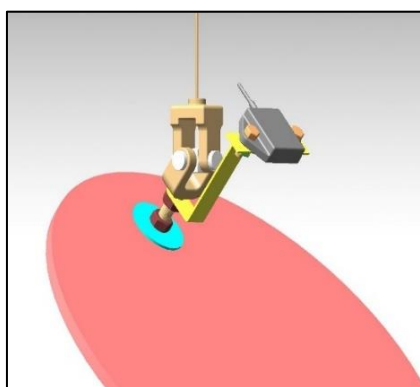


Figure 18 *Sensor mount position view with the disk*

In the Figure 17, the sensor is mounted at the centre of the wheel rim since the point of mount of the Cardan joint to the body has a different angle of inclination than the actual angle of inclination due to complex geometry. But to determine the torsional stiffness, we can mount the sensor on the U- joint itself since it has a uniform geometry.



The connection to the pin board is through a 4-wire configuration, with one for input, one for ground and two for output. Two outputs provide separate signals for both the x- axis and y- axis inclinations. With a supply voltage of 6 to 15V DC and a sinusoidal output voltage characteristic ranging from 0.3V to 4.7V, we get separate graphs for both the inclinations w.r.t time. The output wire type is a 4-wire configuration.

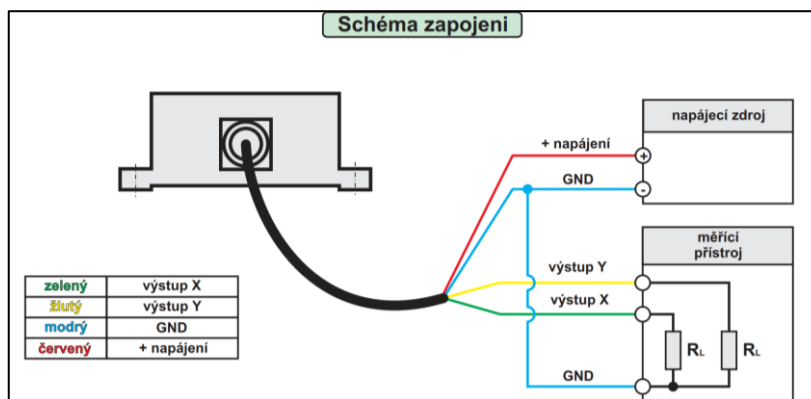


Figure 19 Scheme of sensor connection ^[19]

In case of external power supply to the sensor, the ground connection from the power source must be connected to the terminal board to get the correct readings. The pinout of the above given sensor is given as –

Table A-6 4-wire configuration

Pin	Function	Description	Wire colour
1	V _{cc}	6 - 15V DC supply input (+)	Red
2	GND	GND	Blue
3	Output X	0.3 to 4.7V, X axis output	Green
4	Output Y	0.3 to 4.7V, Y axis output	Yellow

For each pin, in order to differentiate the type of output, we have a different colour to each pin. Hence, it is red colour for positive voltage supply (Pin 1), blue colour for ground voltage (Pin 2), green colour for output on the x-axis (Pin 3) and yellow for the output on the y-axis (Pin 4).

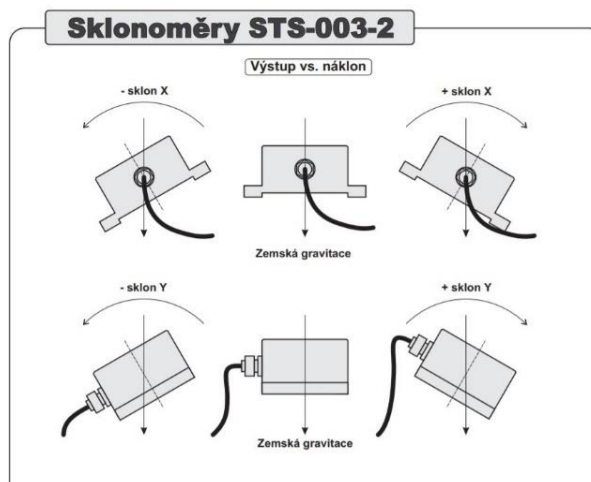


Figure 20 STS-003-2-180-U MEMS Inclinator from SITALL Sensors ^[19]

Since the sensor is small in dimension, it can be fitted easily to the test bench by means of a steel plate of 2mm thickness which can be laser cut according to the dimensions given. Four small holes of 3.2mm diameter are made by the punch plier to accommodate the sensor on the plate. Similarly, a 12mm diameter hole is cut at the bottom to facilitate the placement of the assembly with the U – joint. The diagram of the plate is shown below, and the technical drawing is given in “[Attachment 1.2](#)”–

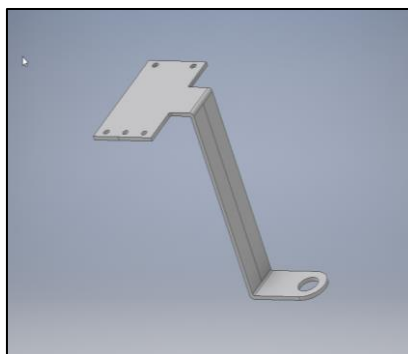


Figure 21 The sensor mounting plate of Stainless Steel

The bent and longitudinal shape of the stand has been given instead of a plain plate without a vertical protrusion because in case of cylinders which are quite narrow, a normal plate would be difficult to mount. But this has been designed with calculations taking in the dimension of the Cardan joints and their inclination capabilities. This plate can be tilted till the maximum inclination of the joint and hence it is favourable.

5.5 Connection of sensors with old and new customized PCBs

The above-mentioned NI terminal board has 68 pin screw terminals, of which we utilize only 7 pins totally for our measurement. Hence, to reduce the size and make the connections more compact, a new PCB has been designed to accommodate just the two components of the experiment i.e., the light gate and the inclinometer. The design and connection of the new PCB has been given in this sub-section.

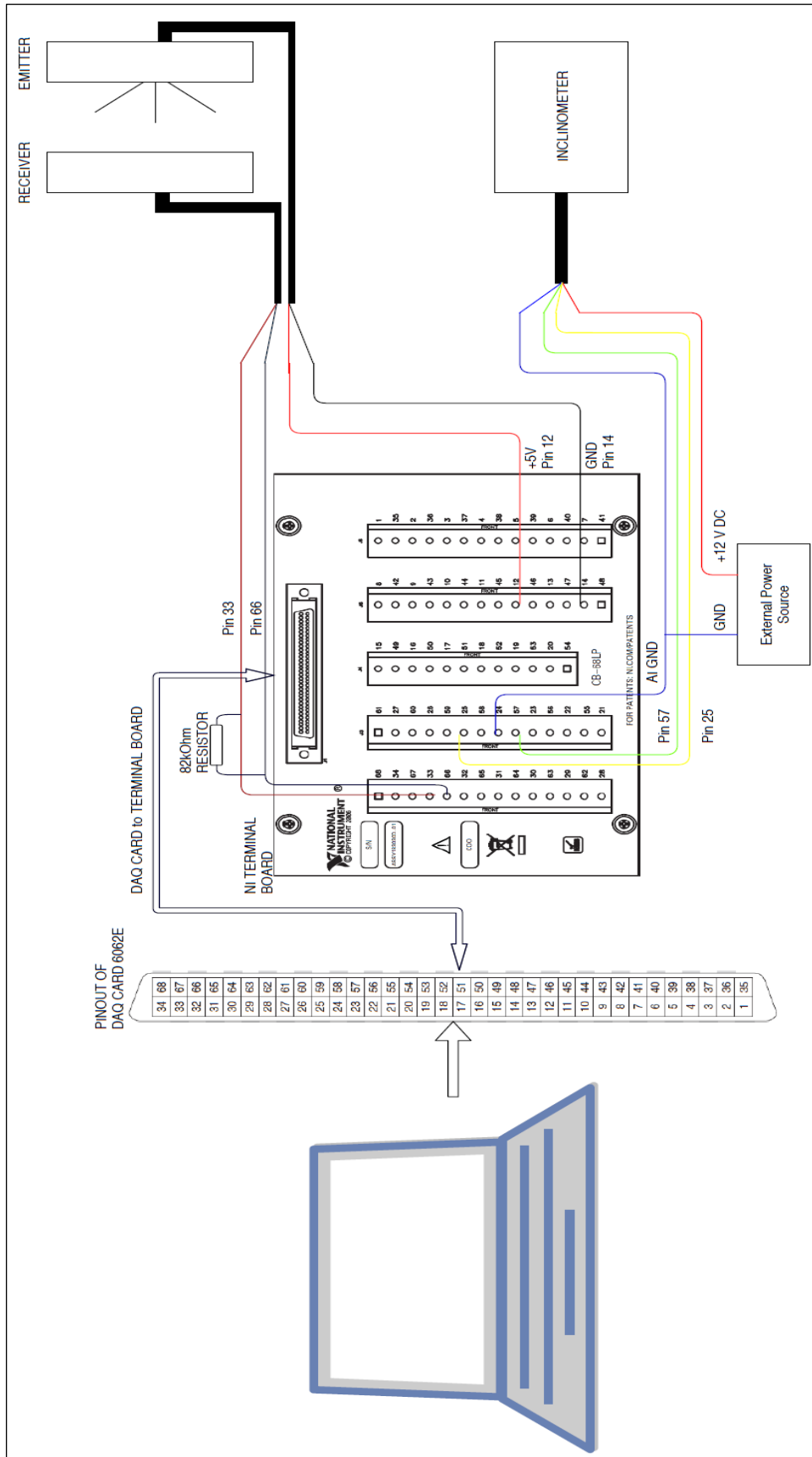


Figure 22 Scheme of old PCB electrical connection



The new electrical designs were done in AutoDesk Eagle, manufactured by Pragoboard, Czech Republic and assembled with the help of Dr. Jiri Novak of FEL at CVUT, Prague. Since the inclinometer inputs +12 VDC and the maximum output of DAQCard is +5VDC, a DC/DC converter from Meanwell – “SBT01L-12” was used.

The new PCB which was to be installed, was first a failure as there was a fault with Autodesk EAGLE library in the 68-pin connector. In a right-angled PCB connector of the 68-pin, the pins are four columns with 17 terminals in each column as seen in the figure below. In the figure below, starting from top right is the number “1” pin, “2” pin to its left slightly down followed by the “3” pin directly below pin “1”. This should have been the case for the second set of columns i.e., from “35” pin to “68” pin. But due to a library fault in Autodesk EAGLE, the pin directly below “35” is “36”, which correctly should have been “37”. This led to the wrong terminal connection design for pin “66”.

Also, the inclinometer is attached to the 15-pin connection as shown. It intakes its input voltage from the DAQCard and converts it into +12V DC through the DC/DC converter. The output from the inclinometer and the ground of power supply had to be connected to a common ground for the measurement to happen, due to a load resistance as seen in the description figure of the inclinometer in the previous chapter. This implies that the input “-ve” (or) GND of the DC/DC converter – “Pin 1” and ground connection from the inclinometer – “Pin 4” need to be interconnected for proper functioning. In the old NI board connection, the connection was done from Pin 24 (AI GND) to the GND of power supply and hence the result was obtained. Hence, due to the above-mentioned facts, the PCB had to be re-designed and given for fabrication to Pragoboard.

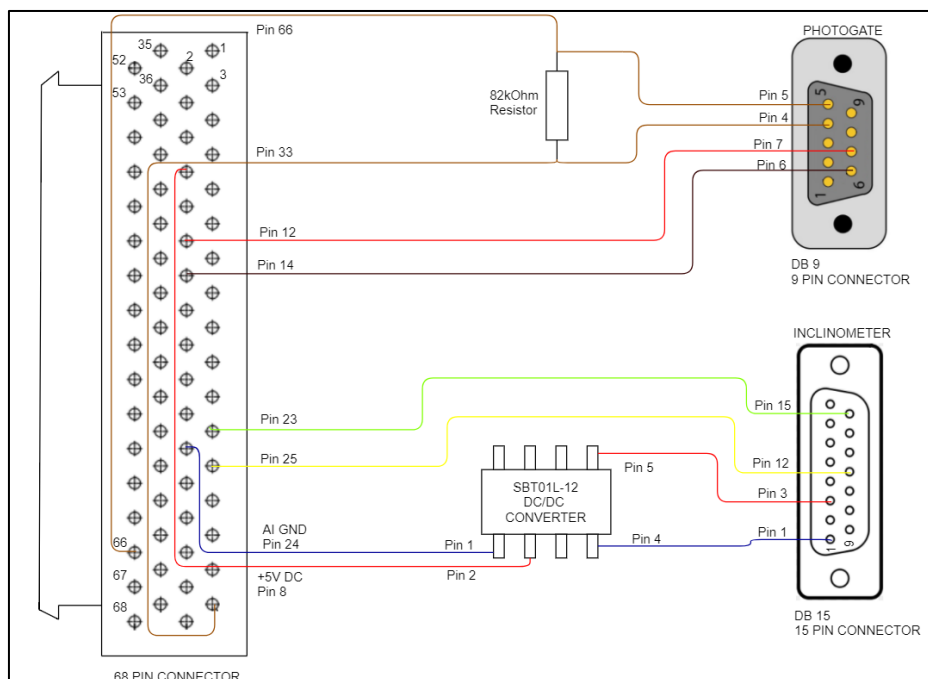


Figure 23 Faulty connection of new customized PCB



The new design with the above mistakes rectified has been done and given for manufacturing. The pins have been rectified and electrical connection between the pads of the DC/DC converter – Pin 1 and Pin 4 has been given.

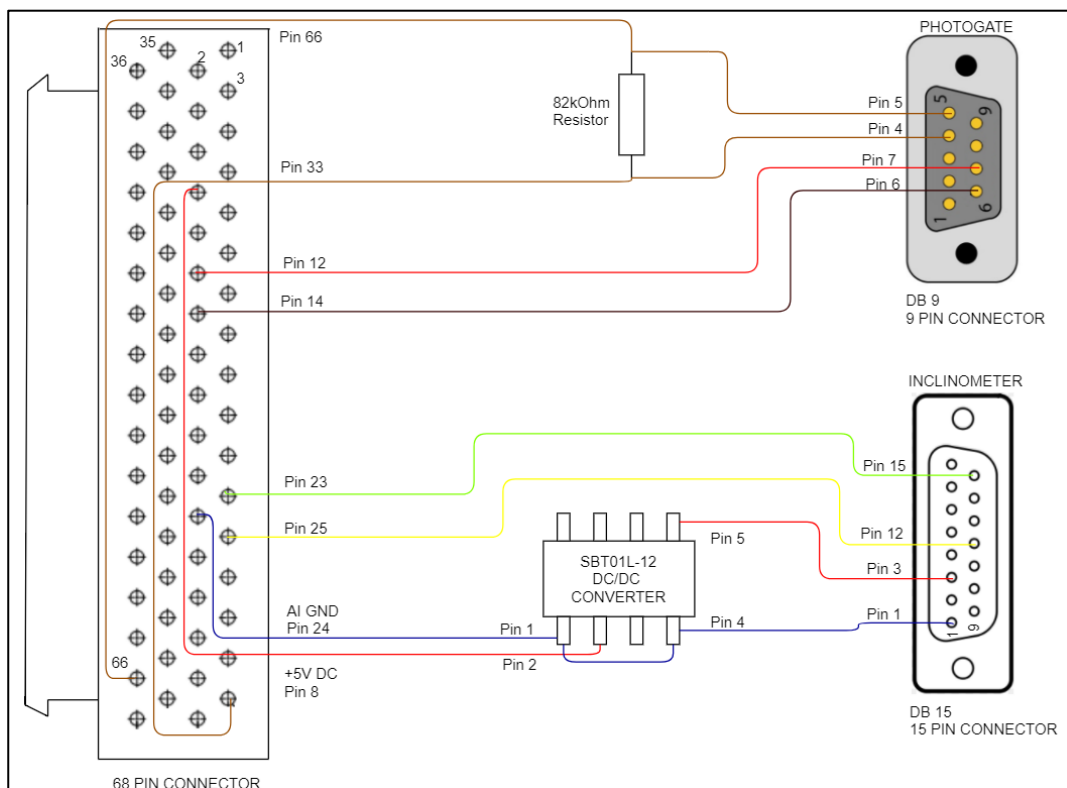


Figure 24 Scheme of new corrected customized PCB

5.6 LabVIEW programming for angle acquisition

The angle values are obtained in voltage from the inclinometer, and this is measured and modified by programming in LabVIEW software, by National Instruments. The provided DAQCard 6062E can process two Analog inputs only if they are on same task.

To measure the principle moments of the body, ellipsoid of inertia method was implemented (given in the Annexure at the end of this document). The moment of inertias I_1 and I_2 about two different mounting positions of the body and the angle it makes with the vertical axis - α and β was obtained. But, to get the angle α two angles of inclination of both axes - θ_1 and θ_2 , that are obtained from the sensor are resolved, since α is the resultant of the two planar inclinations. This is given as ^[33]

$$\theta = \sqrt{(\theta_1^2) + (\theta_2^2)}. \quad (1.33)$$

Where θ can be substituted with α and β in degrees. The sampling is given as 1 Sample on Demand. Inside the program, 500 samples are collected to take the average of them to eliminate any noise present.



Hence the order of measurement is –

- Run the program, obtain the first resultant angle α .
- Measure the half period of oscillation at α inclination.
- Remount the body or wheel to second pivot point.
- Measure resultant angle β .
- Measure the half period of oscillation at β inclination.

My task is to calculate the moment of inertia for the given different mounting positions from the *COG* of the body. the distance of co-ordinates between the mounting positions and *COG* are measured, and input on the front panel of the program. The program for angle acquisition is in “[Attachment 1.3](#)”.

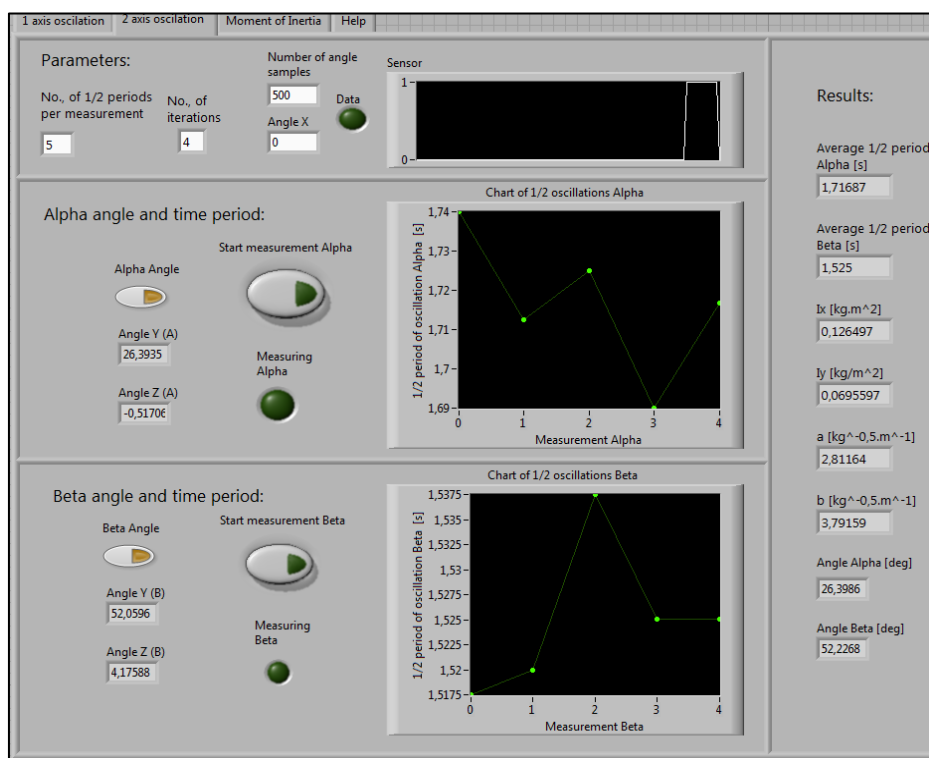


Figure 25 Front Panel of LabVIEW program

By implementing transformation matrices for translation and rotation, and co-ordinates of mounting position that is input on the panel, the final inertia tensor for the moment of inertia of the body is obtained with given program, in “[Attachment 1.4](#)”.

Table A-7 LabVIEW parameters configuration

Task constant – TaskDAQCard					
Channel name	Physical channel	Signal Input range [V]		Order	Acquisition mode
		Min	Max		
Voltage	Dev1/ai1	-5	+5	0	1 Sample (On Demand)
Voltage_0	Dev1/ai6	0	+5	1	
Voltage_1	Dev1/ai7	0	+5	2	



The calculation procedure along with the steps to be followed for execution of the program is given at the end of this report. Thus, following the above steps, the moment of inertia of the body is measured.

5.7 Example check of moment of inertia result with modelling software

To validate and check the accurate function of the sensor and the program, the moment of inertia of a designable object from the laboratory has been found out by LabVIEW program above-mentioned, and also with CATIA V5 software. In this case, a drum brake housing of a passenger car has been taken from the laboratory, as shown in the figure below. The object is made of iron material and weighs about 5.4kg.



Figure 26 Selected drum brake

The housing was mounted on the test stand in a similar fashion as the wheel rim as shown in figure below.



Figure 27 Mounted drum brake housing on Cardan joint

When run with the written program in LabVIEW, the above setup showed the following results as below. Also, the x , y and z axes of the measurement from LabVIEW correspond to z , x and y axes respectively in CATIA V5 throughout the experimentation.

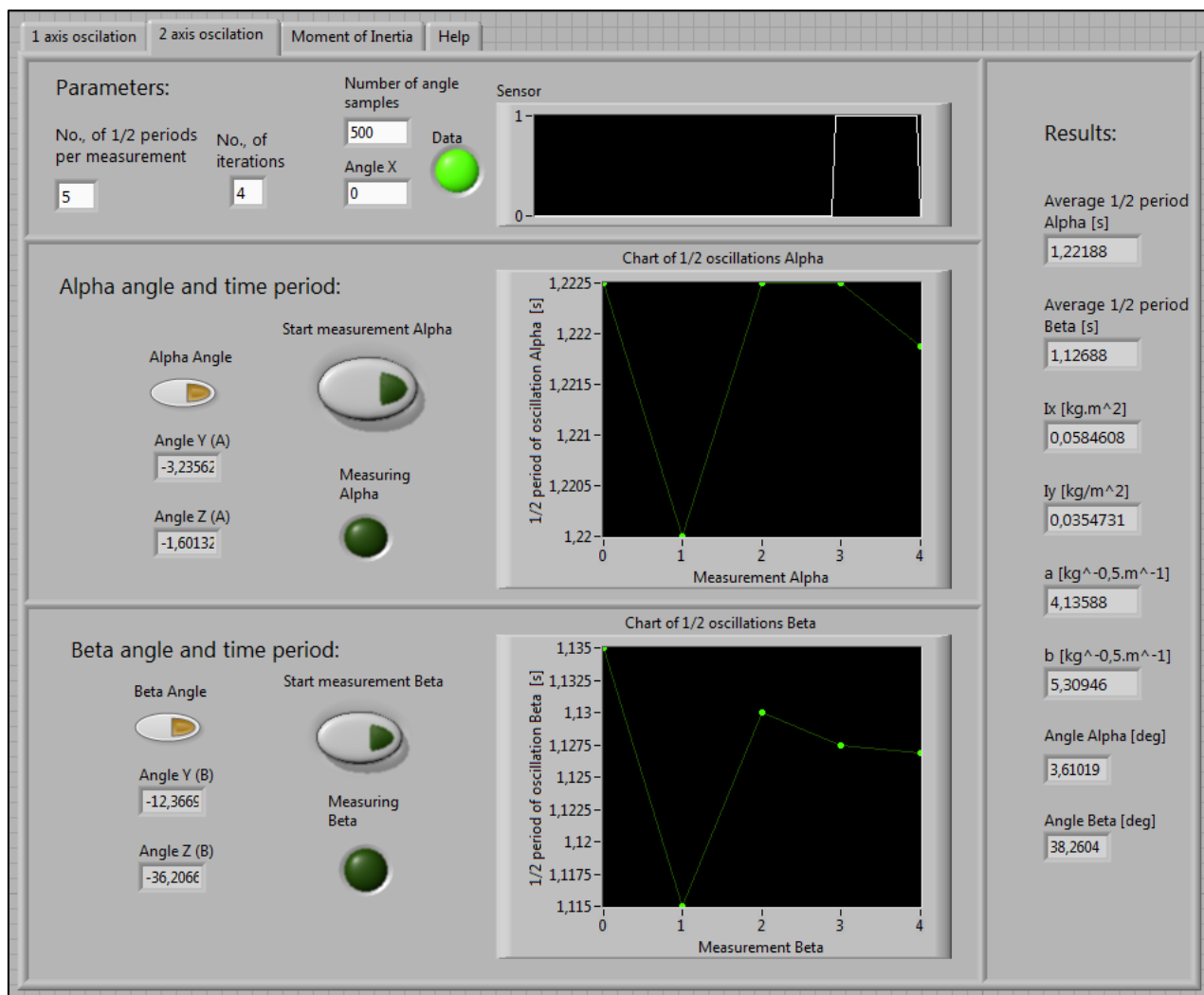


Figure 28 Front panel displaying principle moments of inertia

For the respective angles of inclination – α and β , the moments of inertia change, and so do the mounting positions. When calculated with approximate distances from the principle axes, the results were obtained as shown below.

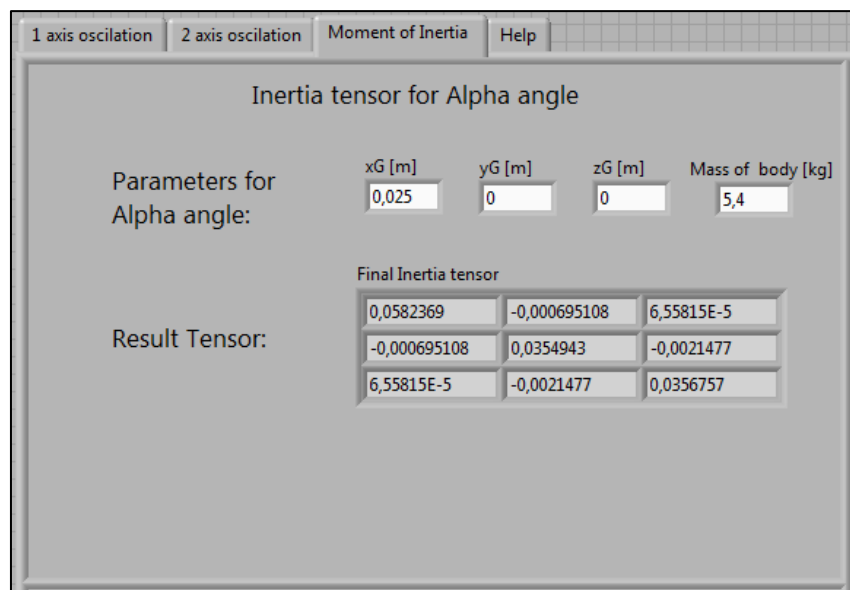


Figure 29 Inertia tensor for angle α

The experiment was intended to measure with angle α as zero by mounting at the centre, but due to slight mounting imperfections it was $\sim 3^\circ$. The corresponding result from CATIA has been given below. The values vary marginally as the exact design could not be done which can change the mass distribution.

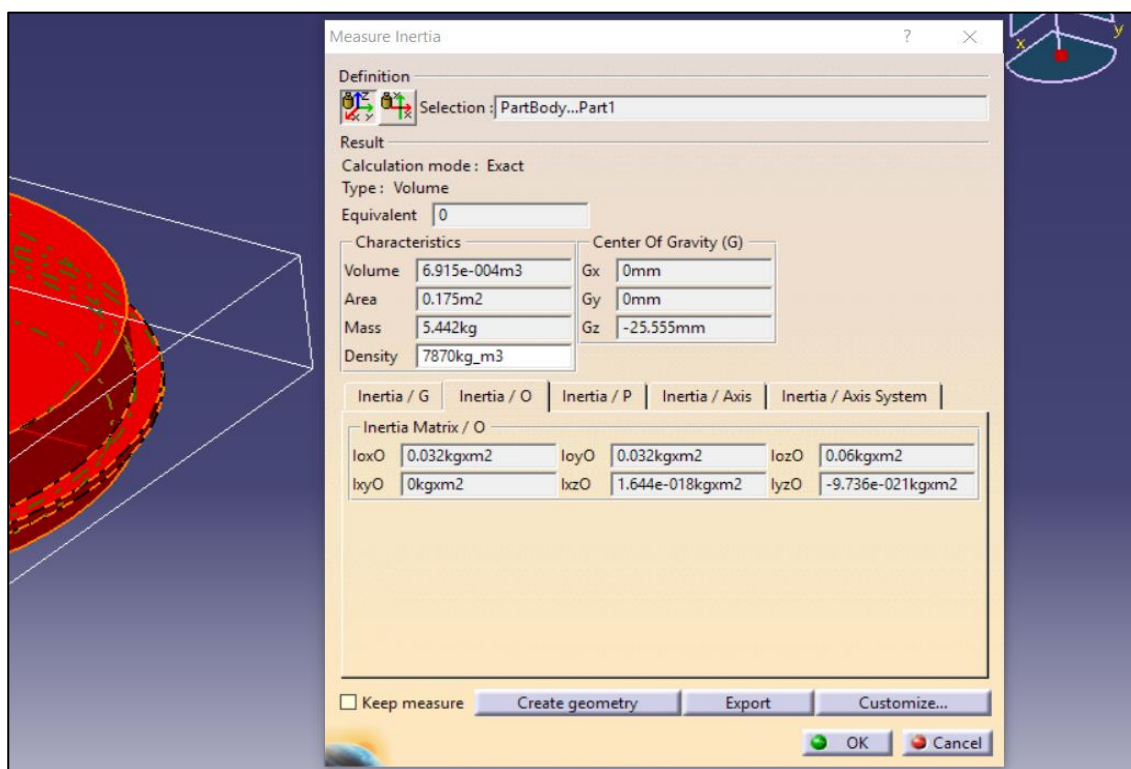


Figure 30 Moment of inertia with CATIA V5, corresponding to angle " α "



The figure from LabVIEW for the angle β measurements is shown below.

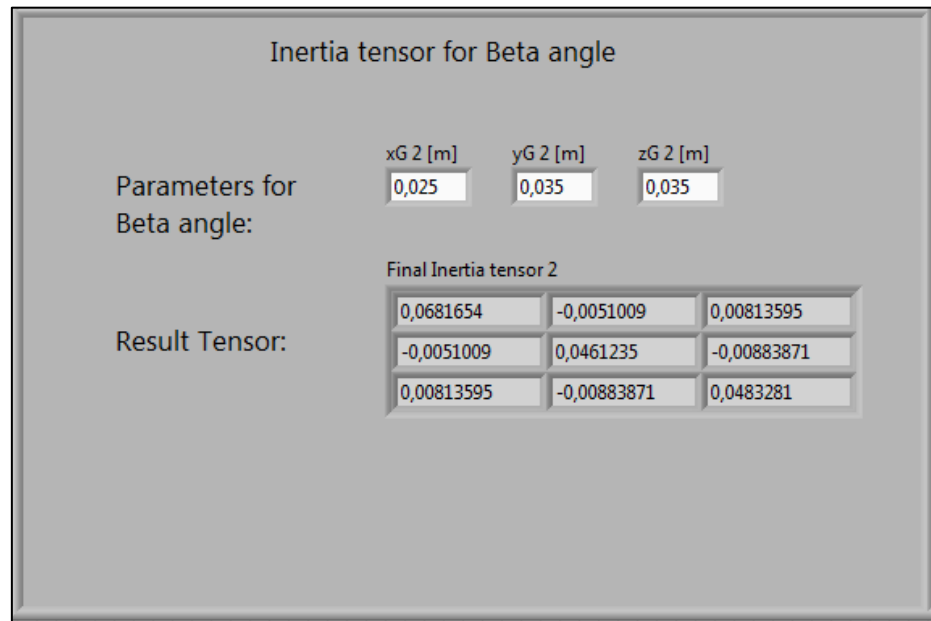


Figure 31 Measurement result from LabVIEW

Corresponding results from CATIA modelling from angle β measurement are as in the figure below.

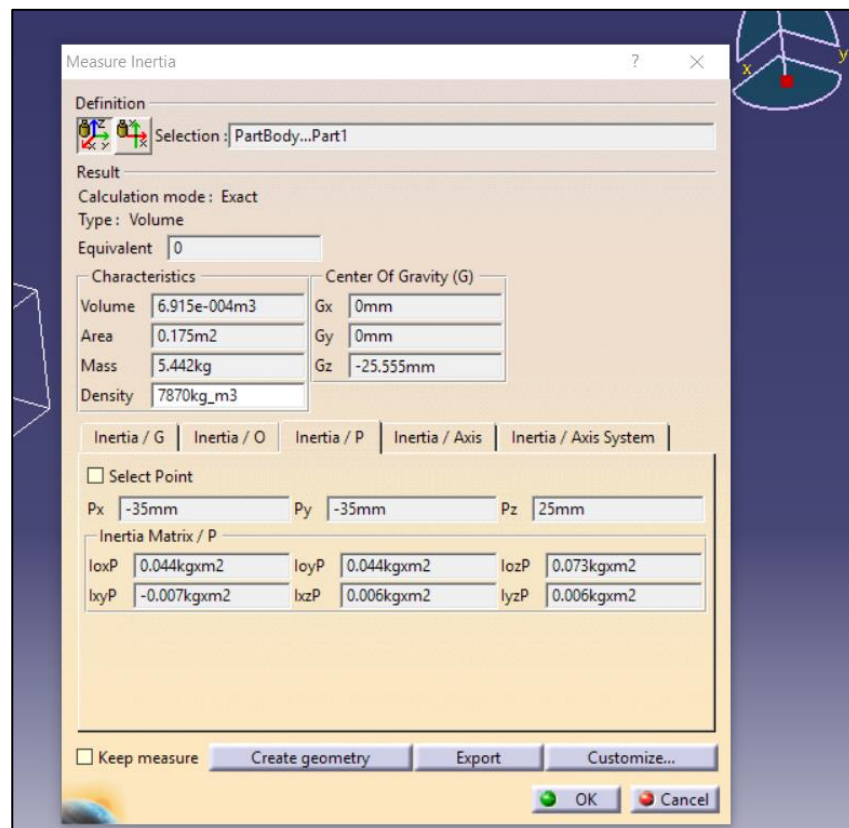


Figure 32 Results from CATIA V5 for the angle β measurement



As seen from both the results, they are almost similar and hence can be concluded that the functioning of the sensor and the procedure which was followed can be accepted for further usage and reference.

6. Conclusion for sub-topic

From this part of the experimentation, it can be concluded that –

- The moment of inertia changes for different points of mounting of the body and different angles of inclination as the distance of rotation from the *COG* of the object varies.
- Eventual mounting at different points would yield deviation moments in the plane at which it is offset.
- DAQCards are the most compact method to connect the hardware and software interfaces but prove slightly difficult to program when using two analog tasks.
- On the other hand, NI modules require additional installation space, but we have the freedom to program more easily the same task at hand.
- There is more than one defined method to determine the *COG* and correspondingly the moment of inertia of the object.

7. Prospects and future work

Few of the probable future works can be –

- In case of variation in movement or other play, development of a program to dynamically provide the moment of inertia tensor according to the additional sway or movement.
- For other complex geometry bodies, a permanent solution must be made for the mounting the sensor if the mounting angle of Cardan joint and the actual inclination are different.



B. MEASUREMENT OF GEARBOX TRANSMISSION ERROR

1. Introduction

Transmission error is a measure of the difference between the theoretical rotations of a gear pair to the actual rotation which might be caused due to the flexibility of the gear and contact ratio of gears. Hence, in addition to the rotation of the gear in mesh, we will have a linear displacement at the base circle radius. Transmission error can also be caused due to manufacturing inaccuracies such as profile errors or run-out and bad design of the gear. The main problem which arises due to the transmission error is the gear noise of the gear set.

Gears made have a finite mesh stiffness and hence deflection of the tooth involute occurs when loaded. In other words, the tooth contact stiffness varies which is one of the main parameters to consider during this measurement as it raises vibration and noise. The formula for transmission error is given as –

$$TE(\mu m) = \left(\phi_2 - \frac{n_1}{n_2} \phi_1 \right) r_2. \quad (2.1)$$

Where n_1 and n_2 are the number of teeth of pinion and wheel respectively.

ϕ_1 and ϕ_2 are the angles of rotation (in radians) of the pinion and wheel respectively.

r_2 is the radius of the output gear (in μm).

There are several methods to determine the transmission error of a gear pair in a gearbox. Some of them include using accelerometers at the end of the shafts of the gearbox, using rotary encoders at the ends of shafts of gearbox and so on. But, implementing accelerometers to measure the torsional accelerations causes the problem of signal transfer from rotational parts and its double integration.^[21]

This experiment has been conducted with two incremental rotary encoders on the gearbox which have a few advantages over accelerometers i.e., the entire gearbox housing noise need not be considered as the instantaneous revolution from the ends of the shafts is obtained. This should save the time for post-processing, if the running is smooth. But in any case, the irregularities due to the components attached to the shaft cannot be neglected, for example the bearings and shaft eccentricity, since they might influence the result significantly.

2. Literature review and previous works

As mentioned above, to determine the transmission error several common previous methodologies were to implement accelerometers on the gearbox housing to detect the vibration signals of all components.



The most noticeable work, which is by Prof. Tuma of Technical University of Ostrava has been done by implementing two Heidenhain encoders of ERN 460-500 type at the ends of two shafts of gearbox and an accelerometer on the housing. ^[21] They produce 500 pulses per revolution of the shaft and the signal obtained is sinusoidal voltage. The noise from the signals are eliminated after FFT with digital filtration about the Gear Mesh Frequency, either low-pass or high-pass filter. The entire measurement is done in “orders” rather than frequency in Hz, which is acceptable since the measurement is cyclic. The sampling is done at constant frequency and resampled according to the rotational frequency to utilize it for DFT and FFT calculation. According to the speed of rotation or order, the amplitude of the vibration is obtained simultaneously from the accelerometer, in dB. Filtering it as mentioned above and averaging the data points provided the average transmission error.

Another method that has been implemented to find the transmission error has been given by Antonio Palermo, with SIEMENS and *Universita' della Calabria, Italy*. ^[22] The method he has used is similar to that, which will be implemented in our laboratory, where he has used two encoders at the ends of shafts and sampled it with internal sampling clocks of high frequency. He has compared the results of Transmission Error from two types of encoders in his test bed.

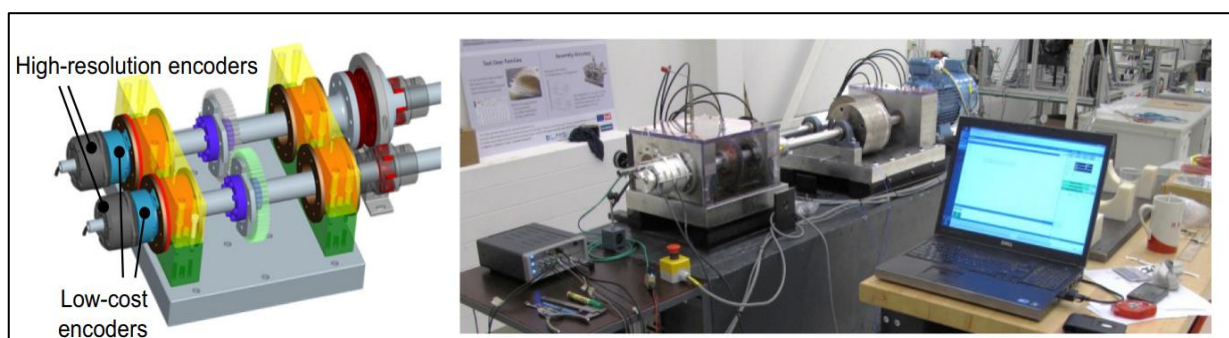


Figure 33 *Test rig implemented with encoders*

The author has considered in the process, 4 types of errors – timing error due to high-frequency clock, rise time error to get the TTL signal from 0 to 1, propagation error in acquisition due to long cable and uneven grating error of the encoder. Since the encoder grating error has been given by the publisher, he has taken other three into account which are indeed significant. He has also obtained the data as impulse in voltage, performed “Order Analysis” and determined the average error similar to the method by Prof. Tuma. Since the end results are satisfactory with the encoder method, it for the experimentation at the laboratory.

3. Concepts related to transmission error

Before delving into the measurement of transmission error, a few related concepts which are essential for the better understanding of transmission error are discussed.



3.1 Root Mean Square (RMS) or Standard Deviation of a signal

When it comes to signal, the change of attributes of a signal with some other independent quantity is specified. Usually, these are changes with respect to time, denoted by 't'. Root Mean Square (RMS) is nothing but the derivation from the variance of the signal. RMS is used to determine the deviation or amplitudes of the signal from the time mean value, T . It is given by the order of its name in the formula –

$$RMS = \sqrt{\frac{1}{T} \int_0^T x(t)^2 dt}. \quad (2.2)$$

Every signal carries a certain amount of energy with it and the signal power is defined by energy per unit of time. It is also mentioned as Power Spectral Density (PSD) in few cases.

$$PWR = \frac{1}{T} \int_0^T x(t)^2 dt = RMS^2. \quad (2.3)$$

3.2 Nyquist- Shannon Sampling theorem

Analog signals need to be converted into digital signals with the help of Analog-to-Digital Converter (ADC) in computer. To do this, samples must be taken frequently, and number of samples taken per second is called as sampling rate or sampling frequency.

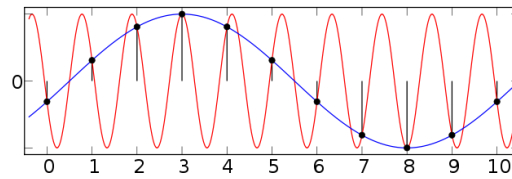


Figure 34 Curves at different sampling rates ^[35]

From the above diagram, taking one sample for each second and joining them will give the blue curve. But, the samples are also a part of the red curve with higher frequency. As they were under-sampled, major portions of the red curve were lost, resulting in different curve altogether. To solve this crisis, Nyquist and Shannon proposed a theory that the sampling frequency (or) the sampling rate must be more than two times the frequency of the signal. Thus, it can be said that if ' f_s ' is the sampling frequency and the highest signal frequency is ' f ', according to the theorem,

$$f_s > 2f. \quad (2.4)$$

3.3 Aliasing

Aliasing is a mistake which occurs when the frequency of the signal is greater than half of sampling frequency but lesser than sampling frequency itself ^[21] i.e.,

$$\frac{f_s}{2} < f < f_s. \quad (2.5)$$

This phenomenon would again lead to wrong information and representation to the computer. Hence to make the conversion valid, two ways are possibly implemented. The



sampling frequency must handle the maximum frequency of the signal or the signal's frequency must be adjusted according to the sampling frequency, by the converter. For the second scenario, a filter is used to counter the aliasing and hence it is termed as anti-aliasing filter or low pass filter. The low pass filter or the LP-filter makes way for signals with frequencies lower than a cut-off frequency and blocks the higher frequency signals. But, there exists a transition band in between the pass band and the stop band and the maximum frequency of the passband is the cut off frequency of the LP filter.

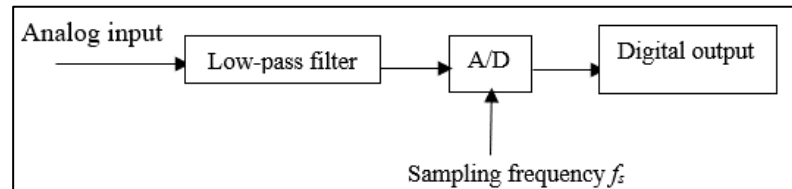


Figure 35 Anti-aliasing or Low-Pass Filter

Usually, more the frequency of a signal, more the corresponding bandwidth. With the low pass filter, the frequency of signal is reduced and derived as $10 \log (f_s/2BW)$ ^[23].

3.4 Fourier Transformation

The original signals that are generated in the machine are usually with respect to real-time. The vibration or acoustic signals which are sinusoidal, seem to be non-periodic and random in the time domain.

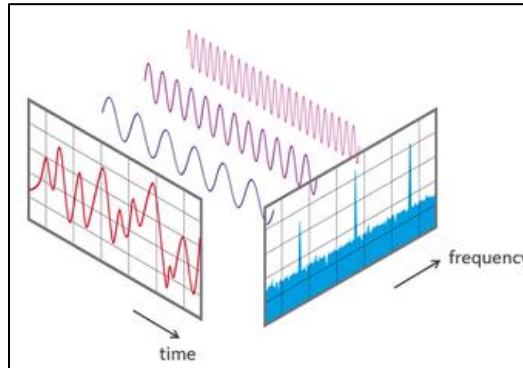


Figure 36 Transformation of sinusoidal signals in spectrum ^[36]

As seen above, even though a combined signal may look random, if it is converted into the frequency domain, it is possible to learn about its individual components. For a periodic signal $x(t)$ with a period of T , the condition for periodicity is –

$$x(t) = x(t + T). \quad (2.6)$$

The above-mentioned function is integrated with t from 0 to T and the Fourier series of the signal or the infinite sum is given by ^[23]

$$\frac{a_0}{2} + \sum_{k=1}^{\infty} [a_k \cos\left(\frac{2\pi kt}{T}\right) + b_k \sin\left(\frac{2\pi kt}{T}\right)]. \quad (2.7)$$



Where a_k and b_k are the Fourier coefficients, which are –

$$a_k = \frac{1}{T} \int_0^T x(t) \cos\left(\frac{2\pi kt}{T}\right) dt.$$

$$b_k = \frac{1}{T} \int_0^T x(t) \sin\left(\frac{2\pi kt}{T}\right) dt.$$

3.4.1 Spectrum scales of DFT

In the time domain, the x – axis of the representing graph can be the index n or the time scale, t_n . In the frequency domain of DFT, the x – axis can be frequency, time or index k .^[23]

$$t_n = nT_s.$$

$$f_k = \frac{k}{NT_s} = \frac{k}{T}. \quad (2.8)$$

Where $n, k = 0, 1, 2, \dots, N - 1$, T_s is the sampling interval, N is the number of samples for calculating DFT and T is the total time for N samples at a sampling interval of T_s . In real-time signals, since they are symmetrical, a one-sided spectrum is used and hence only till $N/2$ samples are used for calculation.

Similarly, the vertical axis of frequency domain can be Root Mean Square (RMS), power (PWR) or Power Spectral Density (PSD). The usage of each of these terms depends on the type of signal acquired.

Table B-1 *Signal spectrum usage*

SIGNAL NAME	SIGNAL USAGE	FORMULA
Root Mean Square (RMS)	Diagnose machines	$RMS = \frac{Amplitude}{\sqrt{2}}$
Power (PWR)	Sound and pressure	$PWR = RMS^2$
Power Spectral Density (PSD)	Random processes and vibrations	$PSD = PWR / \Delta f$

Where $\Delta f = f_s/N$, which is the distance in Hertz (Hz) between adjacent spectrum components.

These are the powers related to the frequency band of 1 Hz. The frequency spectrum for DFT relies on the length of record used for the calculation of DFT.

3.4.2 Fast Fourier Transform

Suppose, there are N samples at hand, the Discrete Fourier Transformation (DFT) undergoes $(N)^2$ operations totally. James W. Cooley and John W. Tukey improved this method, where they published their method as Fast Fourier Transformation (FFT)^[24]. In general, it can be said as the condition for FFT to happen, the total required number of samples should be $(2)^n$, where n is the number of times the operation is conducted. The Cooley-Tukey algorithm requires only $(N \log_2 N)$ mathematical operations and the time taken would only be $O(N \log_2 N)$ ^[24].



Matteo Frigo and Steven G. Johnson in 1998 improvised FFT, which was termed as Fast Fourier Transformation in the West (FFTW) ^[25]. It simplified the existing FFT method to any N number of samples, removing the constraint of necessity for 2^n multiple previously required.

3.4.3 Time window selection

When Fast Fourier Transformation is done, a finite periodic sampling is assumed, which means that the signal has a whole number of period of waveforms. This gives an absolute FFT spectrum which is accurate without any sidebands. But in many cases, the signal may not be of a complete period at the end, which gives extra frequency signals with different amplitudes which may yield inaccurate results. This is termed as *Spectral Leakage*.

To reduce such inaccuracies, a function called Time Window function is implemented. This might not yield only the actual peaks, but it reduces the amplitude of side bands of the desired frequency towards zero which is acceptable in many cases. Choosing a time window is done considering a wide range of factors, depending on the frequencies of the signal.

Hence, in general the Hanning window is sought, which yields satisfactory results. When the nature of the signal is unknown, this window can be applied for proper initial analysis. Even without a window, there is a default windowing effect while performing the FFT and hence is called uniform or rectangular window.

Based on the characteristic functions of the various windows, the most suitable signal for each of them is given in “[Attachment 2.1](#)”, by National Instruments ^[26].

3.5 Comb Filter

Since transmission error is caused due to bending of gears while rotating, fluctuations of rotational speed in frequencies of meshing occur. Theoretically if gears are of infinite stiffness, uniform rotational speed is the result. Hence, the transmission error is determined by isolating the fluctuation values from the rotating speed of both the gear shafts. This is done by implementing “Comb Filter” as shown in figure below, which is like a comb as it allows material to go through at only certain periodic gaps.

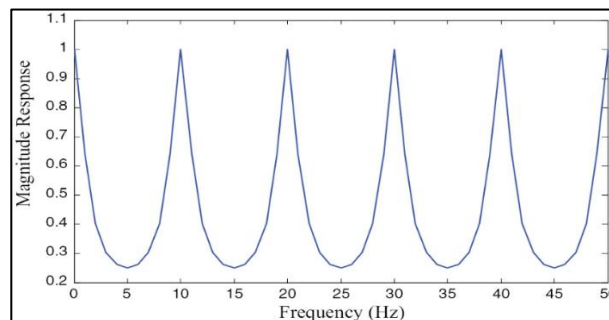


Figure 37 Example of Comb Filter in frequency spectrum ^[34]



4. Experimental setup for measurement

The picture below shows the entire setup of the test bench at the CTU laboratory at Juliska, which consists of a disk brake combined with the rotating inertial mass on its axis of rotation on the left, the inertial mass itself at the centre which is run by a motor connected through a belt and pulley mechanism, and finally the gearbox to be tested on the right side which is coupled to the inertial mass as well, by a half axle shaft which runs through the differential cage of gearbox.



Figure 38 Entire test bench used for experimentation

The entire test bench, except the encoders work on a power supply of 24 VDC with 1A current, which is obtained after converting the 230V AC from the power line. The AC/DC converter power supply was not available at the start of measurement. Hence, this was searched and ordered from a manufacturer - Meanwell and the corresponding model was “EDR-75-24”. It fulfilled the power requirement of the test bench and hence was installed in it.

To measure the transmission error of unloaded gearbox, incremental rotary encoders have been used on the hardware side to collect the rotational period and then send it to the computer for display and post processing, while the other side has a running motor.

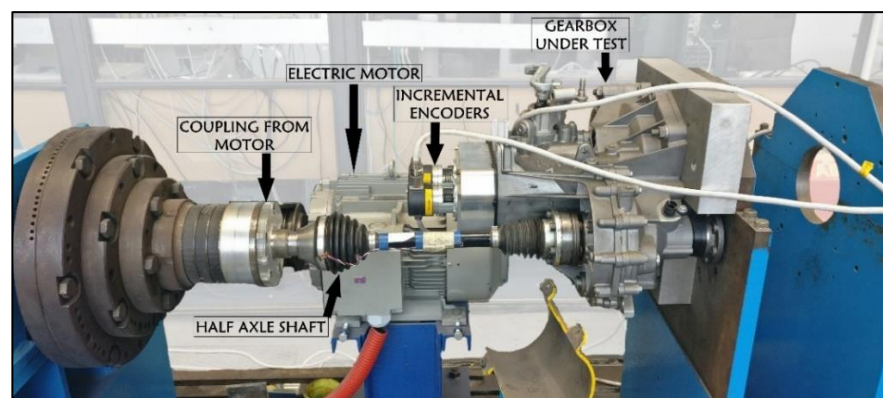


Figure 39 Installed gearbox with the test bench



The test bed comprises of a gearbox on the chassis of the stand in one end and a disk brake setup on the other end, which is used only when we need to stop the setup after measurement. A large inertia mass is provided to simulate the weight of a quarter car. The detailed process is explained in the further steps. The flowchart for the process is –

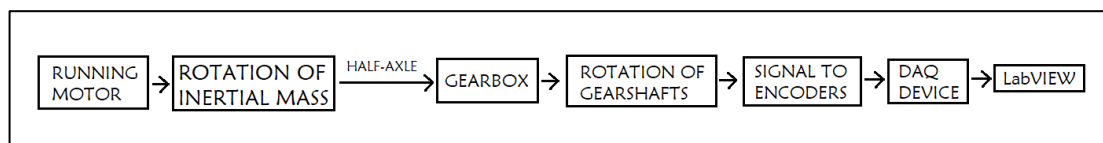


Figure 40 Flowchart of procedure followed during acquisition

Main idea for data acquisition is to obtain the period from the “Counter” signals of Channel A of encoder, with a constant 80 MHz internal clock of the Data Acquisition (DAQ) device. The device counts the number of ticks of internal clock elapsed between successive rising or falling edges of the TTL signal from encoder channel A, once triggered.

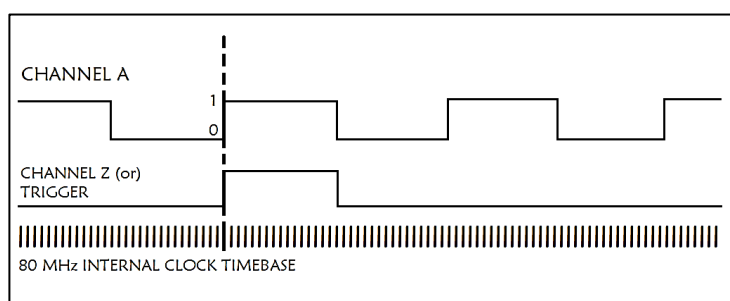


Figure 41 Working of data acquisition from NI DAQ device

Firstly, the components implemented are described below and then the working is described in the following chapters.

4.1 Asynchronous electric motor

The electric motor used to run the setup is a 3-phase asynchronous motor from the manufacturer Elektra. It is powered by ABB industrial drive – **ABB ACS800 – 01 – 0016 – 3**. The performance parameters of the drive are given in “[Attachment 2.2](#)”.

It is a 4 pole, 3-phase asynchronous motor from Elektra, as mentioned above. The specific model is the **7AA160L04**. It is coupled to the test bed with the help of a V – belt, where the diameter of the pulley at the output side is slightly lesser than on the input side resulting in a geometric ratio of 0.8.



Figure 42 Asynchronous motor used

The motor works at operating frequency power of 50 Hz for current test bench, but also can work at 60 Hz, according to which the speed and other electric parameters differ. The working parameter of the motor is provided in “[Attachment 2.3](#)” [28].

4.2 Gearbox on test stand

The gearbox under test is a manual one of Volkswagen make, from MQ 200 series. It is a two-shaft gearbox with an additional shaft for the engagement if the reverse gear. In addition, all change gears are run with needle bearings to minimize the vibration. The 1st and 2nd gears are engaged on the output shaft, whereas the 3rd, 4th and 5th gears are engaged on the input shaft. The 1st and 2nd gears are engaged with the help of double synchronizers. The encoders are attached to the ends of shafts of the gearbox as shown in figure below.

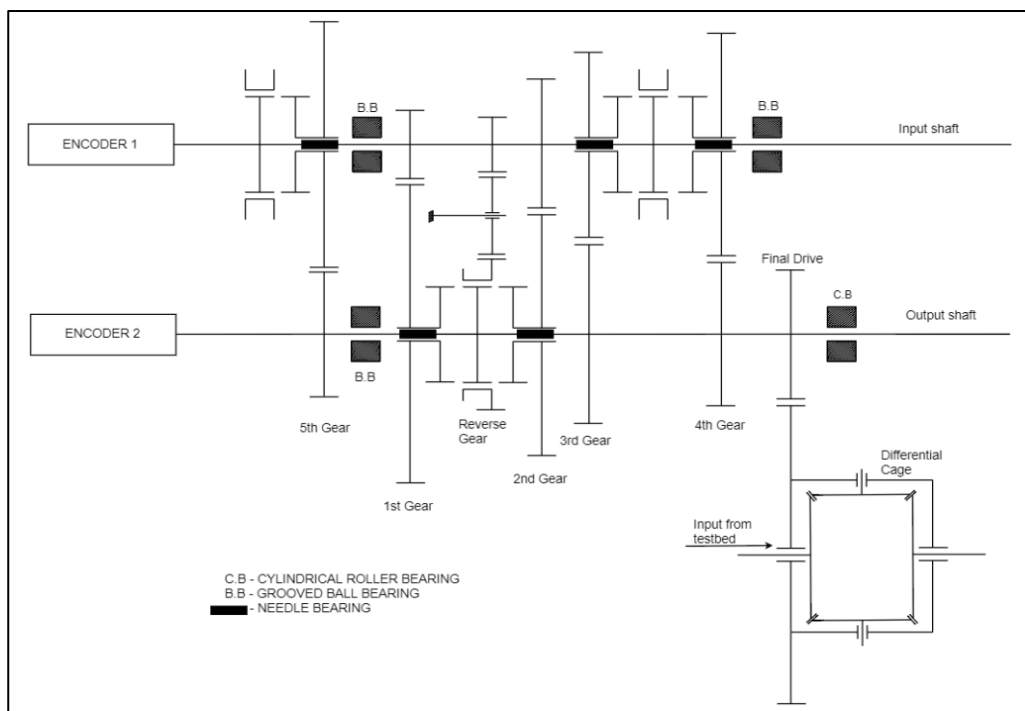


Figure 43 Simple sketch to show the location of encoders



There are many variants of the gearbox whose number of teeth configurations are different. Currently, the LNR type is used, whose specification is given in table below.

Table B-2 Parameters of the tested gearbox

PARAMETERS OF GEARWHEEL						
Gear speed	1	2	3	4	5	Final Drive
Teeth on input shaft	13	21	32	41	50	16
Teeth on output shaft	49	44	41	38	37	67
Gear Ratio	3.769	2.095	1.28125	0.92683	0.74	4.1875

4.3 Incremental Rotary Encoders LARM IRC 305/6000 PA

This experiment is based on the determination of time taken to cover every successive 0.06° of revolution of each shaft of the gearbox. Hence an incremental rotary encoder with equidistant angle separation is implemented, which here is of 6000 pulses and hence 0.06° . The encoder works based on counter signal pulse acquisition with NI instruments. The terminology is as follows^[27]–

Table B-3 Definition of each term of encoder

LARM IRC 3XX XXXX XX	
3	Type of encoder: IRC with LED source
X	Shaft diameter: “0” – External shaft diameter 6 mm
X	Input/ Output parameters: “5” – +5VDC/ line driver
XXXX	Pulses per revolution: “6000” – 6000 pulses
XX	Output connection: “PA” – Axial connection

The general parameters of the encoder have been established and the electrical parameters are given in “[Attachment 2.4](#)”^[27] The encoder has 12 pins with 3 signals, their negation, power supply, shield, No Connect (NC) and ground signal (GND). The distance between consecutive rising or falling edge is 0.06° as shown in figure below. For our experimentation, we consider only the positive signals i.e., we neglect the “non” signals. The Z channel or “3” serves as the digital trigger to start the measurement.

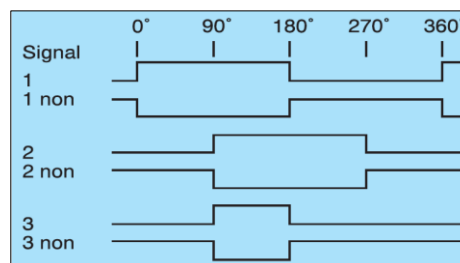


Figure 44 Electrical angle of impulse from encoder

To connect the hardware to the data acquisition device, we use an ADAM terminal board, connected to the NI device by a cable. The terminal board consists of same number



and pin configuration as that of the DAQ device. In the terminal board, each wire is assigned a different colour. The colour codes are given in “[Attachment 2.5](#)”.

The encoders are attached to the gear shafts at the end of the gearbox through a custom-built housing. The shaft of the encoder is of 6 mm and hence provision is made that the coupling from the gearbox shaft is also of the same dimension.

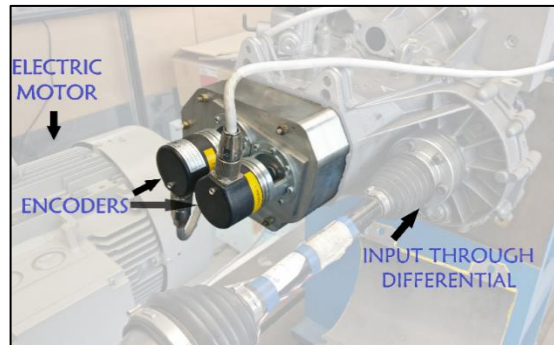


Figure 45 Mounted position of encoder on gearbox

As it is evident from the picture, the input is given from the motor through the half axle via the differential, to the gear shafts. The output from the encoders are obtained through the wires which get impulses according to the slits on the encoders. This is relayed to the computer through a set of components, given in following chapters.

4.4 Advantech ADAM terminal board

The two 12 pin wires from both encoders are attached to ADAM-3925 DB25 DIN-rail terminal board interface, produced by Advantech Solutions ^[30], mounted on a DIN rail of 35 mm. This board relays to NI DAQ device by a 25-pin DSUB cable. Scheme for connecting the incremental encoders with terminal board is given in “[Attachment 2.11](#)”.

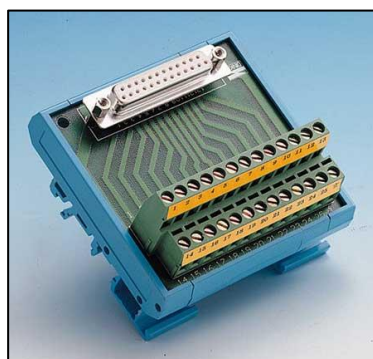


Figure 46 ADAM terminal board

4.5 NI 9401 DAQ module

The 25-pin DSUB cable above-mentioned, is connected to NI 9401 module on the other end. NI 9401 is exclusively used for TTL input. It is compatible with Counter readings also by programming, which is favourable for this experimental test bench.



Figure 47 NI 9401 module implemented

The device relays the data from the hardware to the computer through a CompactDAQ device or CompactRIO and for this experiment CompactDAQ NI 9174 chassis is taken, whose function is explained in the consecutive sub-topic. The characteristics of the NI module are given in “[Attachment 2.6](#)”.

The PFI channels for signal acquisition ranging from 0 to 7, are mainly used for this measurement. The module is used for encoder measurements in many cases due to its favourable internal configuration.

4.6 CompactDAQ chassis cDAQ-9174

The chassis has 4 slots to run 4 modules simultaneously and each has a separate timing engine. Although the board supports all three Analog, Digital and Counter signals, Counters in detail are of interest since they are implemented in the current test bench.



Figure 48 NI 9174 Chassis to dock NI 9401 module

The performance parameters of the Counter tasks and Timers are given in “[Attachment 2.7](#)”. There are also Digital Triggers, which we will be using to synchronize the measurement of the two encoders to start at the same time. A few types of Digital Triggers are Start, Reference and Pause Triggers.

5. Data acquisition from LabVIEW 14

Now that the components required for the experimentation have been established, data acquisition from this setup is explained. The concept to obtain transmission error, i.e., the deviation of angle of rotation from the ideal value, is through the determination of difference



in the period of revolution at every impulse of the encoder. For this purpose, LabVIEW by National Instruments has been implemented. The entire program is classified into 3 steps –

- Configuring the terminals (PFI) and trigger for the tasks
- Initializing the tasks and data acquisition
 - Data acquisition of time period of every impulse of encoder
 - Changing it to instantaneous RPM and display on graph for viewing
- Saving the acquired data

Since the instantaneous speed of revolution from the period between each consecutive pulse is to be determined, the period function of Counter input is used. The analysis of these readings will be explained in the following chapters. To create the tasks from the NI module, a software called NI MAX (or) Measurement and Automation Explorer is used. The steps to create the task are discussed in the “Annex 3”, of this thesis. Similarly, the description of sub-program for configuring terminals is given in “[Attachment 2.8](#)”. Also, the description for initialization and saving the data are given in “[Attachment 2.9](#)” and “[Attachment 2.10](#)” respectively.

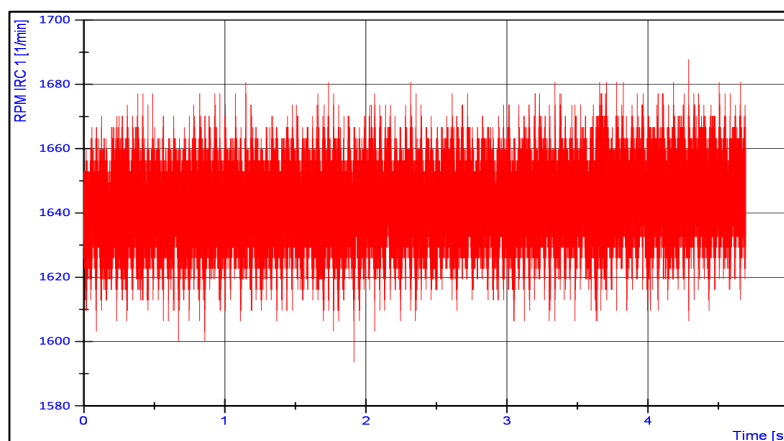


Figure 49 "RPM (vs) time" graph of input shaft of 1st gear

6. Processing obtained data with NI DIAdem

The data obtained from LabVIEW contains a lot of noise as seen above i.e., the instantaneous speed of rotation varies over a large range for every reading of the encoder. This is problematic as a steady transmission error for a gear mesh without load, at a particular speed cannot be finalized. Hence, a specialized software for post processing of data “NI DIAdem” is used, as it is concentrated on vibration and crash analysis of a body. The obtained data is analysed in the frequency spectrum and unwanted fluctuations are attenuated to get only the rotational speed of the shaft at Gear Mesh Frequency (*GMF*) harmonics for processing. The process is explained in the topic below.



6.1 Data preparation for analysis

To analyse the data in DIAdem, a monotonously increasing time of revolution data and the corresponding speed of revolution is needed. Hence a running total of the period of revolution is performed in the Excel worksheet, after importing from the “.txt” file. After the total is done, the Excel file can be imported into the software where new channels are created, data is written, and calculations are done.

6.2 Transmission Error measurement of RPM signal

In the “Analysis” sub-section of the software, there are several curve and crash analysis options. FFT option is chosen for analysis, where the X and Y axes channels are selected. Since RPM vs time is needed in the graph, speed is taken on the Y – axis and monotonously increasing time on the X – axis. The parameters used for FFT analysis are given in the table below –

Table B-4 Parameters of FFT Analysis

PARAMETER	VALUE	
Window type	Hanning	
Amplitude attenuation correction	Periodic	
FFT Parameters	FFT Functions	Amplitude
		Real and Imaginary part
	Type of Amplitude	Peak amplitude
	Third/ Octave	No
Average amplitudes	No averaging	
Time Intervals	Number/ Start/ Overlap	
	Number of intervals	1
	Interval length	//Default entire data//
	Start	1
	Overlap [%]	0

The resulting FFT graph contains the frequency spectrum and its corresponding amplitude. The amplitude is interpreted as the value of fluctuation of speed of rotation which occurs in that frequency. For this experiment, the harmonics of the Gear Mesh Frequency is taken which is the deflection on two teeth of the shaft gears during meshing contact and rotating.

Above-mentioned frequencies are isolated and used further for digital filtration of the signal by either using “Comb Filter” or “Synchronized Averaging in Time Domain”. Only the harmonics of GMF would remain or also sometimes small attenuated peaks of sidebands if the latter method is used.

Also, in the absence of Comb Filters, a different method with “Inverse Fast Fourier Transform” (IFFT) is used, to analyse in a similar manner. But this is more effective due



to the elimination of even the attenuated small peaks of sidebands present in the spectrum, with just the peaks of interest remaining. Initially the FFT of a signal is taken and the vibrational peaks of the spectrum is characterized with “Amplitude” and “Real and Imaginary” parts. The mesh frequencies and their amplitudes are only retained, making the real and imaginary part values of other unnecessary frequencies as zero. Only till the 5th or 7th harmonic of the mesh frequency is taken since higher harmonics have negligible amplitude and hence less effect on the spectrum. The steps for “Averaging” process and IFFT in NI DIAdem is explained in the Annex 4.

6.2.1 Measurement of Gear 1

The gearwheel parameters of the 1st gear mesh is given in the table below –

Table B-5 1st Gear mesh parameters

GEAR 1 –		
Teeth – Input shaft		13
Teeth – Output shaft		49
Gear Ratio		3.769
Module, m		1.8
α		20°
β		28°21'11"
PCD of input gear [mm]		26.5897
PCD of output gear [mm]		100.2229
Running condition	Bench Speed	~100 rpm
	1 × GMF	342 Hz

The experiment was conducted with almost constant speed at the input through the half-axle. The readings were taken with LARM 6000 Pulse encoders after almost steady state condition was seen at the input, to facilitate easier understanding of the data as speed variation can lead to complex 3D “Waterfall plot” charts and consequently complex analysis. The resulting graphs from the two encoders’ measurements are as follow –

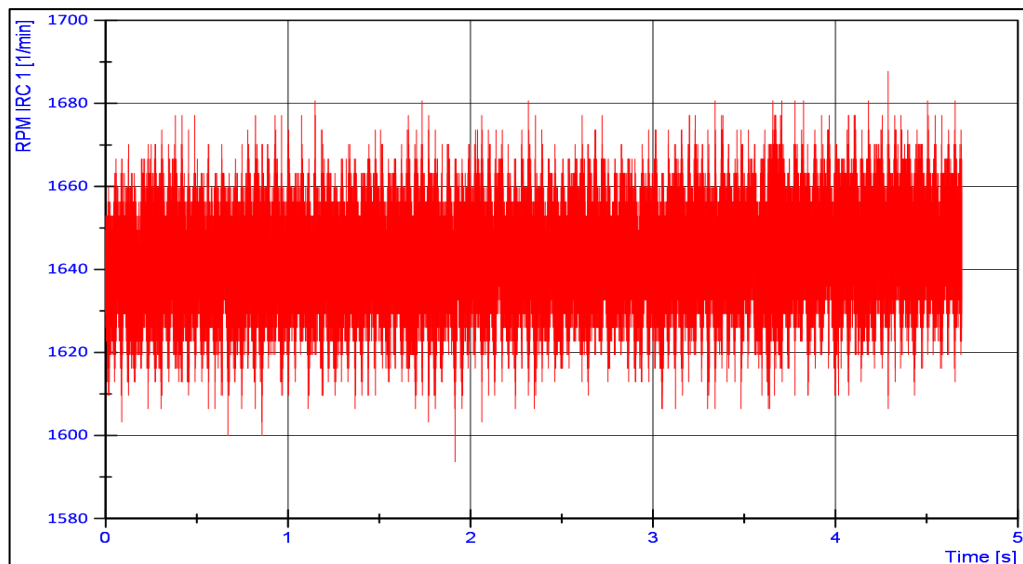


Figure 50 "RPM (vs) time" graph of input shaft of 1st gear

For the encoder 2, the graph is shown below –

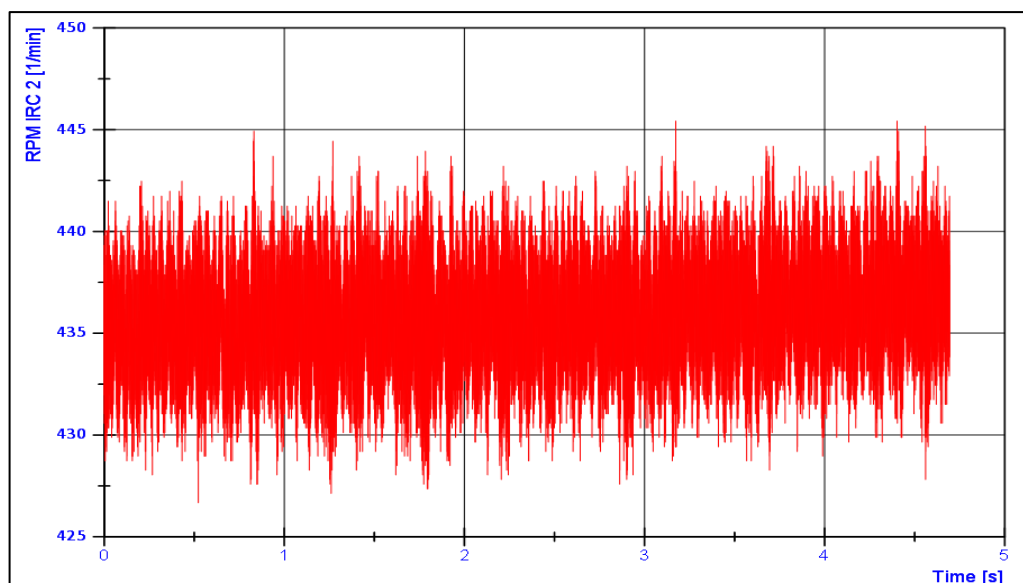


Figure 51 "RPM (vs) time" graph of output shaft of 2nd gear

As it can be seen, there is a lot of fluctuation from the actual speed due to noise from other components. The above graph has been taken for about 5 seconds and approximately 700,000 "RPM vs period of revolution" data points were obtained in the test file, for the gear with higher speed. To remove abnormalities in speed, firstly the FFT Analysis function of DIAdem is used to differentiate individual frequencies. The low frequency section of spectrum, which is the gear shaft eccentricity is filtered out. The image below shows the magnified frequency spectrum of the rotational speed of both shafts of gearbox at Gear 1.

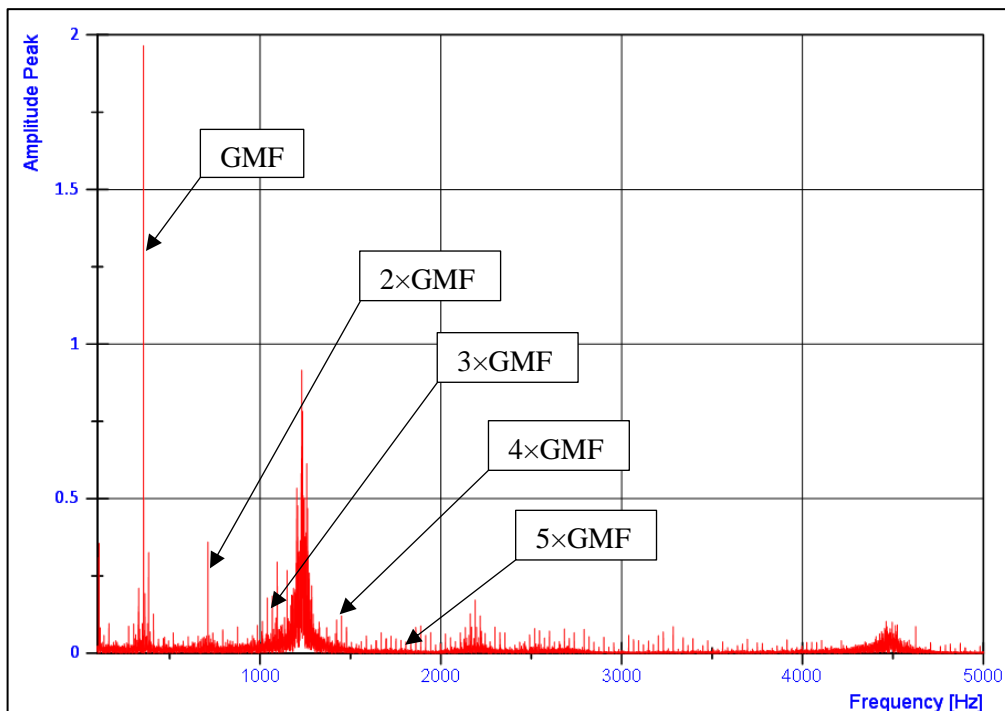


Figure 52 Frequency Spectrum of rotational speed of input shaft (vs) Amplitude – 1st gear

As it is evident, at higher frequencies till an extent, the amplitude diminishes, nevertheless it influences the actual rotational speed of the shafts. Similarly, the two graphs for the output gear of the gearbox are shown below. The noise at approximately 1230 Hz is constant for every speed and every gear, which might be caused due to electrical noise from nearby machinery.

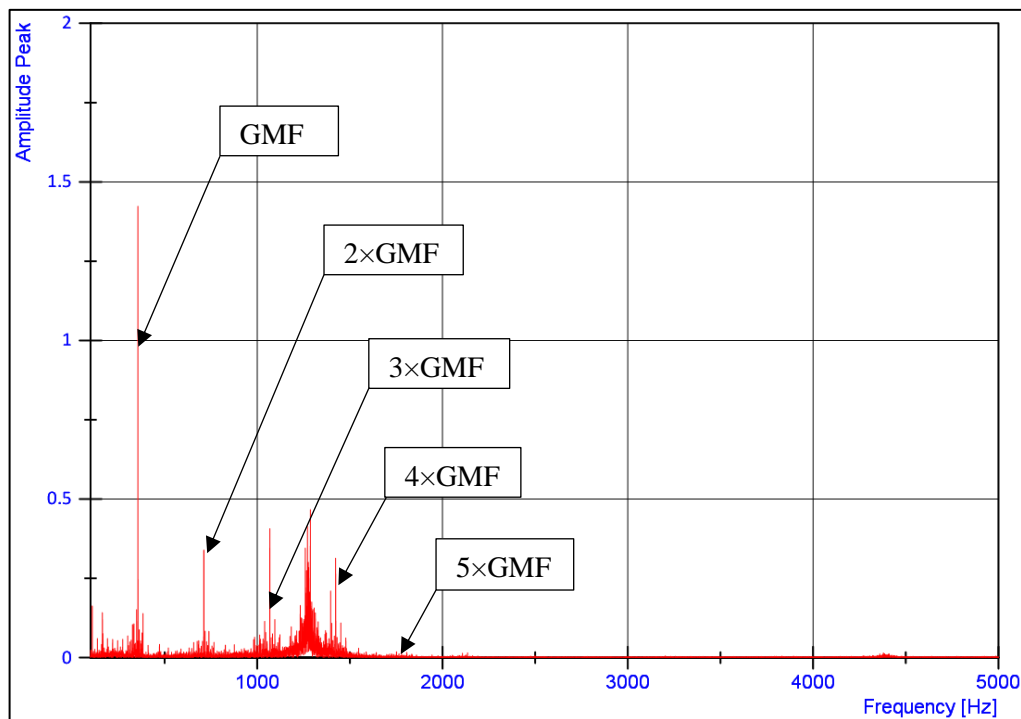


Figure 53 Frequency Spectrum of rotational speed of output shaft (vs) Amplitude – 1st gear



The above graphs show the noise associated with the signal and the side bands of the required frequencies in the spectrum. To reduce random noises in the spectrum, corresponding angle of rotation of every two revolutions is averaged. Every grating of 6000 pulse encoder is at an interval of 0.06° and hence the time value obtained from Counter output would be the time for every 0.06° . The time period data points' list is split at an interval of 12,000, which is 2 complete revolutions and entered as new columns of length 12,000. Now, the corresponding data points of a row on all columns i.e., 0.06° with 360.06° , 720.06° reading value and so on till the last column of the data set are averaged. This can either be done in DIAdem with VBS Script or in Microsoft Excel.

As a result of above averaging, a final set of 12,000 data points of time period of every 0.06° (or) from 0° to 720° angle of rotation is obtained, thus eliminating several random peaks and obtaining the average peaks of gear mesh frequency harmonics, which can be seen in the frequency spectrum. Now, the remaining sidebands of unwanted noise in the spectrum are eliminated with Inverse FFT procedure as explained in the previous sub-topic. The resulting values would give the speed fluctuations at gear mesh frequency harmonics in specified time interval.

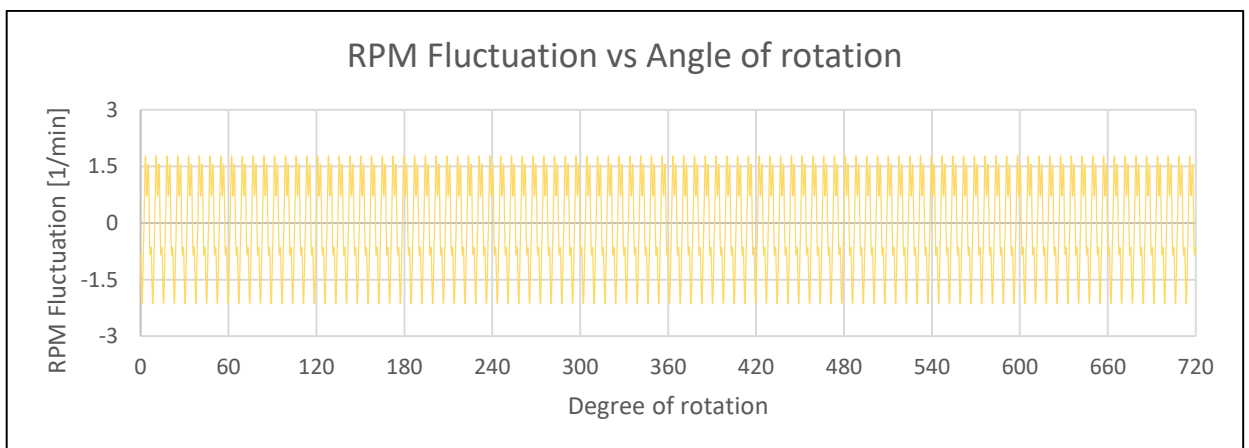


Figure 54 RPM Fluctuation of input shaft of 1st gear by gear mesh (vs) Angle of rotation

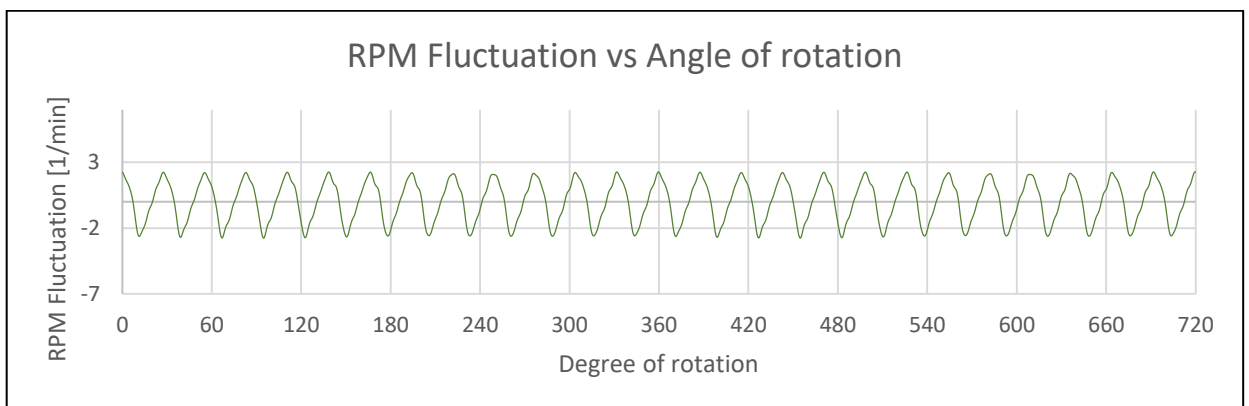


Figure 55 RPM Fluctuation of output shaft of 1st gear by gear mesh (vs) Angle of rotation



With each value of time and speed fluctuation the angle of fluctuation caused due to the gear mesh can be evaluated, which can be converted to radians and when calculated with the formula of Transmission Error, given in (2.1), would result in net deviation of the tooth profile, in micrometre (μm) at given speed and in this case, unloaded condition.

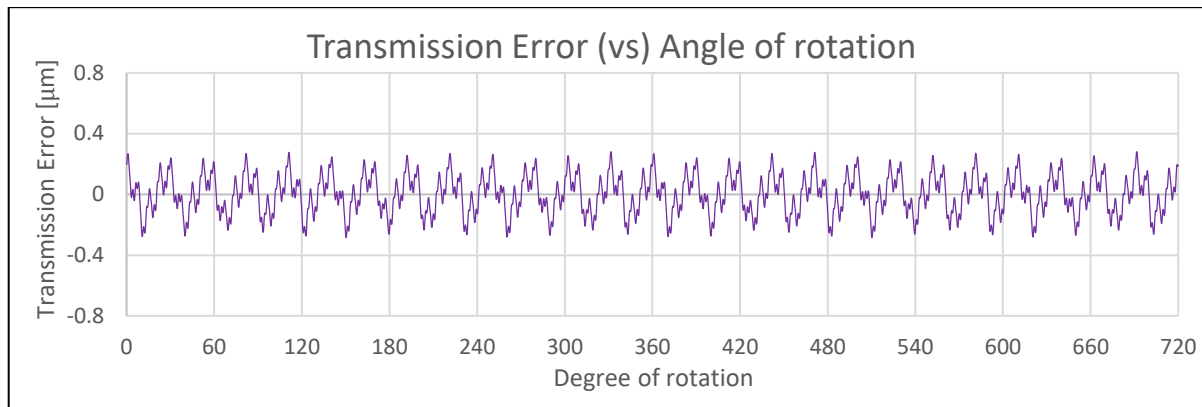


Figure 56 *Transmission Error (vs) Angle of rotation of 1st gear*

6.2.2 Measurement of Gear 2

The gearwheel parameters of the 2nd gear mesh is given in the table below –

Table B-6 *Parameters of 2nd gear*

GEAR 2 –		
Teeth – Input shaft	21	
Teeth – Output shaft	44	
Gear Ratio	2.095	
Module, m	1.63	
α	15°	
β	33°45'	
PCD of input gear [mm]	41.16807	
PCD of output gear [mm]	86.2569	
Running condition	Bench Speed	~200 rpm
	1 × GMF	614 Hz



Like the 1st gear, noise exists in rotational speed as seen in graphs below.

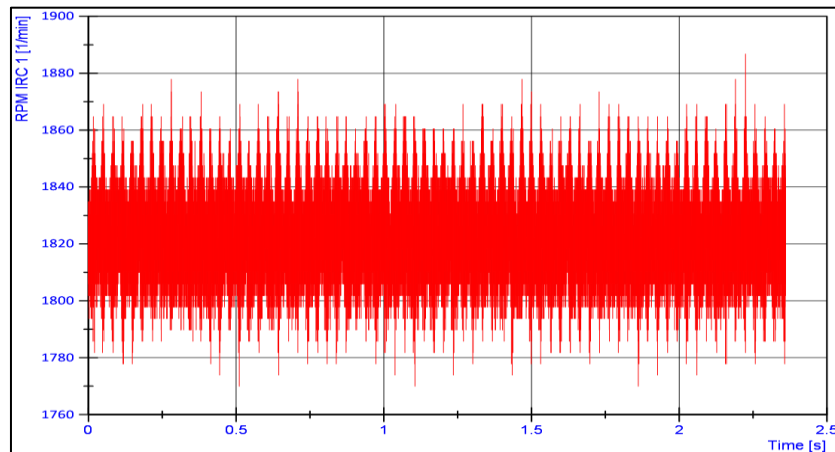


Figure 57 "RPM (vs) time" graph for input shaft of 2nd gear

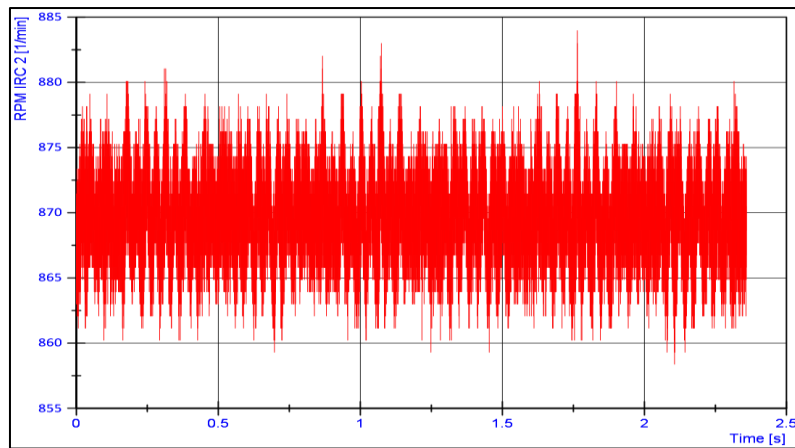


Figure 58 "RPM (vs) time" of output shaft of 2nd gear

The frequency spectra and their respective amplitudes of both encoders along with the graphs of RPM fluctuation influenced by gear mesh are given in "[Attachment 2.12](#)". The resulting transmission error graph is given below.

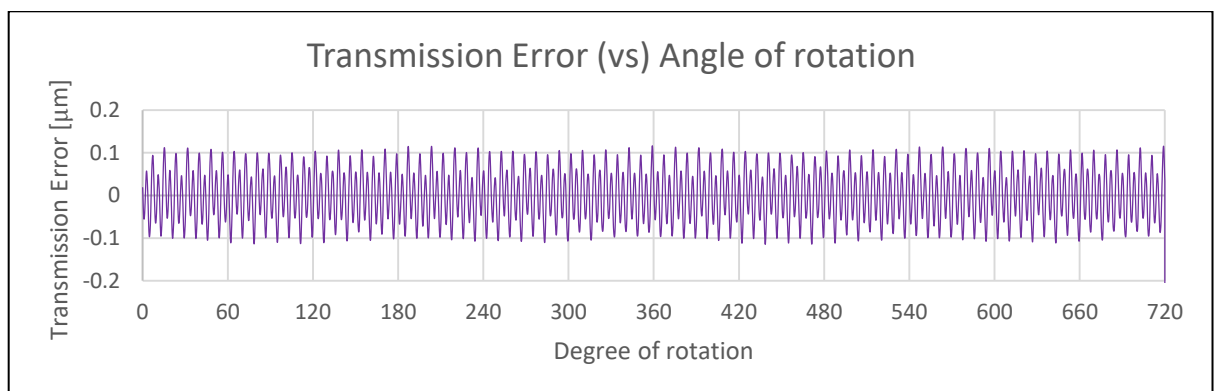


Figure 59 Transmission Error (vs) Angle of rotation of 2nd gear



6.2.3 Measurement of Gear 3

The gearwheel parameters of the 3rd gear mesh is given in the table below –

Table B-7 Parameters of 3rd gear

GEAR 3 –		
Teeth – Input shaft		32
Teeth – Output shaft		41
Gear ratio		1.28125
Module, m		1.5
α		15°
β		32°
PCD of input gear [mm]		56.6006
PCD of output gear [mm]		72.5195
Running condition	Bench Speed	~200 rpm
	1 × GMF	572 Hz

The graph shown below contains the speed of rotation of input and output gear shafts.

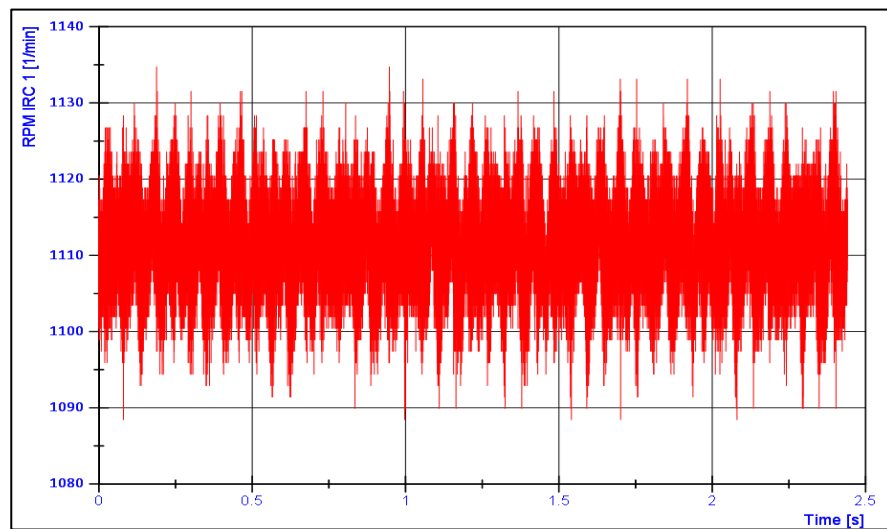


Figure 60 "RPM (vs) time" of input shaft of 3rd gear

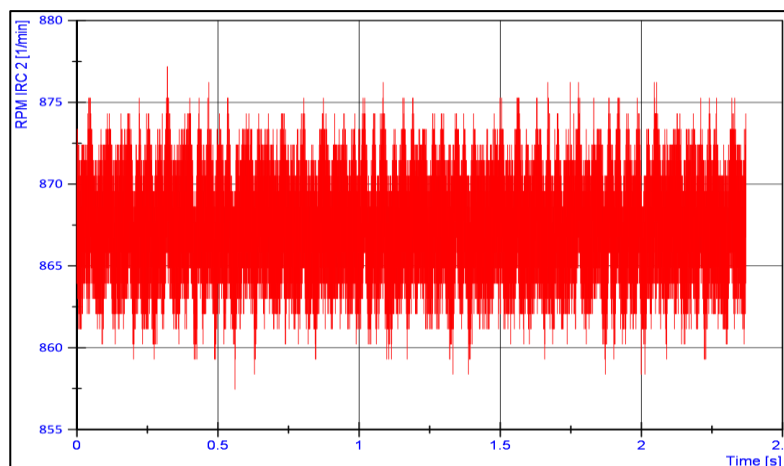


Figure 61 "RPM (vs) time" of output shaft of 3rd gear

The frequency spectrum of the signal and the filtered rotational speed is given in “Attachment 2.13”. Following the procedure mentioned for Gear 1, we obtain the transmission error at the given speed without load in diagram below.

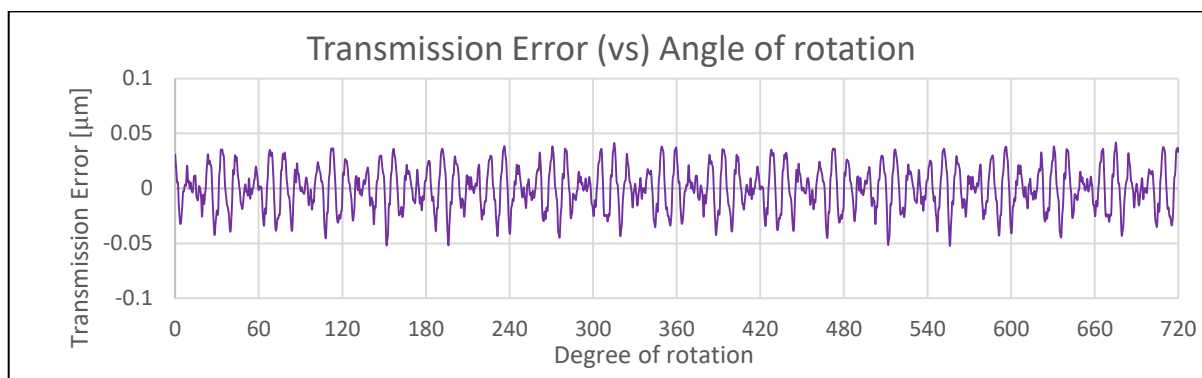


Figure 62 Transmission Error (vs) Angle of rotation of 3rd gear

6.2.4 Measurement of Gear 4

The gearwheel parameters of the 4th gear mesh is given in the table below –

Table B-8 Parameters of Gear 4

GEAR 4 –		
Teeth – Input shaft		41
Teeth – Output shaft		38
Gear ratio		0.927
Module, m		1.38
α		15°
β		33°
PCD of input gear [mm]		67.4639
PCD of output gear [mm]		62.5275
Running condition	Bench Speed	~200 rpm
	1 × GMF	530.5Hz



The graph shown below represents rotational speed vs time taken of both gears during measurement.

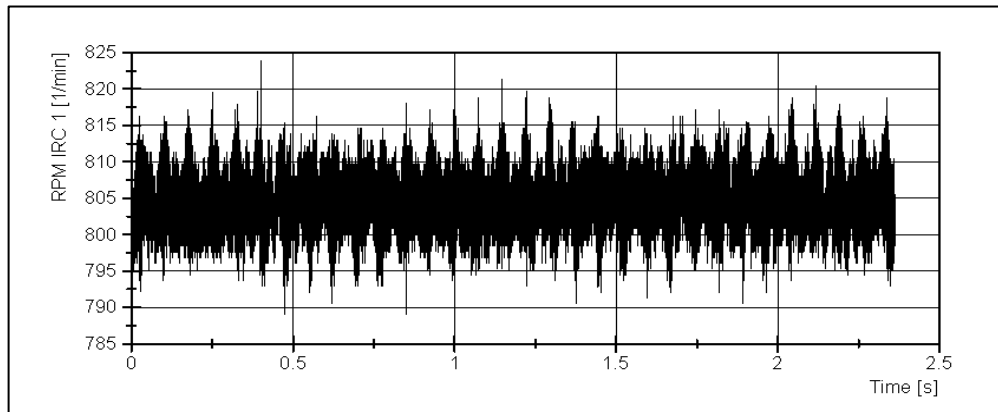


Figure 63 "RPM (vs) time" of input shaft of 4th gear

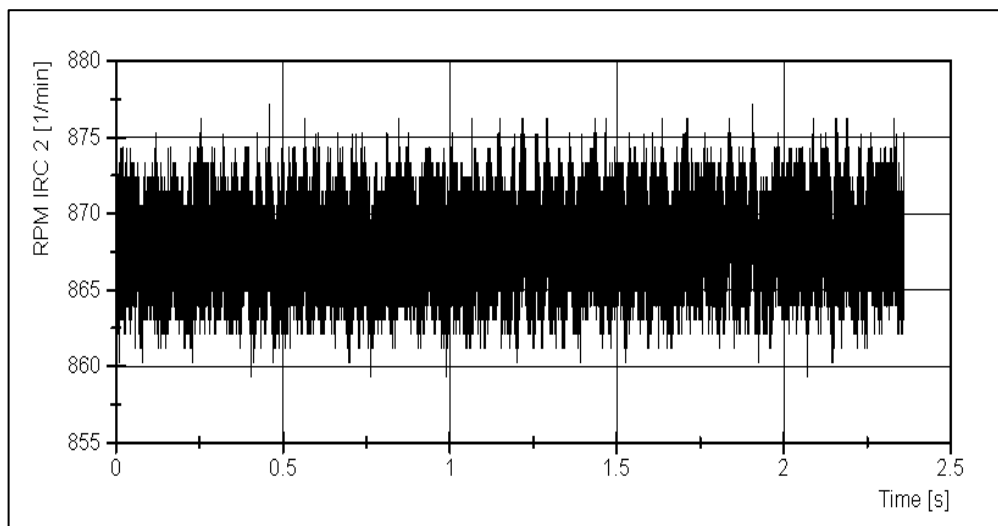


Figure 64 "RPM (vs) time" of output shaft of 4th gear

The frequency spectrum and the amplitude peaks of the signal are given in "[Attachment 2.14](#)". The resultant graph of Transmission Error (T.E) for the given gear at given speed is seen in the diagram below.

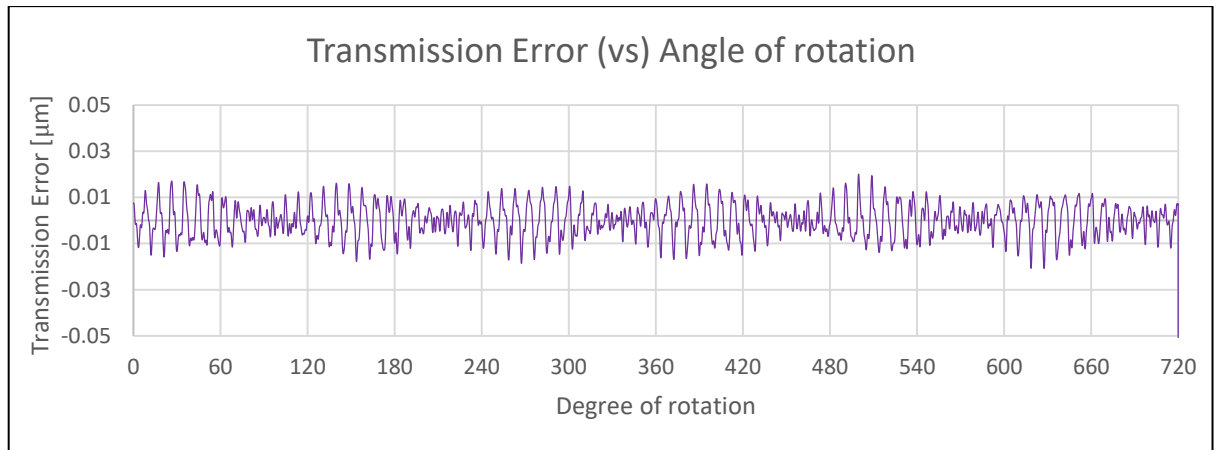


Figure 65 *Transmission Error (vs) Angle of rotation of 4th gear*

6.2.5 Measurement of Gear 5

The gearwheel parameters of the 5th gear mesh is given in the table below –

Table B-9 *Parameters of 5th gear*

GEAR 5 –		
Teeth – Input shaft		50
Teeth – Output shaft		37
Gear ratio		0.74
Module, m		1.25
α		14°30'
β		33°
PCD of input gear [mm]		74.5227
PCD of output gear [mm]		55.1468
Running condition	Bench Speed	~200 rpm
	1 × GMF	516.5 Hz

As seen in the previous gears, noise exists also for the 5th gear. The rotational speeds of both gears are shown in the diagram below.

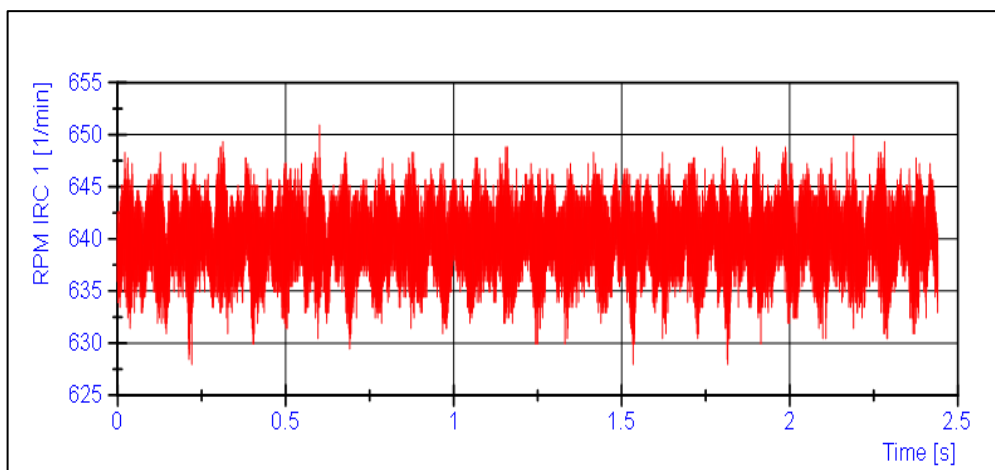


Figure 66 "RPM (vs) time" of input shaft of 5th gear

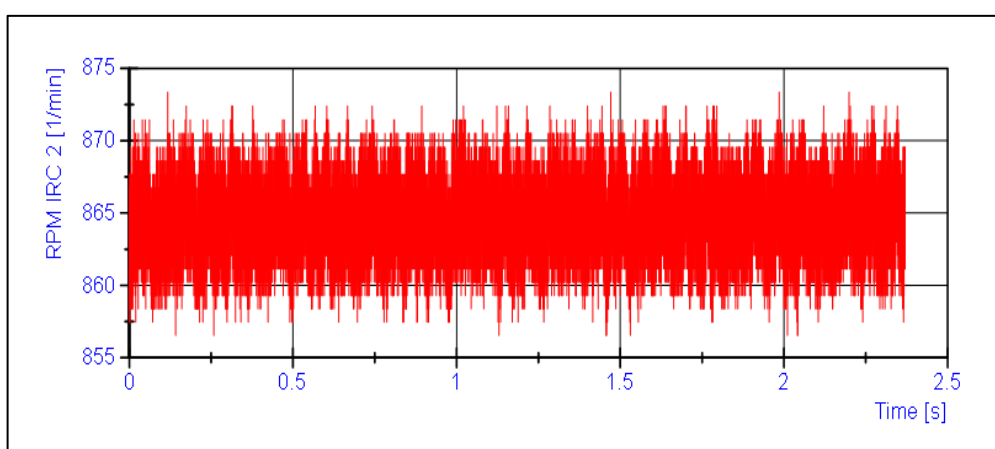


Figure 67 "RPM (vs) time" of output shaft of 5th gear

The frequency spectrum of the signals above and the respective amplitudes are given in "[Attachment 2.15](#)". The transmission error for the 5th gear at the given speed and without load is given below.

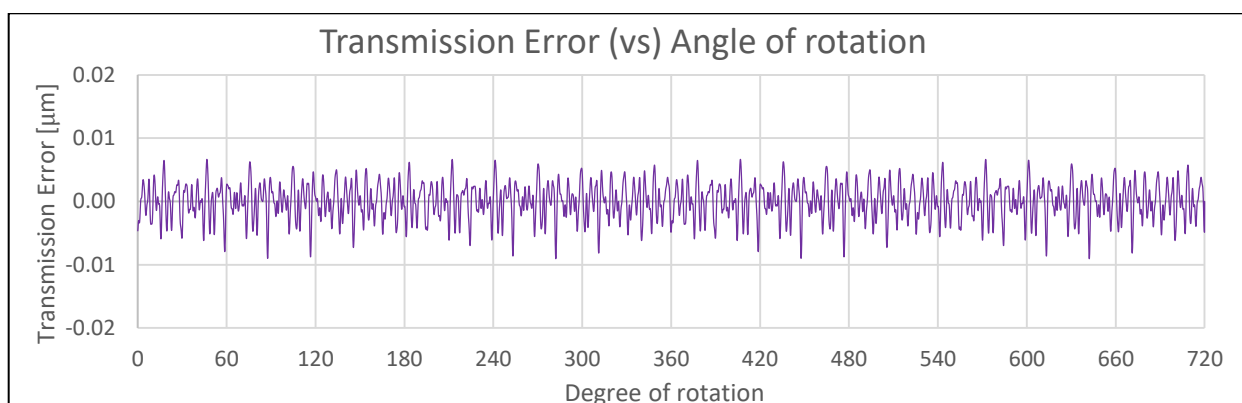


Figure 68 Transmission Error (vs) Angle of rotation of 5th gear



7. Inference and conclusion

For the above experimentation, given procedure has been followed –

- Recorded the time period of every pulse of given encoder - LARM KB 6000 PA, with NI LabVIEW.
- Experiment has been conducted at low speed of test bed due to limited output frequency of the encoders.
- From the time period, instantaneous RPM of the gear shaft has been obtained.
- Unwanted random noise has been eliminated and gear mesh frequency fluctuations have been isolated and processed.
- Finally obtained the Transmission Error of the given gearbox at given speed and no-load condition.

Following points have been observed from the results and are documented below –

- The averaged transmission error has been found out for two nominal revolutions.
- The amplitude of transmission error decreases as the gear ratio decreases as the torque multiplication is reduced because of similar number of tooth on both shafts.
- Amplitude of transmission error in μm of all gear pairs is low also because of low speed and unloaded condition of gearbox.
- There might be few errors with the amplitude of peaks since
 - Accuracy of the given encoders are unknown
 - Propagation losses might occur in the cable which are unknown
 - Rise-fall time of Counter Input of NI 9401 module is up to 500 ns.

8. Future work and prospects

If gears are theoretically of infinite stiffness, this error would not exist. But, since gears bend due to high loads, the output speed and torque differ from ideal value. Transmission Error of a vehicle must be minimized to reduce the noise of gearbox, especially at high loads an acceleration, to provide a smoother and quieter performance. And so, to improvise a gearbox in this regard, the future work can be focused on –

- Different conditions of load (or) torque on gear shafts.
- Experimentation at various constant speeds to study the behaviour of transmission error.
- Determining the error in gear shafts with different types of gear profiles and defects, to know the measure of damage and impact on life of gears.
- Determining the transmission error profile during run-up and slowing down of gearbox with a 3-dimensional plot to study its change and trend.
- Repeating tests with a known encoder configuration and at higher frequencies.



C. ACTUATION OF DISC BRAKE ON TEST BENCH

1. Introduction

An IC engine powered vehicle releases various exhaust gases to the atmosphere where most of them are considerable in sizes and hence human lung cells have the capacity to filter them, preventing potential risk factors. With the evolution of greener cars and emission control these are however reduced, but till date one of the consistent pollution factors is the brake emission from the vehicles, which constitute for about 50% of PM2.5 and PM10 emissions of vehicles. ^[31]

The actuation of disc brake causes the frictional surfaces of the pad to encounter metal linings of disc brake which releases particles in a bandwidth of 6nm - 10 μ m ^[31] into atmosphere which are inhaled by human beings. These cannot be filtered by the lung cells which have a capacity of 27nm, and hence they enter the bloodstream directly. This poses a serious long-term threat and hence studies are being made to control these emissions.

The faculty at Juliska has a test bench to currently study the frictional co-efficient of the mounted disc brake. The proposal has been to design a dilution tunnel to capture these wear emission particles with a filter and study them later. Hence, to observe both the frictional factor and emission rate at different braking conditions, my work is to propose an idea for automatic variable actuation of the braking system, which currently works on single constant value at a time and needs to be manually adjusted for different actuation forces. The experimental setup and consequent proposed idea is discussed in the sections below.

2. Current experimental setup

The current experimental setup to actuate the disc brake consists of the following components –

- Hydraulic pusher or motor
- Lever
- Weight
- Fluid piping
- Pressure feedback sensor
- NI 9201 and NI 9472

The lever with the weight is kept in a tensioned state at rest by the hydraulic pusher and linkage mechanism. The hydraulic pusher can actuate a maximum force of 800N which holds the weight in position above. To actuate the brake, the pusher extends outwards, which slackens the belt and the weight acts on the linkage to push the fluid into hydraulic circuit and clamp the brake. To release the brake, the pusher rod gets back in and consequently pushes the lever upwards, thus releasing the pressure.

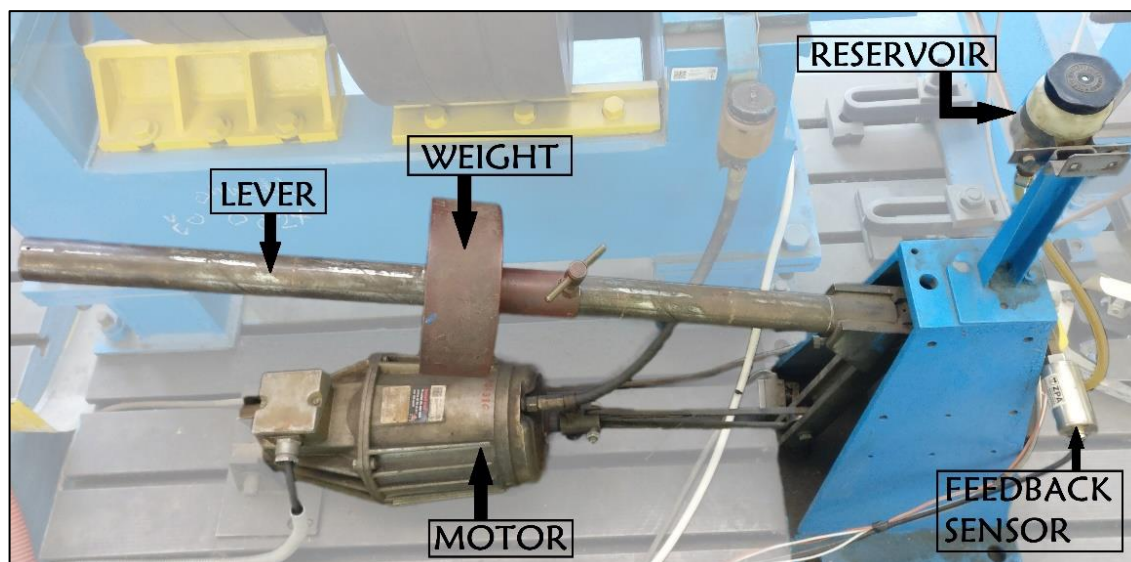


Figure 69 *Current experimental setup for disc brake actuation*

2.1 Hydraulic pusher

The installed hydraulic pusher from VEM Group, “**VEB Elektromotorenwerk Oschersleben DDR**” has a constant stroke length and permissible force, to push and pull the rubber belt which accordingly moves the lever and the weights attached to it. The technical specifications of the hydraulic pusher are given in “[Attachment 3.1](#)”.



Figure 70 *Hydraulic pusher for brake retraction*

2.2 Actuating lever

The actuating lever as shown in Figure. 69, consists of a hollow shaft with a heavy disk attached to it at a distance from the end which affects the force of actuation. The gravitational force of the weight acts on the fluid which presses the clamps on the disc brake. This mechanism is controlled by the motor, mentioned in the section above.

The current length of the shaft used in our laboratory at Juliska is of 90 cm, with the weight of 13.5 kg balanced on it. The current setup provides 41.5 cm distance from the free end, which provides approx., 5MPa pressure in the hydraulic circuit of the brake.



2.3 Pressure feedback sensor



Figure 71 Location of pressure sensor for hydraulic circuit

The sensor by ZPA, “UNIPRES 81” is used to obtain the pressure of the hydraulic circuit which changes with actuation of brake. The specifications of the sensor are given in “[Attachment 3.2](#)”. The sensor is powered by 24V source and the feedback voltage is sent to the measuring card NI 9201.

3. Proposed solution for actuation

As seen in the sections above, the current setup at Juliska allows only for the constant actuation of brake at a time. Hence, to get a variable actuation, a feedback loop must be achieved with a controller and a suitable linear actuator.

To vary it at different rates of deceleration or actuation forces, two probable methods can be used – variable stroke length and variable velocity with a high rated force.

Table C-1 Current working conditions of actuation system

SPECIFICATION		
SETUP	Current	Maximum
Shaft length [cm]	45.5	90
Weight [kg]	13.5	13.5
Pipe diameter [m]	0.014	0.014
Force on circuit [N]	~820	~1620
Pressure in circuit [MPa]	5.4	10.5
Braking time for 1000 rpm [s]	4	< 4
Rise time of actuation [s]	~ 2	~1

Hence, according to the table above, an actuator is needed which can provide a push force working till the limit of feedback sensor, which is 16MPa within a short period of time. Hence the basic requirements for selection of actuator are as follows –

- Easily programmable
- Feedback control system
- Easy installation
- Required thrust force and linear speed
- Required stroke length



Meeting the above requirements is a manufacturer – “**Parker Hannifin Corporation**” which produces linear actuators with inline and parallel mount motors for actuation. An actuator which can comfortably produce the maximum force for the current setup is needed. According to the catalogue of ETH Series of Parker actuators ^[32], the chosen model is **ETH050 M10** with inline motor, which can produce up to a force of 7000 N. The basic parameters of the actuator are given in the table below –

Table C-2 *Linear Actuator specification*

SPECIFICATION – ETH050 M10 series	
Parameters	Value
Stroke length [mm]	50
Max., speed [mm/s]	667
Max., acceleration [m/s ²]	8
Max., thrust force [N]	7000
Input voltage [V]	230V AC
Input current to drive [A]	0.2 A

Now that the basics are established, to meet our necessities a few more specifications are also to be considered such as the mounting method, actuator rod end type, desired stroke, motor used, servo drive and so on. The tabulation for ordering such required factors are given in “[Attachment 3.3](#)”.

As a side mount for the actuator has been selected, the stand has to be designed to support it accordingly. Also, the space constraints and mounting position on the test bed are to be considered. The proposed solution of design is shown below. The technical drawing of the stand is given in “[Attachment 3.4](#)”.

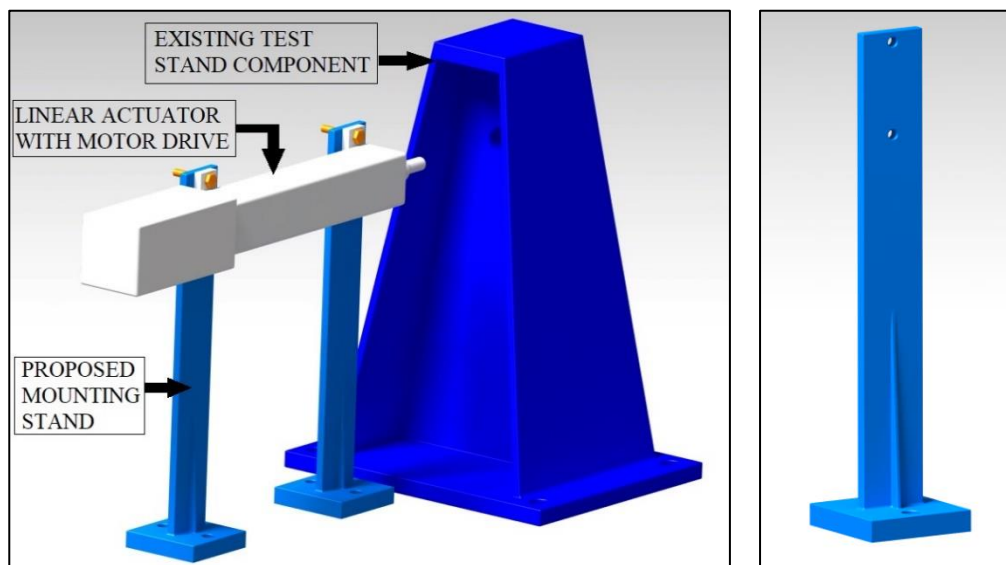


Figure 72 *Assembly of actuator w.r.t existing stand (left), proposed actuator mount (right)*



The below diagram shows the area where the proposed linear actuator would actuate combine with the existing stand and actuate the hydraulic circuit. The exact design of the connection between the existing test stand and the actuator i.e., the mechanical coupling with the piston of the hydraulic circuit (part in red box) could not be designed since the technical drawings of the test stand were not available at the laboratory.

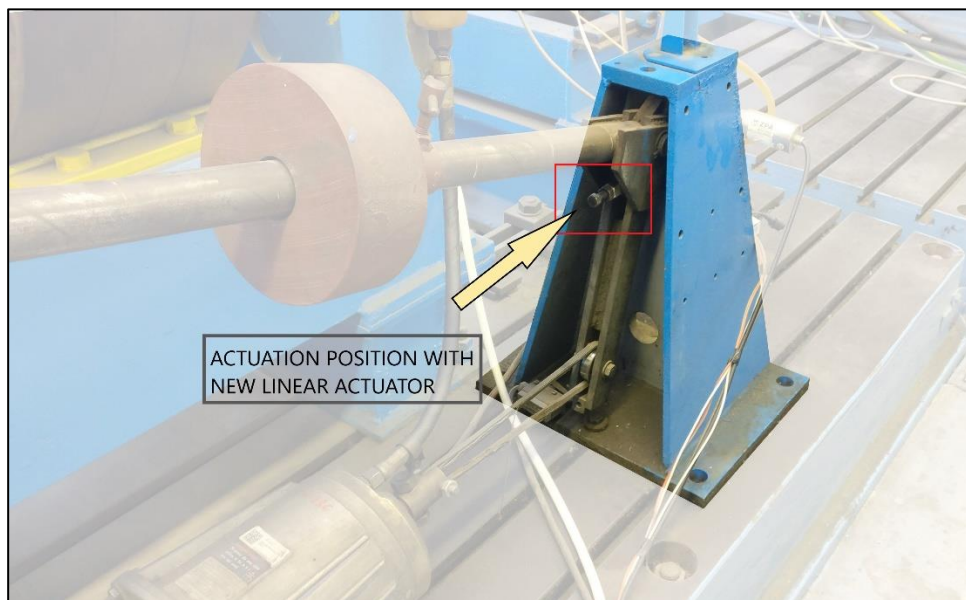


Figure 73 Proposed position of mount and connection of actuator

The level of stand has been kept in line with that of the existing part. The end rod is connected to existing stand's circuit through a mechanical coupling. As the actuator is actuated, its end rod travels back and forth which pushes the fluid in and out of the reservoir to pressurize the caliper against the brake material. The stroke length desired has been given as 100 mm, since the allowance for "Safety Travel" according to the manufacturer which is required to slow down the cylinder in the final stages is given as 10mm for the required velocity of 400 mm/s.

The high velocity is satisfactory for current application. To fulfil the need of variable deceleration of test bench and variable actuation force, variable stroke length of the actuator is fulfilled with the drive/ controller associated with it. Related programming and installation can be done in the future by the next student who undertakes this assignment in detail.

4. Alternate solution proposal for actuation

The CVUT laboratory at Juliska currently possesses a test stand to measure the elastokinematics of a vehicle, in which a hydraulic aggregate has been implemented for actuating the piston/ hydraulic cylinders to apply load on wheel of the vehicle. Hence these aggregates can apply high loads to push and pull the resting platform of the wheel which can be used for brake actuation purpose where an actuating piston which can move the fluid along the line to produce clamp force to the brakes can be used. Details of the aggregate and its adaptation to current usage are given in the following section.



4.1 Hydraulic aggregate

The hydraulic aggregate currently used in the test bench is from the manufacturer “**Naradi Vrchlabi**”, of the model “**PA2-40-1**”. The technical specification of the aggregate was not available from the internet and hence the available preliminary details from the imprint on setup has been written. The aggregate pushes the hydraulic cylinder model – “**HM 1.2 63/32/125 121A111**” from the local Czech manufacturer “**Elotechnik**”^[37]. The specification of the setup is given in the table below –

Table C-3 *Specification of hydraulic aggregate and piston*

	PARAMETER	VALUE
Hydraulic aggregate	Input Voltage [V]	380
	Current [A]	2
	Frequency [Hz]	50
	Power [kW]	0.75
	Maximum allowable pressure [mPa]	4
Hydraulic cylinder/ piston	Maximum force from aggregate [N]	9200
	Nominal pressure [mPa]	16
	Max., working speed [ms ⁻¹]	0.5

As seen in the table above, the piston or hydraulic cylinder that is currently used has a maximum speed of 0.5 ms⁻¹, which is as fast as the linear actuator, can provide high amount of force to the test bench hydraulic circuit and can be used for actuation. If the rate of pressure change of aggregate can be varied to give high velocities within the limit, this option can be readily used which is much more budget friendly than buying the actuator.

The proposed mounting position of the new setup with the existing one is shown in the figure below. It is mounted at the same position as that of the actuator, and the real-time position can be seen from the previous chapter. The technical drawing of the mounting stand is given in “[Attachment 3.5](#)” for future fabrication and reference.

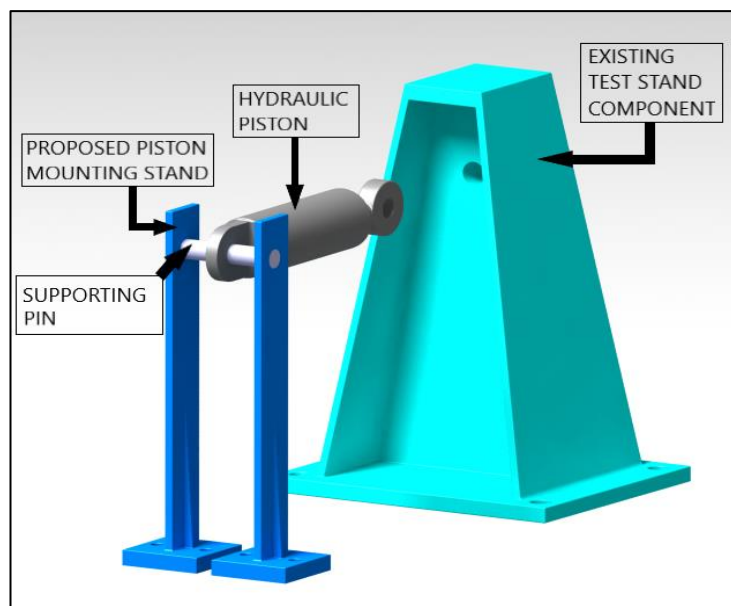


Figure 74 Proposed mount with hydraulic piston

In the figure above, one end of the hydraulic piston rests on a supporting metal shaft/pin, which is fitted into the test stand. The movable end is attached by a coupling with the existing test stand, but the exact diagram of this mechanism could not be drawn since the exact design of the existing components is not available. This can be designed when the stand is dismantled, and each part can be analysed before the detailed work on this test bench. The hydraulic cylinder is mounted in level with the piston of the existing test bench and when there is a rigid coupling between them, will prevent the piston from sway or any other non-intended motion from its original position, hence resulting only in linear travel. Hence to summarize, utilization of hydraulic aggregate for disc brake actuation is a viable option when the necessary conditions of mounting, space constraint and pressure variation of aggregate are met.

5. Conclusion

The proposed motor, its specification and corresponding design for the test stand has been given in this document. When compared with the current test stand, lot of manual effort and error percentage can be reduced while shifting weight on the lever, to actuate different forces acting on disc brakes.

A Czech manufacturer for the actuator could not be found at the point of submission of this work, but the next student can try to obtain one if any new supplier or manufacturer is available during his experimentation period.

The hydraulic aggregate can provide a high force to the hydraulic piston which can be utilized to our advantage. The future student working on the test bench should design the coupling between the cylinder and brake circuit and can modify the proposed design to his current spacing options, due to addition of wind-tunnel for capturing the brake emission particles.



D. LIST OF FIGURES

Figure 1 Irregular body with COG.....	- 9 -
Figure 2 COG through moments method.....	- 10 -
Figure 3 COG of a 3D object.....	- 11 -
Figure 4 Computing longitudinal COG position for a car.....	- 11 -
Figure 5 Computing the height of COG of a car.....	- 12 -
Figure 6 Co-ordinate system on a 3D plane.....	- 13 -
Figure 7 Translation of axes to a new co-ordinate system.....	- 15 -
Figure 8 Experimental setup for wheel moment of inertia.....	- 17 -
Figure 9 Experimental setup for light sensing.....	- 18 -
Figure 10 DAQ Card 6062E.....	- 19 -
Figure 11 NI CB - 68LP (left) and SHC68-68-EP (right).....	- 19 -
Figure 12 Photo gate with emitter and receiver.....	- 20 -
Figure 13 Schematic of the light sensing connection with old PCB ^[10]	- 21 -
Figure 14 Potentiometer diagram and circuit connection ^[11]	- 22 -
Figure 15 Hall Effect angular sensor IC from Allegro Microsystems ^[12]	- 22 -
Figure 16 Two axes inclinometer IC from Murata ^[13]	- 22 -
Figure 17 Mounting of sensor with wheel.....	- 24 -
Figure 18 Sensor mount position view with the disk.....	- 24 -
Figure 19 Scheme of sensor connection ^[19]	- 25 -
Figure 20 STS-003-2-180-U MEMS Inclinometer from SITALL Sensors ^[19]	- 26 -
Figure 21 The sensor mounting plate of Stainless Steel.....	- 26 -
Figure 22 Scheme of old PCB electrical connection.....	- 27 -
Figure 23 Faulty connection of new customized PCB.....	- 28 -
Figure 24 Scheme of new corrected customized PCB.....	- 29 -
Figure 25 Front Panel of LabVIEW program.....	- 30 -
Figure 26 Selected drum brake.....	- 31 -
Figure 27 Mounted drum brake housing on Cardan joint.....	- 31 -
Figure 28 Front panel displaying principle moments of inertia.....	- 32 -
Figure 29 Inertia tensor for angle α	- 33 -
Figure 30 Moment of inertia with CATIA V5, corresponding to angle “ α ”.....	- 33 -
Figure 31 Measurement result from LabVIEW.....	- 34 -
Figure 32 Results from CATIA V5 for the angle β measurement.....	- 34 -
Figure 33 Test rig implemented with encoders.....	- 37 -
Figure 34 Curves at different sampling rates ^[35]	- 38 -
Figure 35 Anti-aliasing or Low-Pass Filter.....	- 39 -
Figure 36 Transformation of sinusoidal signals in spectrum ^[36]	- 39 -
Figure 37 Example of Comb Filter in frequency spectrum ^[34]	- 41 -
Figure 38 Entire test bench used for experimentation.....	- 42 -
Figure 39 Installed gearbox with the test bench.....	- 42 -
Figure 40 Flowchart of procedure followed during acquisition.....	- 43 -
Figure 41 Working of data acquisition from NI DAQ device.....	- 43 -
Figure 42 Asynchronous motor used.....	- 44 -



Figure 43 Simple sketch to show the location of encoders.....	- 44 -
Figure 44 Electrical angle of impulse from encoder.....	- 45 -
Figure 45 Mounted position of encoder on gearbox.....	- 46 -
Figure 46 ADAM terminal board.....	- 46 -
Figure 47 NI 9401 module implemented.....	- 47 -
Figure 48 NI 9174 Chassis to dock NI 9401 module.....	- 47 -
Figure 49 "RPM (vs) time" graph of input shaft of 1 st gear.....	- 48 -
Figure 50 "RPM (vs) time" graph of input shaft of 1 st gear.....	- 51 -
Figure 51 "RPM (vs) time" graph of output shaft of 2 nd gear.....	- 51 -
Figure 52 Frequency Spectrum of rotational speed of input shaft (vs) Amplitude – 1 st gear.....	- 52 -
Figure 53 Frequency Spectrum of rotational speed of output shaft (vs) Amplitude – 1 st gear.....	- 52 -
Figure 54 RPM Fluctuation of input shaft of 1 st gear by gear mesh (vs) Angle of rotation.....	- 53 -
Figure 55 RPM Fluctuation of output shaft of 1 st gear by gear mesh (vs) Angle of rotation.....	- 53 -
Figure 56 Transmission Error (vs) Angle of rotation of 1 st gear.....	- 54 -
Figure 57 "RPM (vs) time" graph for input shaft of 2 nd gear.....	- 55 -
Figure 58 "RPM (vs) time" of output shaft of 2 nd gear.....	- 55 -
Figure 59 Transmission Error (vs) Angle of rotation of 2 nd gear.....	- 55 -
Figure 60 "RPM (vs) time" of input shaft of 3 rd gear.....	- 56 -
Figure 61 "RPM (vs) time" of output shaft of 3 rd gear.....	- 57 -
Figure 62 Transmission Error (vs) Angle of rotation of 3 rd gear.....	- 57 -
Figure 63 "RPM (vs) time" of input shaft of 4 th gear.....	- 58 -
Figure 64 "RPM (vs) time" of output shaft of 4 th gear.....	- 58 -
Figure 65 Transmission Error (vs) Angle of rotation of 4 th gear.....	- 59 -
Figure 66 "RPM (vs) time" of input shaft of 5 th gear.....	- 60 -
Figure 67 "RPM (vs) time" of output shaft of 5 th gear.....	- 60 -
Figure 68 Transmission Error (vs) Angle of rotation of 5 th gear.....	- 60 -
Figure 69 Current experimental setup for disc brake actuation.....	- 63 -
Figure 70 Hydraulic pusher for brake retraction.....	- 63 -
Figure 71 Location of pressure sensor for hydraulic circuit.....	- 64 -
Figure 72 Assembly of actuator w.r.t existing stand (left), proposed actuator mount (right).....	- 65 -
Figure 73 Proposed position of mount and connection of actuator.....	- 66 -
Figure 74 Proposed mount with hydraulic piston.....	- 68 -
Figure 75 Installation scheme of sensors with old NI terminal board.....	- 75 -
Figure 76 New electrical connection scheme with customized PCB.....	- 76 -
Figure 77 Task configuration in NI MAX software.....	- 83 -
Figure 78 VBA script for channel split in DIAdem.....	- 85 -
Figure 79 Sensor mount technical drawing.....	- 88 -
Figure 80 LabVIEW program for angle acquisition.....	- 89 -
Figure 81 Math Script for moment of inertia tensor calculation.....	- 90 -
Figure 82 Sub-section of program for configuring terminals.....	- 94 -
Figure 83 Reading and display of acquired signals.....	- 95 -
Figure 84 Saving the acquired data.....	- 97 -
Figure 85 Scheme of terminal connection with ADAM board.....	- 98 -
Figure 86 Frequency spectrum of rotational speed of input shaft (vs) Amplitude– 2 nd gear.....	- 99 -



Figure 87 Frequency spectrum of rotational speed of output shaft (vs) Amplitude– 2nd gear - 100 -
Figure 88 RPM Fluctuation of input shaft of 2nd gear by gear mesh (vs) Angle of rotation..... - 101 -
Figure 89 RPM Fluctuation of output shaft of 2nd gear by gear mesh (vs) Angle of rotation - 101 -
Figure 90 Frequency Spectrum of rotational speed of input shaft (vs) Amplitude – 3rd gear - 102 -
Figure 91 Frequency Spectrum of rotational speed of output shaft (vs) Amplitude – 3rd gear - 103 -
Figure 92 RPM Fluctuation of input shaft of 3rd gear by gear mesh (vs) Angle of rotation - 104 -
Figure 93 RPM Fluctuation of output shaft of 3rd gear by gear mesh (vs) Angle of rotation - 104 -
Figure 94 Frequency spectrum of rotational speed of input shaft (vs) Amplitude – 4th gear..... - 105 -
Figure 95 Frequency spectrum of rotational speed of output shaft (vs) Amplitude – 4th gear..... - 106 -
Figure 96 RPM Fluctuation of input shaft of 4th gear by gear mesh (vs) Angle of rotation - 107 -
Figure 97 RPM Fluctuation of output shaft of 4th gear by gear mesh (vs) Angle of rotation - 107 -
Figure 98 Frequency spectrum of rotational speed of input shaft (vs) Amplitude – 5th gear..... - 108 -
Figure 99 Frequency spectrum of rotational speed of output shaft (vs) Amplitude – 5th gear..... - 109 -
Figure 100 RPM Fluctuation of input shaft of 5th gear by gear mesh (vs) Angle of rotation - 110 -
Figure 101 RPM Fluctuation of output shaft of 5th gear by gear mesh (vs) Angle of rotation - 110 -
Figure 102 Actuator stand design and technical drawing - 112 -
Figure 103 Proposed stand for hydraulic cylinder mounting - 113 -



E. LIST OF TABLES

Table A-1 Specification of NI CB - 68LP	- 19 -
Table A-2 Parameters of Photo gate used	- 20 -
Table A-3 Comparison of advantages and disadvantages between sensors.....	- 22 -
Table A-4 Final criteria for selection of sensor	- 23 -
Table A-5 Specification of selected inclinometer from Sitall.....	- 24 -
Table A-6 4-wire configuration	- 25 -
Table A-7 LabVIEW parameters configuration.....	- 30 -
Table B-1 Signal spectrum usage.....	- 40 -
Table B-2 Parameters of the tested gearbox	- 45 -
Table B-3 Definition of each term of encoder	- 45 -
Table B-4 Parameters of FFT Analysis.....	- 49 -
Table B-5 1 st Gear mesh parameters	- 50 -
Table B-6 Parameters of 2nd gear.....	- 54 -
Table B-7 Parameters of 3 rd gear	- 56 -
Table B-8 Parameters of Gear 4.....	- 57 -
Table B-9 Parameters of 5th gear	- 59 -
Table C-1 Current working conditions of actuation system	- 64 -
Table C-2 Linear Actuator specification.....	- 65 -
Table C-3 Specification of hydraulic aggregate and piston	- 67 -
Table G-1 Specification of DAQCard 6062E.....	- 87 -
Table G-2 Preferred FFT window type for acquired signals.	- 91 -
Table G-3 Main specification of the ABB industrial drive used	- 91 -
Table G-4 The main working parameters of motor	- 92 -
Table G-5 Electrical parameters of LARM Incremental Rotary Encoder	- 92 -
Table G-6 Wiring specification of encoder.....	- 92 -
Table G-7 Specification of NI 9401 DAQ device.....	- 93 -
Table G-8 Working parameter of the NI cDAQ 9174 chassis	- 93 -
Table G-9 Parameters of hydraulic pusher	- 110 -
Table G-10 Specification of UNIPRES pressure sensor.....	- 111 -
Table G-11 Tabulation for ordering required actuator.....	- 111 -



F. LIST OF ANNEXURES

- | | |
|---------|--|
| Annex 1 | Installation manual for the sensors with the DAQ Card 6062E and PCBs |
| Annex 2 | Instruction for moment of inertia calculation and obtained results |
| Annex 3 | Instruction to create the task for Counter Input in NI MAX application |
| Annex 4 | Instruction manual for data analysis in NI DIAdem |



Annex 1 – Instruction to connect the sensors with DAQCard 6062E and PCBs

Hereby written is the installation manual for dual axis inclinometer with the DAQCard through old NI terminal board and the new customized manufactured PCB.

- With terminal board NI CB-68 LP –
 - 1) The electrical connections are turned off in the power supply. Emitter and receiver wires are inserted in the pins 12 and 14 in the pin board, with the GND (blue) wire in Pin 12 and +5V or supply voltage (red) in Pin 14.
 - 2) Similarly, the receiver end's red wire is inserted into the Pin 33 and the black wire in Pin 66. Insert the 82k Ω resistor wire ends into the board at Pin 33 and 66.
 - 3) Wire the positive and negative connections of the sensor to the red and black junctions of 12 VDC of the supply. Another wire from the ground of power supply is connected to an Analog Input Ground (AI GND) of the PCB.
 - 4) The other two junctions, for X and Y axes are connected to the Analog Input terminals of the board, to the pins 25 and 57, respectively.
 - 5) The sensor is mounted by a bolt and nut through the centre of the wheel with the help of a thin plate on either side to support the sensor to be steady.
 - 6) Turn on the electrical connection of the power supply and proceed with the measurement of the moment of inertia of the body.

The electrical connection scheme for the old connection with NI terminal board CB-68 LP is given in the next page for future reference.

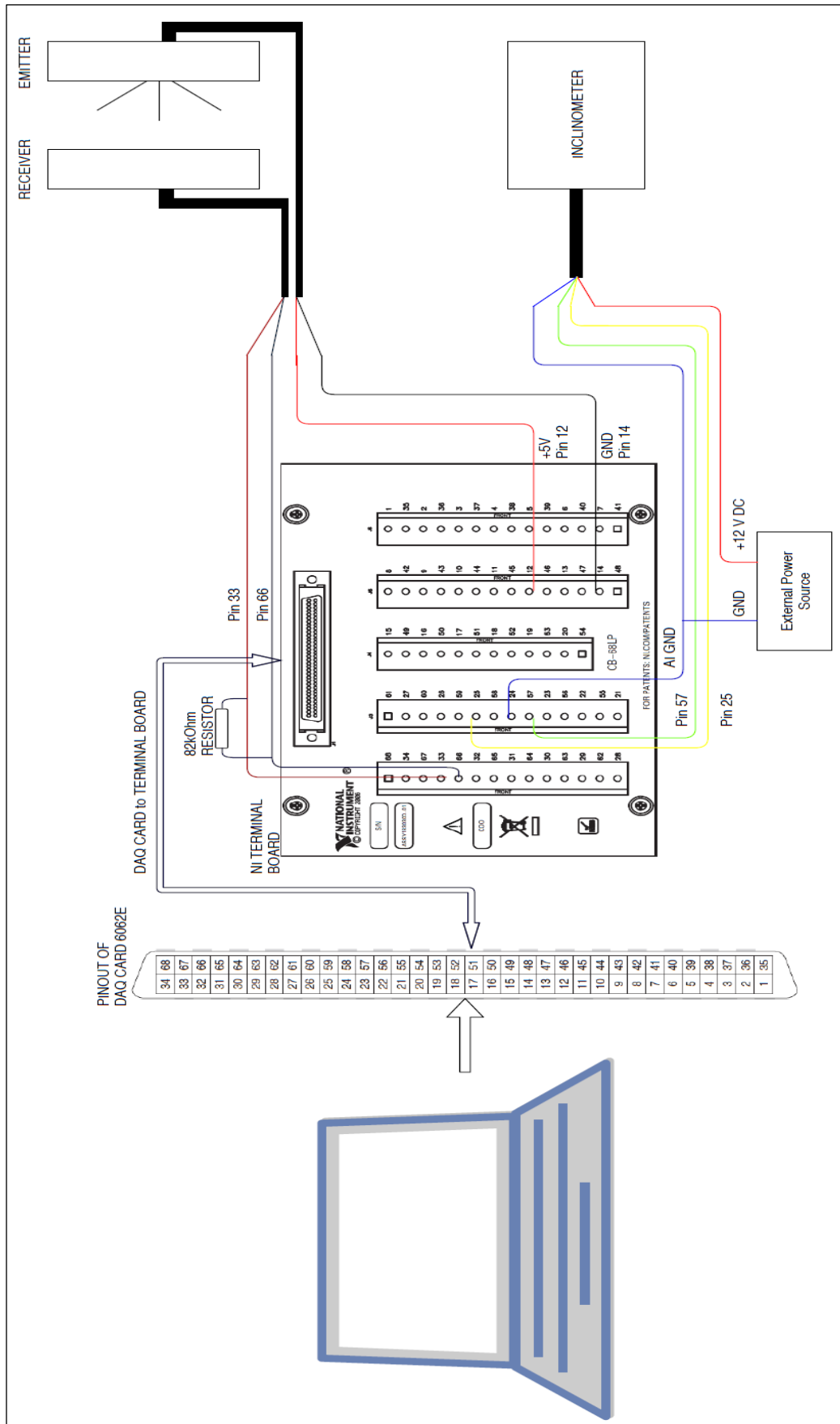


Figure 75 Installation scheme of sensors with old NI terminal board



- With new customized PCB –
 - 1) Make sure that the electrical connections are turned off in the power supply. The DAQ Card 6062E is not plugged into the computer while fitting other connectors to the PCB.
 - 2) The 68-pin cable wire is plugged into the corresponding terminal in the PCB. Make sure that the connection is firm.
 - 3) The 9-pin connector for the photogate is plugged into the corresponding adapter in the PCB. The DB-15 type wire i.e., 15-pin connector for the inclinometer is plugged into the corresponding adapter in the PCB.
 - 4) The DAQCard 6062E is now connected to the computer in its slot and the computer is powered on. The measurement can be started with the written program in LabVIEW software.

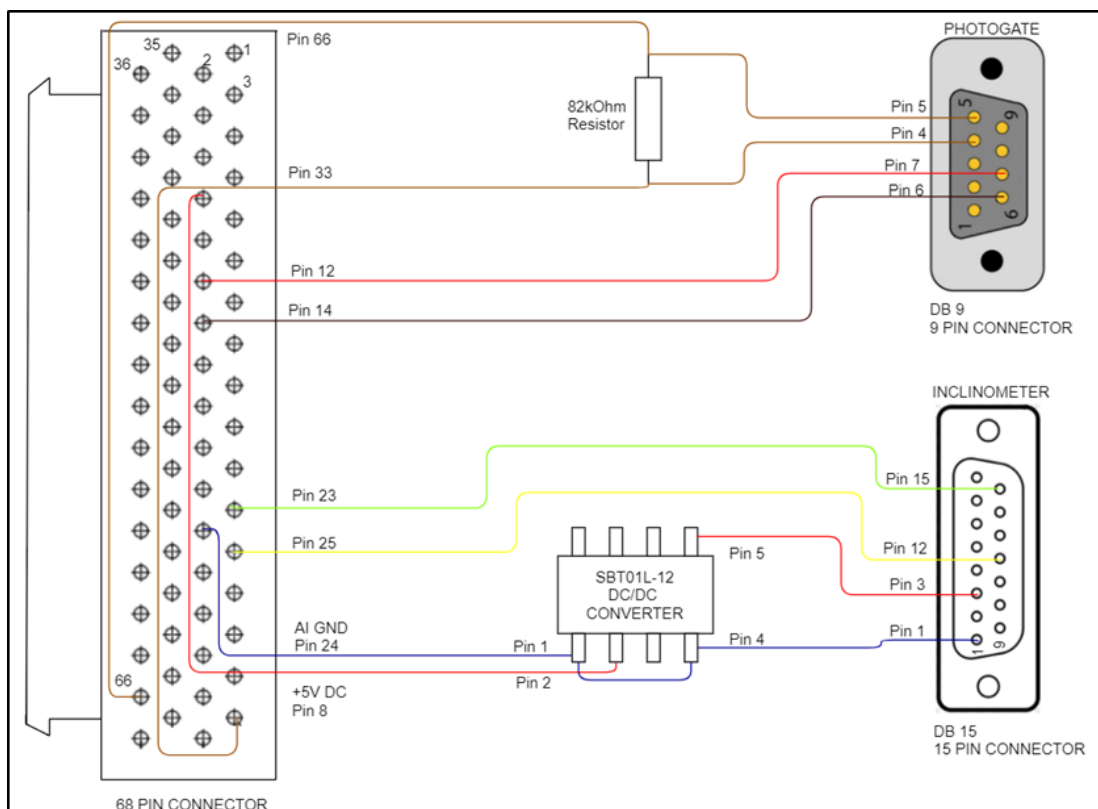


Figure 76 New electrical connection scheme with customized PCB



Annex 2 – Instruction for moment of inertia calculation and obtained results

(a) Known terms and concepts –

The basic formula/ equation for moment of inertia of an object in the integral form is given by –

$$I = \int_M r^2 dm$$

As an inertia tensor form, the equation is re-written as,

$$I = \begin{bmatrix} I_{x'x'} & -I_{x'y'} & -I_{x'z'} \\ -I_{y'x'} & I_{y'y'} & -I_{y'z'} \\ -I_{z'x'} & -I_{z'y'} & I_{z'z'} \end{bmatrix}$$

Where the diagonal terms are called as the principal moment of inertia terms and the others are product of inertia terms. For an object symmetrical about two axes, the product of inertia terms would be zero and we would obtain a diagonal matrix.

(b) Ellipsoid of inertia –

We know that the ellipsoid of inertia's equation is given by –

$$I_x x^2 + I_y y^2 + I_z z^2 + 2I_{xy} xy + 2I_{yz} yz + 2I_{xz} xz = 1$$

And the moment of inertia of the body w.r.t the centre as

$$I_o = I_1 \cdot \cos(\alpha) + I_2 \cdot \cos(\beta) + I_3 \cdot \cos(\gamma)$$

Where α , β and γ are the angle of orientation of the x , y , and z respectively.

(c) Transformation of co-ordinate system –

We know that for transformation about the axes, the rotation matrix is given by –

$$T_x = \begin{bmatrix} 1 & 0 & 0 \\ 0 & \cos \alpha & -\sin \alpha \\ 0 & \sin \alpha & \cos \alpha \end{bmatrix}, T_y = \begin{bmatrix} \cos \beta & 0 & \sin \beta \\ 0 & 1 & 0 \\ -\sin \beta & 0 & \cos \beta \end{bmatrix}, T_z = \begin{bmatrix} \cos \gamma & -\sin \gamma & 0 \\ \sin \gamma & \cos \gamma & 0 \\ 0 & 0 & 1 \end{bmatrix}$$

Where T_x , T_y and T_z are the transformation matrices. The inertia tensor matrix is –

$$I = \begin{bmatrix} (I_{xx})_G + m(y_G^2 + z_G^2) & I_{xy} + mx_G y_G & I_{xz} + mx_G z_G \\ I_{yx} + mx_G y_G & (I_{yy})_G + m(x_G^2 + z_G^2) & I_{yz} + my_G z_G \\ I_{zx} + mx_G z_G & I_{zy} + my_G z_G & (I_{zz})_G + m(x_G^2 + y_G^2) \end{bmatrix}$$

The resultant moment of inertia can be calculated with the following relation –

$$I_F = [T_z]^T [T_y]^T [T_x]^T [I] [T_x] [T_y] [T_z]$$

**(d) Measurement procedure –****1. Measuring the stiffness of wire –**

- 1) Firstly, determine the mass moment of inertia of the disk with the radius and the mass of the disk, by the known formula of

$$I = \frac{MR^2}{2}. \quad \boxed{I = \text{_____ kg.m}^2}$$

- 2) Mount the disk to the U – joint and allow it to come to rest without any oscillations.
- 3) Take a piece of paper and stick it to the end of the disk such that half the piece sticks out, to block the light gate.
- 4) Place the sensor stand beside the paper, such that the paper can interrupt the light, but the disk cannot touch the stand.
- 5) The electrical connections of the sensors are given according to the scheme and PCB used, as given before.
- 6) The program “Moment of Inertia” is then opened in LabVIEW and in the front panel, 1 Axis oscillation is selected.
- 7) Set how many measurements would you like to make for the oscillation.
- 8) Gently, hold the disk and slight rotate it horizontally about its centre by 20° or 30° and release it. Make sure that the disk doesn’t sway longitudinally as a pendulum as we would get erroneous results.
- 9) After a few oscillations, as the disk becomes steadier, press the “Start Measurement” button on the front panel after pressing “Run”, which is a white arrow in the front panel.
- 10) According to the number of measurements set, the experiment continues and stops automatically.
- 11) The torsional stiffness of the wire is then calculated according to the oscillation period measured.

Calculation of stiffness –

Average period of oscillation,

$$\boxed{\tau = \text{_____ s}}$$

Torsional stiffness of wire,

$$k = \frac{I_0 \pi^2}{\tau^2}.$$

$$\boxed{\therefore k = \text{_____ N.m.rad}^{-1}}$$



2. Measurement of mass moment of inertia of a body–

This method is for objects which are symmetrically distributed about the axis of rotation and mounted about that axis without any rotation or translation.

- 1) Mount the body to the U – joint and allow it to come to rest without any oscillations.
- 2) Take a piece of paper and stick it to the end of the body such that half the piece sticks out, to block the light gate.
- 3) Place the sensor stand beside the paper, such that the paper can interrupt the light, but the body cannot touch the stand.
- 4) The electrical connections of the sensors are given according to the scheme and PCB used, as given before.
- 5) The program “Moment of Inertia” is then opened in LabVIEW and in the front panel, 1 Axis oscillation is selected.
- 6) Set how many measurements would you like to make for the oscillation.
- 7) Gently, hold the body and slight rotate it horizontally about its centre by 20° or 30° and release it. Make sure that the body doesn’t sway longitudinally as a pendulum as we would get erroneous results.
- 8) After a few oscillations, as the body becomes steadier, press the “Start Measurement” button on the front panel after pressing “Run”, which is a white arrow in the front panel.
- 9) According to the number of measurements set, the experiment continues and stops automatically.
- 10) The moment of inertia of the body is then calculated according to the oscillation period measured.

Calculation of moment of inertia –

The moment of inertia of the body is given by, $I = k \cdot \left(\frac{\tau}{\pi}\right)^2$

Measured data –

Average period of oscillation, $\tau = \boxed{\quad\quad\quad} \text{ s}$

Hence, the moment of inertia, $I = \boxed{\quad\quad\quad} \text{ kg.m}^2$



3. Measurement of moment of inertia of the wheel –

- 1) Mount the dual axis inclinometer on the plate and onto the bolt of the U – joint and tighten the bolt such that the plate and the sensor don't vibrate or move freely.
- 2) Mount the wheel to the U – joint and allow it to come to rest without any oscillations.
- 3) Take a piece of paper and stick it to the end of the wheel on the rubber tire or the rim, such that half the piece sticks out, to block the light gate.
- 4) Place the light sensor stand beside the paper, such that the paper can interrupt the light, but the wheel cannot touch the stand.
- 5) The electrical connections of the sensors are given according to the scheme and PCB used, as given before.
- 6) The program “Moment of Inertia” is then opened in LabVIEW and in the front panel, 2 Axes Oscillations is selected.
- 7) Set how many measurements would you like to make for the oscillation and the number of samples you need to average to determine the static angle of inclination. The default is set to be 500 samples.
- 8) After the body becomes stationary, void of any oscillation, click on the “Run” button, which is a white arrow on top of the front panel.
- 9) Check the angle of inclination “Alpha” by clicking on the Alpha Angle button. Check if the angle is displayed on the screen in the box near it.
- 10) Measure the distance of *COG* of the body to the mounting position of the body and enter the data into the boxes xG , yG and zG .
- 11) Now, gently hold the body and slight rotate it horizontally about its centre by 20° or 30° and release it. Make sure that the body doesn't sway longitudinally as a pendulum as we would get erroneous results.
- 12) After a few oscillations, as the body becomes steadier, press the “Start Measurement” button on the front panel after pressing “Run”, which is a white arrow in the front panel. According to the number of measurements set, the experiment continues and pauses automatically after each iteration is complete.
- 13) After finishing the measurement of “Alpha” angle parameters, repeat the steps 9) to 12) for the “Beta” angle.
- 14) The moment of inertia of the body is then calculated according to the oscillation period measured.



The moment of inertia of the body calculated in the program is according to the steps below –

$$I_1 = k \cdot \left(\frac{\tau_1}{\pi}\right)^2 \text{ and } I_2 = k \cdot \left(\frac{\tau_2}{\pi}\right)^2$$

$$I_{xx} = \frac{I_1 - I_y \sin^2 \alpha}{\cos^2 \alpha} \text{ and } I_{yy} = I_{zz} = \frac{I_2 \frac{\cos^2 \alpha}{\cos^2 \beta} - I_1}{\frac{\cos^2 \alpha}{\cos^2 \beta} (\sin^2 \beta) - \sin^2 \alpha}$$

The above equation gives the principal moments of inertia about the 3 axes. Now, for the moments of inertia about the two different mounting points, substitute the values of I_x , I_y and I_z along with the angles and distances of the mount into the relations given below.

$$T_x = \begin{bmatrix} 1 & 0 & 0 \\ 0 & \cos A & -\sin A \\ 0 & \sin A & \cos A \end{bmatrix}, T_y = \begin{bmatrix} \cos B & 0 & \sin B \\ 0 & 1 & 0 \\ -\sin B & 0 & \cos B \end{bmatrix}, T_z = \begin{bmatrix} \cos C & -\sin C & 0 \\ \sin C & \cos C & 0 \\ 0 & 0 & 1 \end{bmatrix}$$

Where T_x , T_y and T_z are the transformation matrices. The inertia tensor matrix is –

$$I = \begin{bmatrix} (I_{xx}) + m(y_G^2 + z_G^2) & I_{xy} + mx_G y_G & I_{xz} + mx_G z_G \\ I_{yx} + mx_G y_G & (I_{yy}) + m(x_G^2 + z_G^2) & I_{yz} + my_G z_G \\ I_{zx} + mx_G z_G & I_{zy} + my_G z_G & (I_{zz}) + m(x_G^2 + y_G^2) \end{bmatrix}$$

The resultant moment of inertia can be calculated with the following relation –

$$I_F = [T_z]^T [T_y]^T [T_x]^T [I] [T_x] [T_y] [T_z]$$

The moment of inertia tensor about the three new axes are now found out and correspondingly the inertia about the individual axes are also found.

4. Result tabulation –

Measurement of COG					
m _{rim} [kg]		m _{rod} [kg]		m _{tot} [kg]	
a [m]		b [m]		h [m]	

Calculation of wire stiffness -			
Mass of known disk, M [kg]		Avg., period of oscillation, τ [s]	
Radius of disk, r [m]		Torsional wire stiffness, k [Nmrad ⁻¹]	
Moment of inertia, I_o [kg.m ²]			

Moment of inertia of body -			
Angle of inclination, α [°]		Principle MOI in x-axis, I_x [kg.m ²]	
Half period of oscillation, τ_1 [s]		Principle MOI in y-axis, I_y [kg.m ²]	
Moment of inertia, I_1 [kg.m ²]		Principle MOI in z-axis, I_z [kg.m ²]	
Angle of inclination, β [°]		Major axis of ellipsoid, a [kg ^{-1/2} .m ⁻¹]	
Half period of oscillation, τ_2 [s]		Minor axis of ellipsoid, b [kg ^{-1/2} .m ⁻¹]	
Moment of inertia, I_2 [kg.m ²]			



Annex 3 – Instruction to create the task for Counter Input in NI MAX application.

- 1) Open the NI-MAX application.
- 2) Right-click the option “NI-DAQmx Tasks” to display a dialog box – “Create new NI-DAQmx Task”.
- 3) Click on “Acquire Signal” and then “Counter Input”.
- 4) Click “Period” option.
- 5) In the devices shown, select cDAQ3Mod1, since NI 9401 module is connected in the 3rd slot.
- 6) The default counter chosen is the “ctr 2” for the measurement. Click on “Next” and proceed to next step.
- 7) Name the task according to your wish. The default name has been given as “Period_IRC_1” and click “Finish”.
- 8) The default input is set to PFI 2, check the pinout diagram for the corresponding pin for the “ctr”. The default is Pin 17 on the terminal board.
- 9) If the Custom Scaling is anything other than “<No Scale>”, revert it back to that option.
- 10) Set the starting edge option to “Rising” and the measurement method to 1 Counter (Low Frequency).
- 11) The acquisition mode is set to “Continuous Samples” and the Samples to read to “6000”.
- 12) The signal input range by default is set from “12.501ns” to “100ms” and the Scaled Units as “Seconds”.
- 13) Repeat the steps 2) to 12) with “ctr 1” and corresponding terminal, to configure the task for the second encoder.

The photo in the next page shows the task configuration in NI MAX – Measurement and Automation Explorer application.

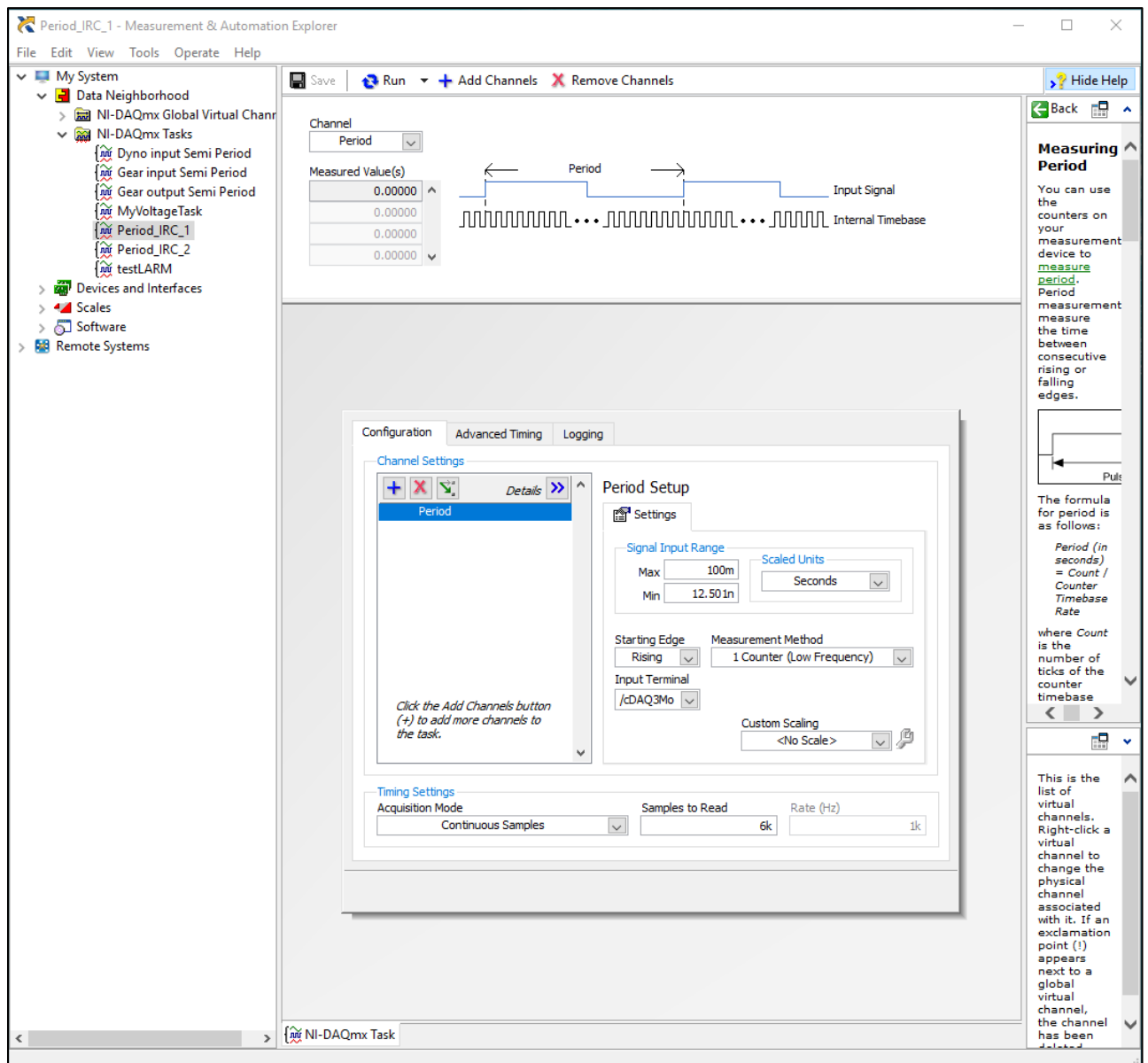


Figure 77 Task configuration in NI MAX software



Annex 4 – Instruction manual for analysis in NI DIAdem

After obtaining the encoder readings as text or Excel file, follow the procedure below –

(a) Importing the data into DIAdem software:

- 1) Open NI DIAdem and go to “NAVIGATOR” window.
- 2) On the top taskbar, select  if you have the data as “.txt” format or  if you have the data as Excel format.
- 3) Select the file which you want to import and click on OK. The data plugin wizard opens where click on “Next” until you reach the end, without changing any property of the sheet.
- 4) Click on “Load” to load the data and give a name for the data plugin. If the default “DataPlugin” has been taken, rename it to own choice and Click on “Finish”.
- 5) In the “VIEW” column, individual columns for speed of each encoder shaft along with time periods are created.

(b) Frequency spectrum/ Fast Fourier Transform(FFT) of data:

- 1) The time period has to be added continuously for every row, which is done by “Sum” function in “ANALYSIS” section, to get the incremental time for every pulse.
- 2) In “ANALYSIS” section, select “FFT with one signal” option and select speed signals as Y-axis data and time channel as X-axis data.
- 3) Input and select parameters given in “Table B-4” in this document and click on “Calculate” and close the window. FFT of given signal is calculated w.r.t time.
- 4) We obtain both the “Amplitude” and “Real and Imaginary Parts” in frequency domain.
- 5) Identify the peaks and note the trend of harmonics of Gear Mesh Frequency in the spectrum to basically analyse if the gear pair is healthy or has any defect.
- 6) Next, we proceed to average the obtained data using VBS script to remove random peaks or also use the IFFT with “Real and Imaginary Parts” obtained above.



(c) Synchronized Averaging method:

- 1) To split the time period data evenly for every 2 revolutions i.e., 12000 data points, type the following script given in the next diagram.

```
Dim i, iValues, iLoopLength, oMyNewChn, sSignalChn, sTimeChn, oChnList
iValues = 12000

iLoopLength = Data.Root.ChannelGroups(1).Channels("Time Period IRC 1 [s]").Properties("length").Value/iValues
sTimeChn = "[1]/Time Period IRC 1 [s]"
sSignalChn = "[1]/Speed"

Set oChnList = data.CreateElementList 'List of split channels

For i = 1 to iLoopLength
Set oMyNewChn = Data.Root.ChannelGroups(1).Channels.Add("new" & i,DataTypeChnFloat64)
Call DataBlCopy(sTimeChn, 1 + (i-1)*12000, 12000, oMyNewChn, 1)
Call oChnList.Add(oMyNewChn) 'Add result channel to list
Next
```

Figure 78 VBA script for channel split in DIAdem

- 2) Now, the entire data is split into distinct channels and has been assigned the new name given in the script which can be changed according to user's wish.
- 3) The averaging of the split columns of data has been done in Microsoft Excel and hence, the new channels created are selected together from "Data Portal" window and copied into a new Excel worksheet.
- 4) The first row of every column has been averaged to give one value in a new column. Similar operation is done for all other rows and final column with averaged time period of 12,000 rows has been created.
- 5) The corresponding speed of rotation has been calculated accordingly for every time period.
- 6) Create new channels in DIAdem and copy the averaged time and corresponding speed into it. Perform the running sum of time period as done before.
- 7) In "ANALYSIS", select "Digital Filters" and "Bandpass" option, in which type lower limit – 1st GMF and upper limit – 5th GMF harmonic of the signal and calculate.
- 8) The RPM fluctuation caused due to the harmonics of gear mesh frequencies are obtained which when multiplied with corresponding time period gives the fluctuation in angular increments.
- 9) Repeat the above steps for the second signal also. The difference in increments given by formula (2.1) gives the transmission error.



The ripple caused due to filtering and presence of small peaks between the limits despite averaging is the disadvantage of this method. Hence, we shift to IFFT method.

(d) IFFT method:

- 1) Average the data as done before till final 12,000 points of time period and speed are obtained (till step 6) of last section). This gives averaged peak of GMF harmonics.
- 2) For the gear mesh, note 5 or 7 harmonics of gear mesh frequency and create two channels with 12,000 beside real and imaginary parts channels, obtained before.
- 3) Copy and paste the corresponding real and imaginary parts at GMF harmonics into the new two channels. Rest of the rows of the new channels are kept as zero.
- 4) IFFT with summed time channel and new real and imaginary part channels give RPM fluctuations as in previous method. Next, following the steps 8) & 9) of previous method gives the required Transmission Error.



G. ATTACHMENTS

1. Moment of Inertia measurement

Attachment 1.1

Table G-1 Specification of DAQCard 6062E

SPECIFICATIONS			
<u>Analog Input</u>			
Number of Channels	16 Single-ended or 8-differential (software selectable)		
Resolution	12 bits		
Max., Sampling rate	500 kS/s		
Input Voltage Range	Bipolar	Unipolar	
	±10 V	-	
	±5 V	0 to 10 V	
	±2.5 V	0 to 5 V	
	±1 V	0 to 2 V	
<u>Analog Output</u>			
Number of Channels	2		
Resolution	12 bits		
Max., update rate	First In First Out (FIFO) mode		
	Internal timer	External timer	
	850 kS/s	850 kS/s	
FIFO buffer size	248 samples		
Voltage output range (DC)	±10 V, ±AO EXT REF		
Output impedance	0.1 Ω max		
Minimum switch on power	±200 mV		
External reference input	±11 V		
Overvoltage protection	±25 V		
<u>Digital I/O</u>			
Number of Channels	8 I/O		
Resolution (Counter/timers)	24 bits		
Input Voltage		Min	Max
	Low	0 V	0.8 V
	High	2 V	5 V
Output Voltage	Low	-	0.4 V
	High	4.35 V	-



Attachment 1.2

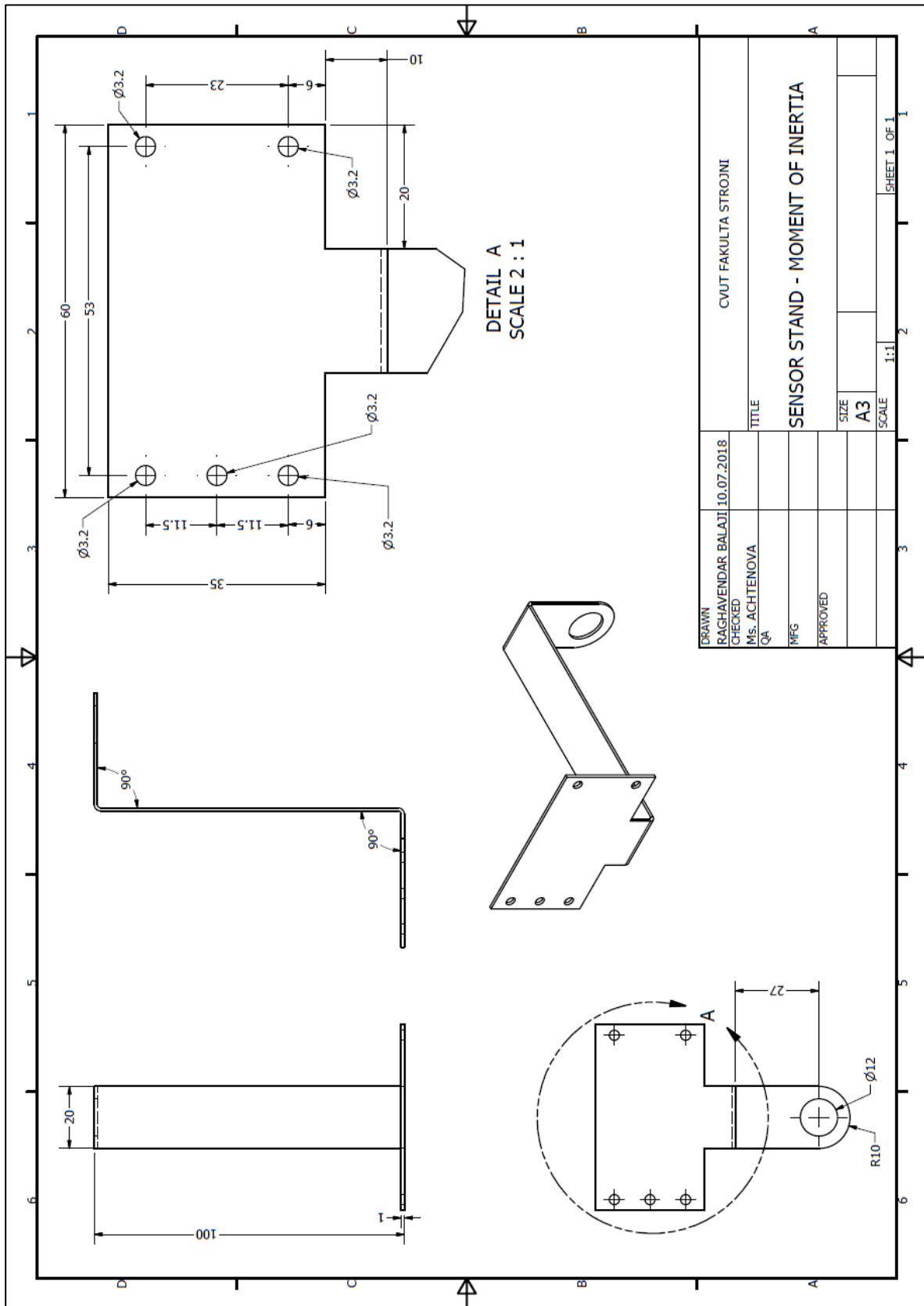


Figure 79 Sensor mount technical drawing



Attachment 1.3

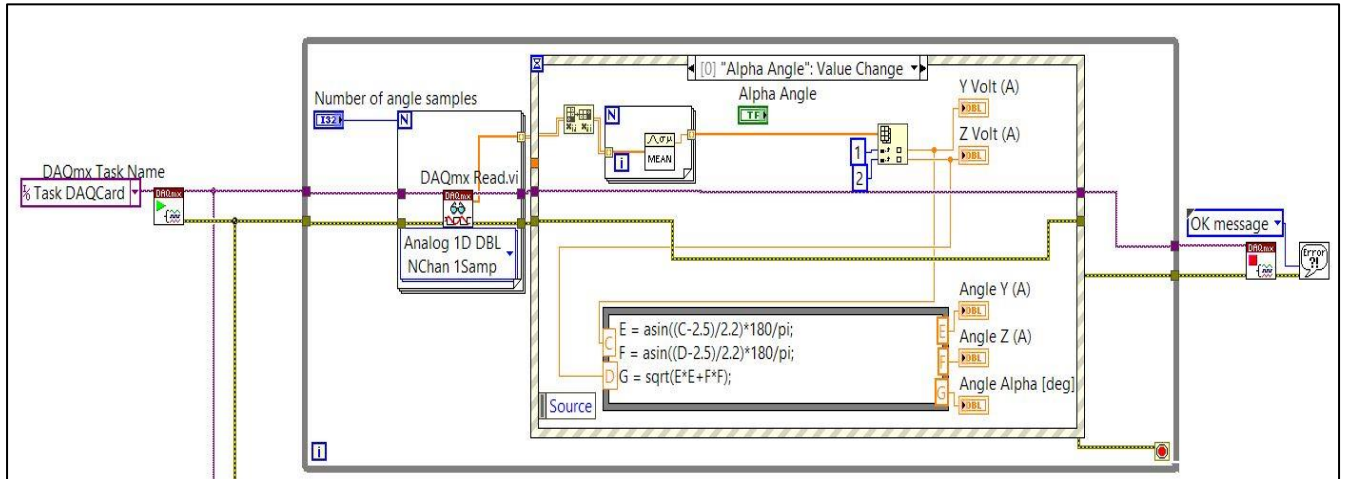


Figure 80 LabVIEW program for angle acquisition

Given below is the individual program written for angle acquisition. The task has been created as “TaskDAQCard” which is then initiated by the Start task  command which then passes the task into the while loop where the data is read. The command which reads “Analog 2D DBL NChan 1Samp” reads the input task and converts into the data which we require. Since we obtain two sets of data, for the ‘x’ and ‘y’ axes, we use indexing of array. The numeric constants 0 and 1 inside the blue box indicate the row of the array which we need to obtain separately. Since the number of angle samples to be taken is given as 500, we take the mean value of the readings and send it to a numeric indicator which displays our result in the front panel.

The gray coloured box given below is the formula node which has two inputs (C, D) and three outputs (E, F, G). The inputs are the voltage values which we obtain above and the outputs (E, F) are the two inclinations on the Y and Z axes of the object which are the X and Y axes of the inclinometer. The output G is the resultant angle of the two inclinations, which we need for the moment of inertia calculation. Since the output is sinusoidal, it is easy to determine the angular value with the parameters of the curve provided in the datasheet.

The voltage task is created outside the While loop and starts the task. The program runs inside an Event structure which has two similar cases for α and β values. The purpose of this setup is to make sure that the task is initialized, and data is recorded on demand, instead of making it run the entire time which would consume a lot of power and data.



Attachment 1.4

Given below is the basic program for calculating the moment of inertia tensor of the object suspended. When integrated as a part of the main program, the values of principle moments of inertia - I_x , I_y and I_z of a complex body are obtained from the method as mentioned in the work by Mr. Pavel Špinka ^[9] or for simpler rotationally symmetrical objects through the ellipsoid of inertia method as described in the above literature. The distances from the principle axes to the mounting co-ordinates – x_G , y_G and z_G are obtained after measuring the position of *COG* of the body according to the methods described above in the chapters. The mass of the object is known which is input into the required field and the angles of inclination - *Angle X*, *Y* and *Z* are connected to the outputs from the program given in “[Attachment 1.3](#)”.

```

1 Tx = [1 0 0;
2   0 cos(K) -sin(K);
3   0 sin(K) cos(K)];
4
5 Ty = [cos(L) 0 sin(L);
6   0 1 0;
7   -sin(L) 0 cos(L)];
8
9 Tz = [cos(M) -sin(M) 0;
10  sin(M) cos(M) 0;
11  0 0 1];
12
13 Ixxo = A + J*(H^2 + I^2);
14 Iyyo = B + J*(G^2 + I^2);
15 Izzo = C + J*(G^2 + H^2);
16
17 Ixyo = J*G*H;
18 Iyzo = J*H*I;
19 Izxo = J*G*I;
20
21 Io = [Ixxo Ixyo Izxo; Ixyo Iyyo Iyzo; Izxo Iyzo Izzo];
22 Ik = Tz.*Ty.*Tx.*Io.*Tx.*Ty.*Tz
    
```

Final Inertia tensor

Figure 81 Math Script for moment of inertia tensor calculation



2. Measurement of gearbox transmission error

Attachments for experimental setup

Attachment 2.1

Table G-2 Preferred FFT window type for acquired signals.

Signal of interest	Window
Sinusoidal wave or its combination	Hanning
Sine wave (Necessary amplitude accuracy)	Flat Top
Narrowband random vibration signal	Hanning
Broadband random (white noise)	Uniform
Closely spaced sine waves	Uniform, Hamming
Excitation signals (hammer blow)	Force
Response signals	Exponential
Unknown signal	Hanning
Two signals of similar frequencies but different amplitudes	Kaiser-Bessel
Two signals of similar frequencies and amplitudes	Uniform
Accurate single tone amplitude measurement	Flat Top

Attachment 2.2

Table G-3 Main specification of the ABB industrial drive used

SPECIFICATION		VALUE	
Electric supply connection	Voltage [V]	3-phase, $U_N = 400$ V	
	Frequency [Hz]	48 to 63 Hz	
	Efficiency [%] (at nominal power)	98%	
	At nominal voltage of 400 V and no overload	Nominal current rating [A]	$I_{CONT. MAX} = 25$ $I_{MAX} = 32$
		Power [kW]	11
		Noise level [dB]	62
	Heat dissipation [W]	340	
Motor connection	Frequency [Hz]	0 to ± 300 Hz	
	Torque control (at nominal torque)	Step rise time: <5 ms	
	Inaccuracy [%]	0.01% of nominal speed	
Operating temperature		-15 to 50°C	



Attachment 2.3

Table G-4 The main working parameters of motor

SPECIFICATION		
Parameter	50 Hz	60 Hz
Power [kW]	15	17.3
RPM [min^{-1}]	1460	1760
Supply current (at nominal voltage)	52 (220 V)	29.6 (440 V)
Effect factor ($\cos \phi$)	0.84	
Efficiency [%]	90.5	
Starting current [I_a/I_n]	7.3	
Starting moment [M_a/M_n]	2.8	
Weight [kg]	93.5	

Attachment 2.4

Table G-5 Electrical parameters of LARM Incremental Rotary Encoder

ELECTRICAL DATA	IRC 305
Supply Voltage U_N [V]	5±5%
Supply current max. I_N [mA]	100
Output frequency max., F_o [kHz]	200
Output max I_o [mA]	±20
Operating temperature [°C]	0 to 60
Output signal	
U_{OH} [V] ($U_N = 30$ V, $I_{ON} = 10$ mA)	>2.5
U_{OL} [V] ($U_N = 30$ V, $I_{ON} = -10$ mA)	<0.4
Max., cable length [m]	50

Attachment 2.5

Table G-6 Wiring specification of encoder

SPECIFICATION		
Pin	Colour	Signal
1	Grey	Signal 2 non
2	Rose	Sensor +5 V
3	Blue	Signal 3
4	Violet	Signal 3 non
5	Yellow	Signal 1
6	White	Signal 1 non
7	-	NC
8	Green	Signal 2
9	Shield	Shield
10	Black	GND
11	Brown	Sensor 0 V
12	Red	$V_{CC} +5$ V



Attachment 2.6

Table G-7 Specification of NI 9401 DAQ device.

NUMBER OF CHANNELS		8 DIO CHANNELS	
I/O type		TTL, single-ended	
Input voltage range [V]		0.8 to 5.25	
Output voltage range [V]		0.1 to 4.7	
Input current [μ A]		\pm 250	
Input rise/fall time maximum [ns]		500	
Max., signal switching frequency, per channel [MHz]	Input	8 channels	9
		4 channels	16
		2 channels	30
	Output	8 channels	5
		4 channels	10
		2 channels	20

Attachment 2.7

Table G-8 Working parameter of the NI cDAQ 9174 chassis

PARAMETER	VALUE
No., of counters/timers	4
Resolution	32 bits
Counter outputs	Edge count, pulse, semi-period, period, pulse width, 2-edge separation
Position outputs	X1, X2, X4 and pulse encoding
Internal base clocks	80 MHz, 20 MHz and 100 kHz
External base clock	0 to 20 MHz
Base clock accuracy	50 ppm
Inputs	Gate, Source, Aux, A, B, Z
Routing option for input	PFI, Analog trigger
FIFO	127-sample FIFO



Attachments for LabVIEW programming

Attachment 2.8

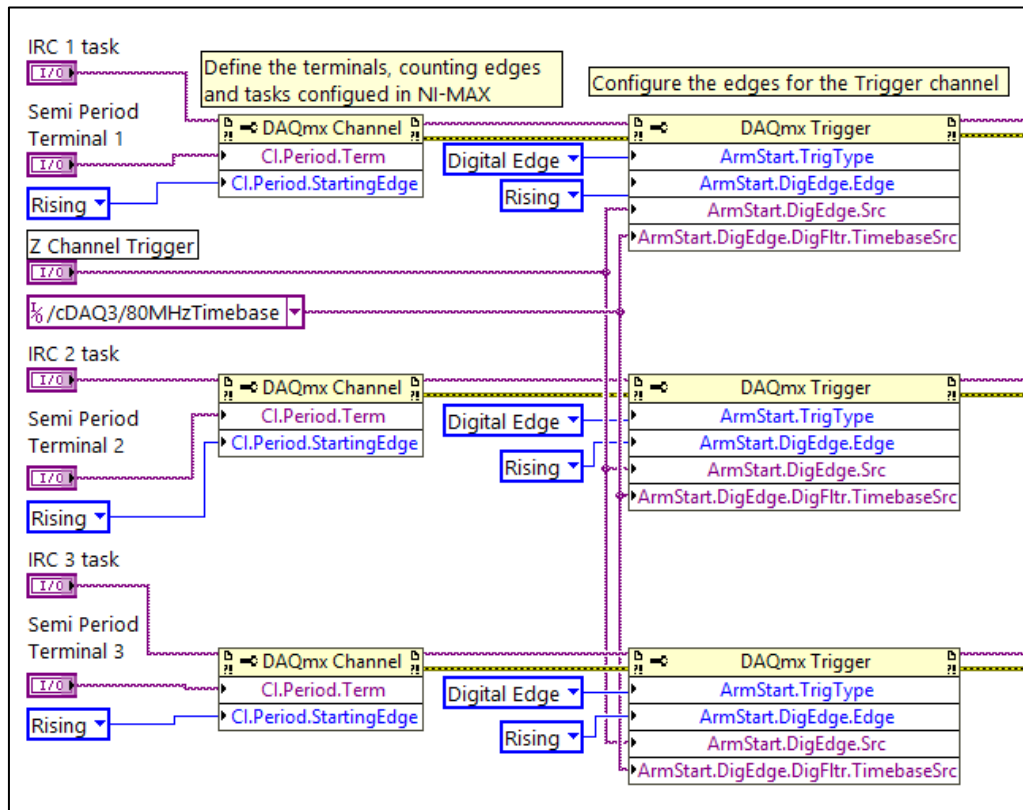


Figure 82 Sub-section of program for configuring terminals

As we can see from the picture above, each of the properties is configured separately on a channel. The task is initialized into the “**DAQmx Channel**”, along with the property of input terminal for the measurement, in “**CI.Period.Term**” and the starting edge to measure, in “**CI.Period.StartingEdge**”. This is obtained by choosing the “**Channel property node**” in LabVIEW and configuring it. The same procedure is done for all the three signals i.e., two from the LARM encoders and one from the input encoder from the inertial test bed.

To start the measurement at the same time for the two encoders, a trigger is configured in a DAQmx channel property node. The Z channel of second encoder is used as a trigger to just start the measurement initially, with “**Digital Edge**” and “**Rising**” as the reference information in trigger channel properties - “**ArmStart.Trig.Type**” and “**ArmStart.DigEdge.Edge**”. The terminal and time-base for the trigger, “**cDAQMod3/PFI 7**” and “**cDAQ/80MHzTimebase**” are the same for all the three channels, which is given through “**ArmStart.DigEdge.Src**” and “**ArmStart.DigEdge.DigFltr.TimebaseSrc**” respectively



Attachment 2.9

Now that the tasks and terminals are configured, we focus on the acquisition and reading of the data transmitted from the encoder. This step follows as shown in the figure below.

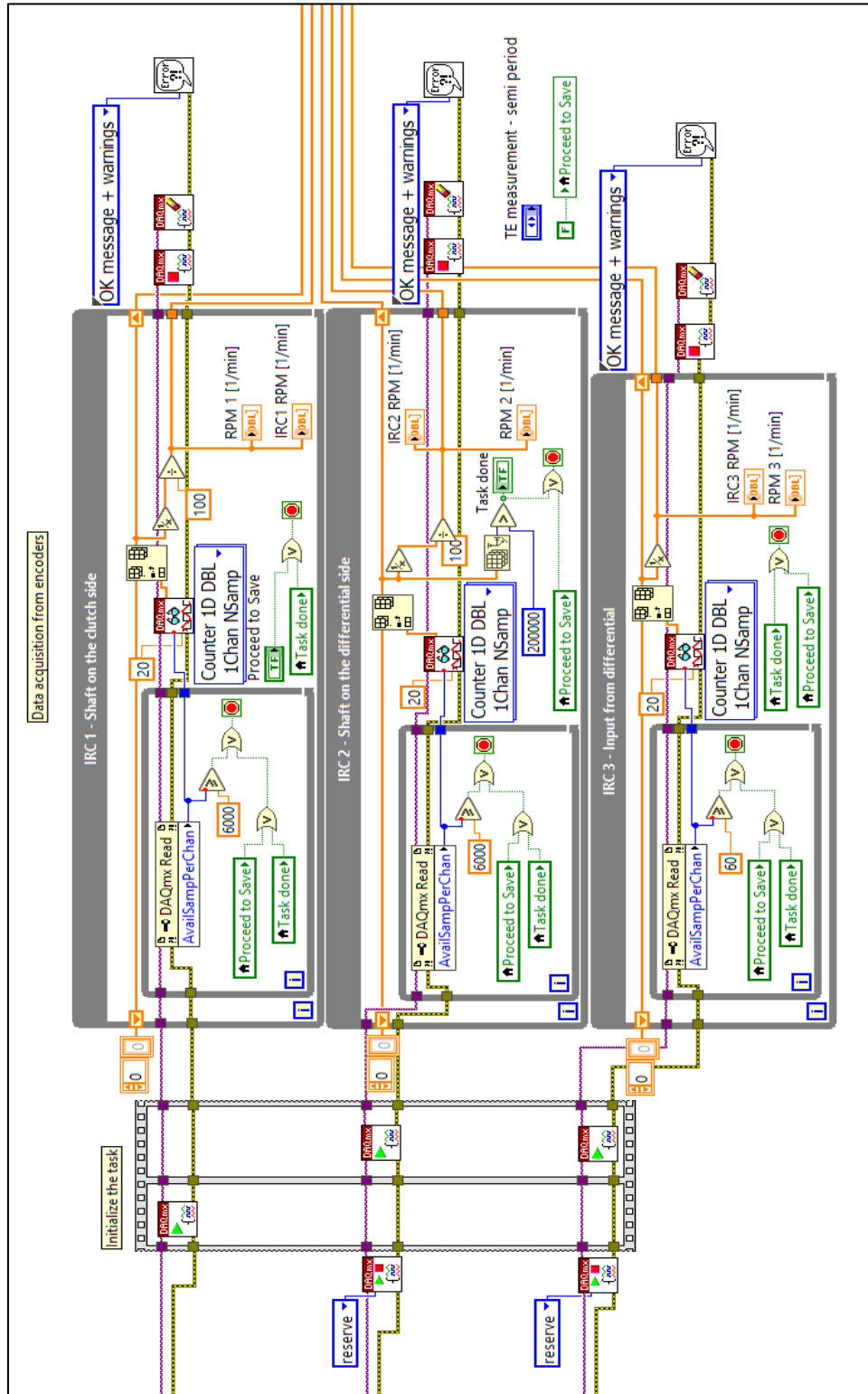


Figure 83 Reading and display of acquired signals



The  button is called as the DAQmx Control Task, which is used to alter the state of the task according to the option we provide to it. In this case, we use “**reserve**” which reserves the hardware to that particular task entirely so that no other task can utilize it simultaneously. Hence, one task is started first in the “**Flat Sequence**” window and the second one is reserved and used later for the loop. The third task involves a different module and hardware and hence it does not affect this measurement. Next the task starts in the Flat Sequence loop, with the task present in the first section starting prior and the moving to the next sequence.

After the initialization, the tasks move to the While loop, which is the grey coloured box. The task is analysed and the data from it is read by the “**DAQmx Read**” command. But before that, since a large amount of data is sent to the computer in a short amount of time during high RPM, it might occupy a large memory during the usage. To prevent that, we place another While loop inside the existing one to collect a few samples in buffer till the condition is met, and then sent to the outer loop for further processing.

This is done with the DAQmx Read channel with three conditions i.e., if the samples in the loop exceed the number provided by the user or if the task is complete or if it is manually stopped before the finish of the task. The first condition is fulfilled when the buffer is full and exceeds the predefined limit. Likewise, the second condition is met when the number of total samples in the array exceeds the limit of “**200000**” set by the user, which is usually sufficient for the encoder type. Finally, the last condition happens when the user needs to abruptly end the program for whatso reason ever.

The output instantaneous RPM is also displayed in the form of a graph in the front panel. A Shift Register is added to the loop to index the array and store the data for every consecutive loop occurring in the program. After the data acquisition is complete, it is transferred to an Event Structure where it is saved by the user in a customized manner.



Attachment 2.10

Now that the data has been acquired, we need to save the acquired data for further processing. The image below shows the method implemented in saving the acquired data to a text file in the prescribed directory of computer.

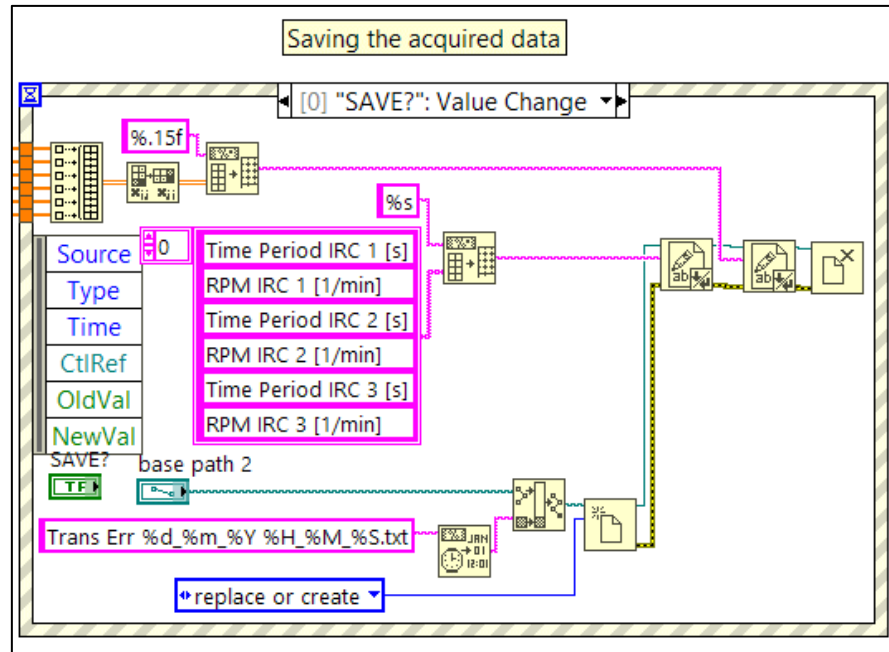


Figure 84 Saving the acquired data

The data of time for every degree of both encoders and their corresponding speeds of rotation along with the speed of rotation of the inertial mass, is sent to be saved in an Event Structure placed outside other loops. A precision of 15 digits is preferred to obtain the most accuracy of reading possible. An option to replace or create a new file is given. To keep a default name for the file, a string with the format “**Trans Err %d_%m_%Y %H_%M_%S.txt**” given along with a path to a default directory to save the file. In the above format, representations are as follows –

- %d – Date of measurement
- %m – Month of measurement in numeric format
- %Y – Year of measurement in 4-digits numeric format
- %H, %M and %S – Time of measurement in Hours, minutes and seconds on day of measurement in 24 Hours format.

The given data is then merged into the file created and saved. As soon as it finishes the saving process, the program stops, and the acquisition is complete. The event is handled by changing the value of the Boolean “SAVE?” placed inside the loop. This is done by “**Edit Events Handled by This Case**”.



Attachment 2.11

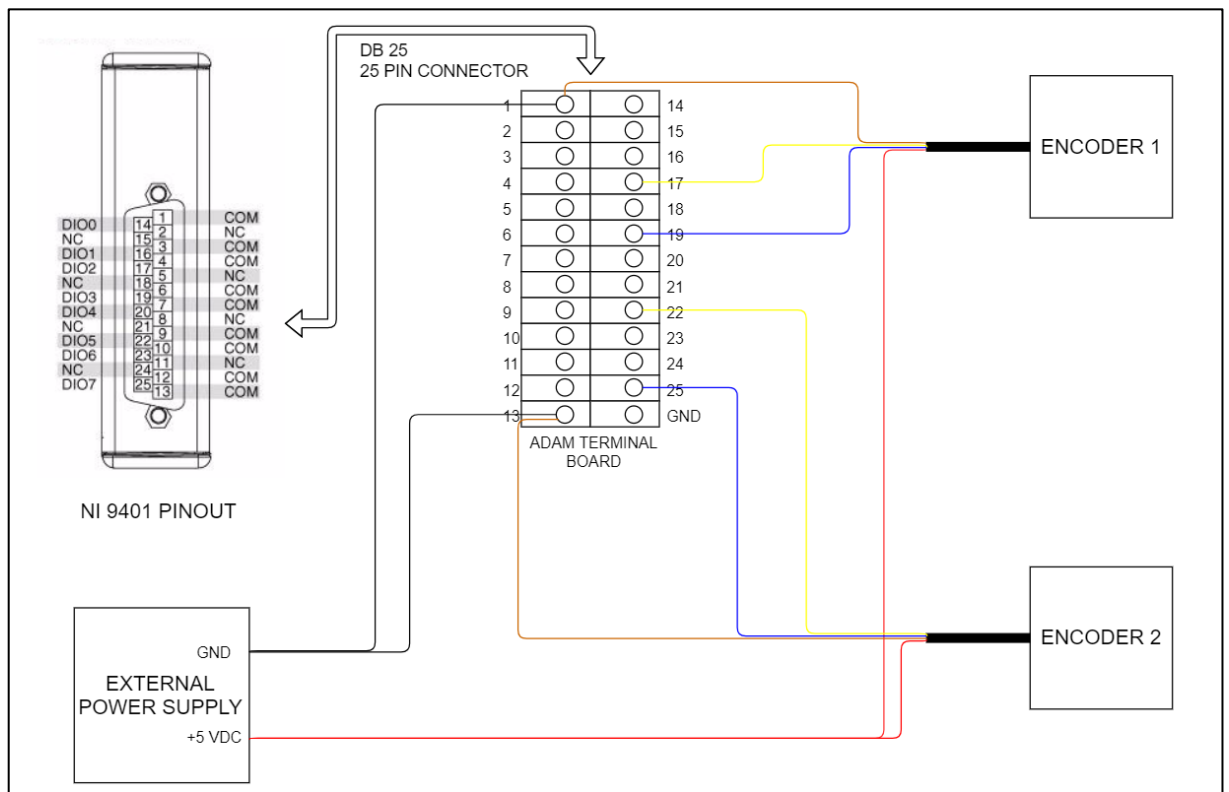


Figure 85 Scheme of terminal connection with ADAM board



Attachments for post-processing in DIAdem

Attachment 2.12

The graph below shows the frequency on the x – axis where we have a noticeable amplitude peak on y – axis though low, which is due to gear mesh frequency and also electric components which can potentially cause disturbance with the readings.

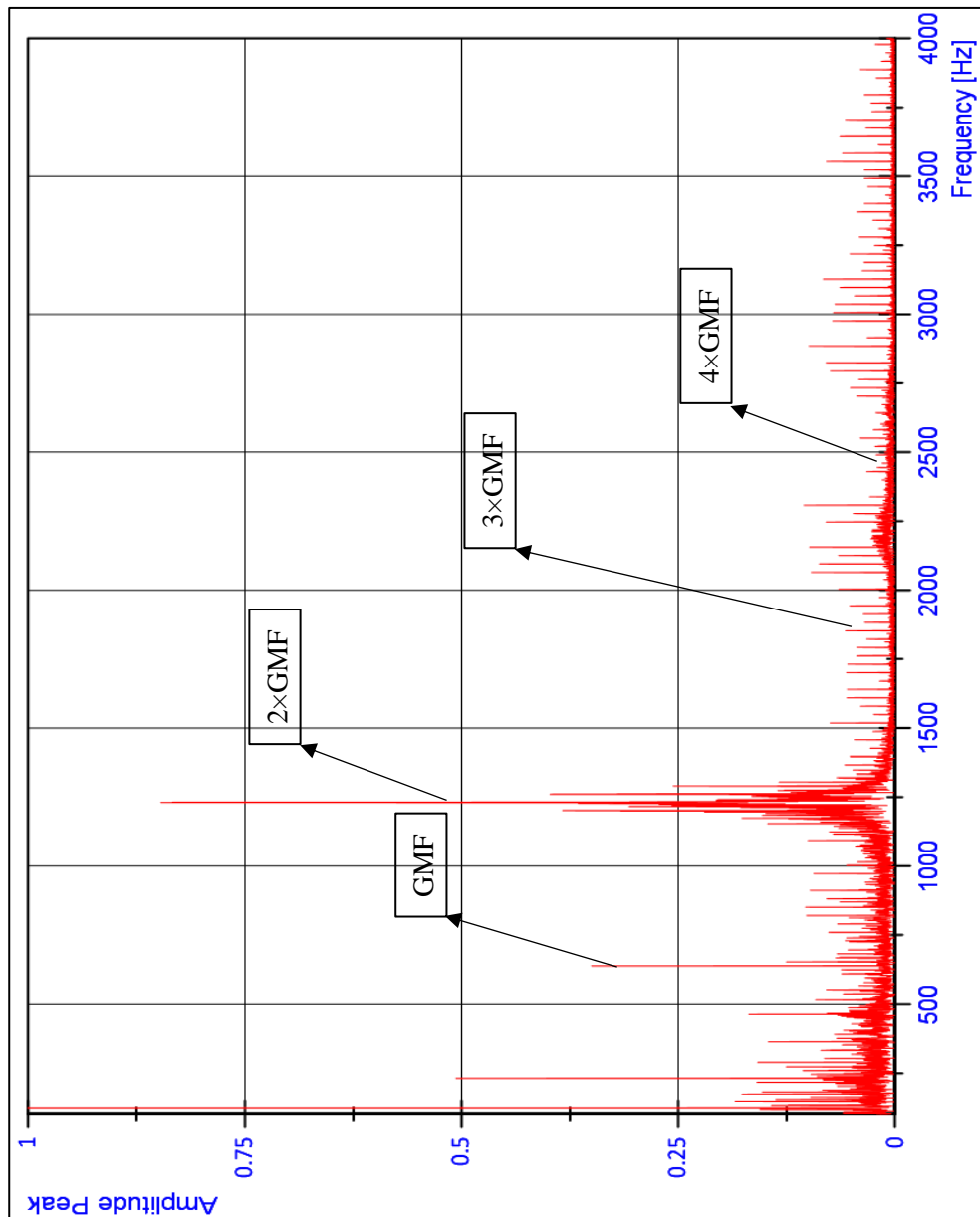


Figure 86 Frequency spectrum of rotational speed of input shaft (vs) Amplitude– 2nd gear

Similar graph has been shown for the output shaft of gearbox below.

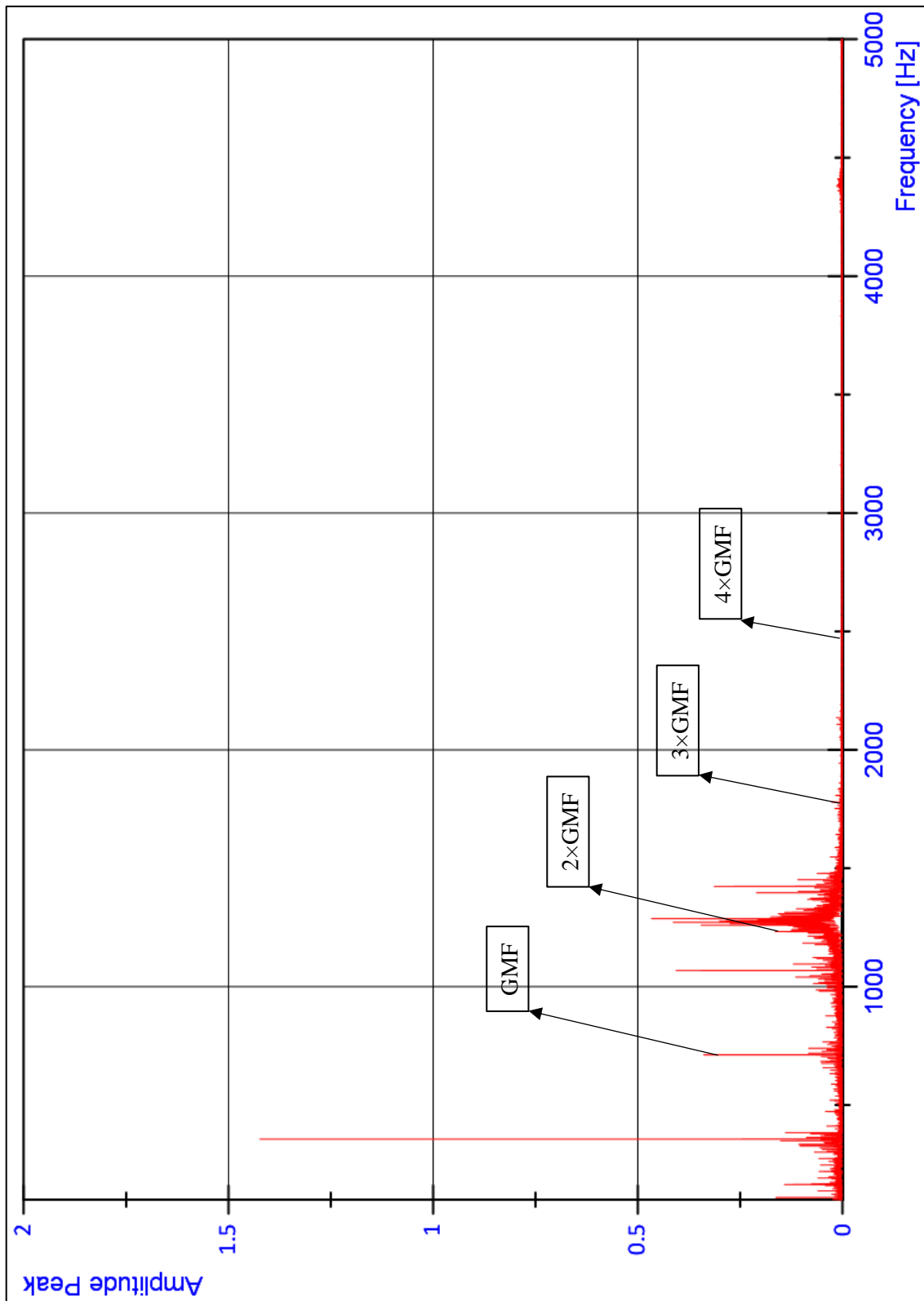


Figure 87 Frequency spectrum of rotational speed of output shaft (vs) Amplitude– 2nd gear



The graphs below have been obtained after filtering with the parameters given above and the method explained in Gear 1.

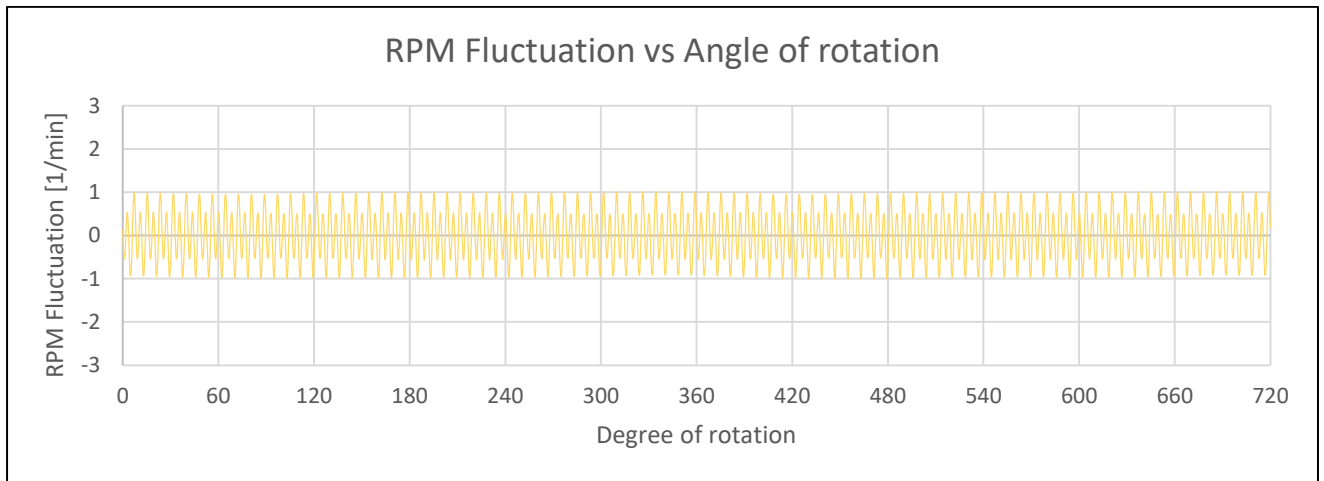


Figure 88 *RPM Fluctuation of input shaft of 2nd gear by gear mesh (vs) Angle of rotation*

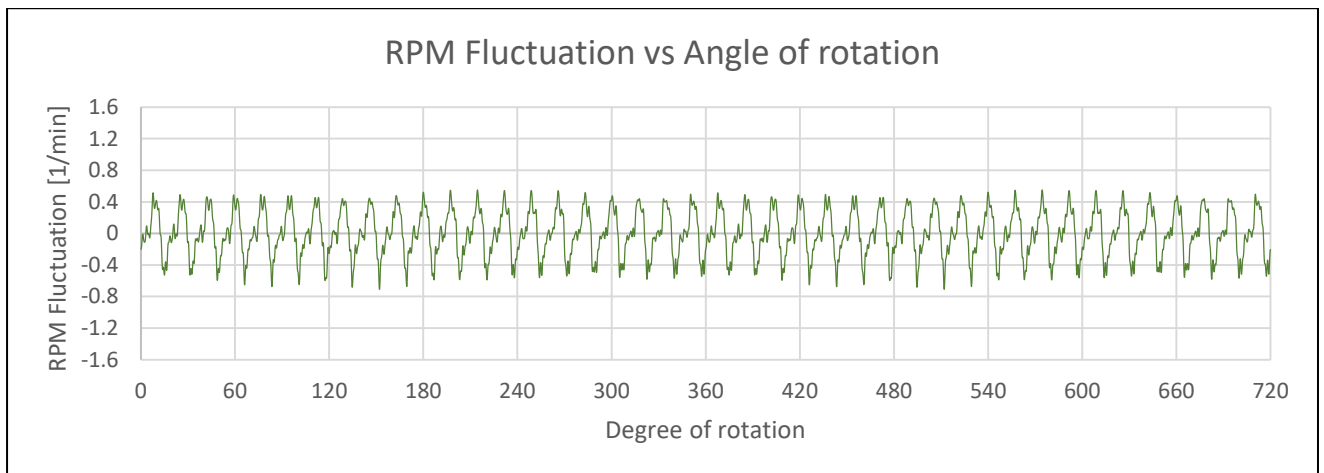


Figure 89 *RPM Fluctuation of output shaft of 2nd gear by gear mesh (vs) Angle of rotation*

[Attachment 2.13](#)

Like the two gears as seen above, we derive the graph between the amplitude peak and frequency for the rotational speed signal of 3rd gear. The respective graphs for the input and output gears' frequency spectrum and corresponding noise are shown below.

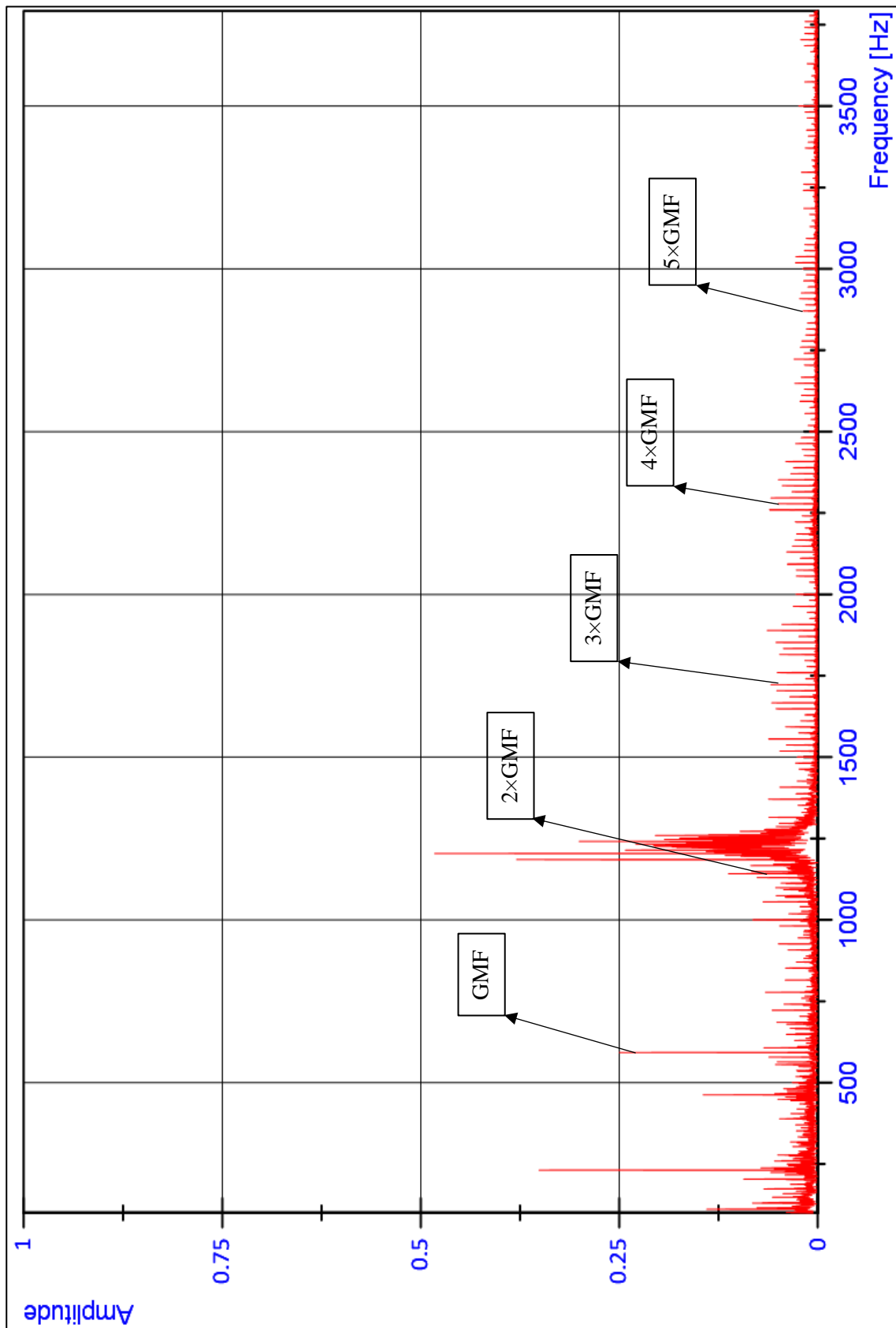


Figure 90 Frequency Spectrum of rotational speed of input shaft (vs) Amplitude – 3rd gear

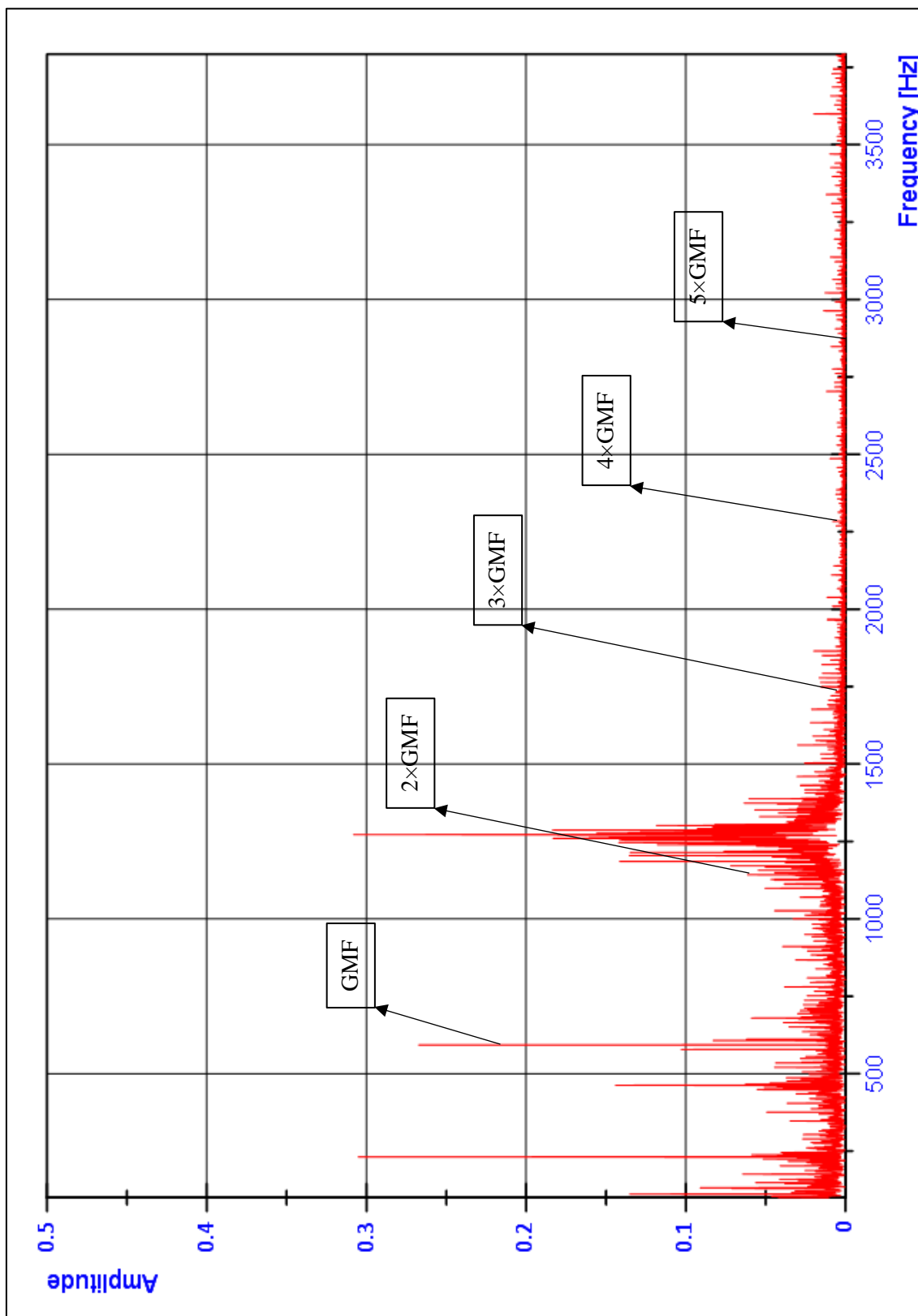


Figure 91 Frequency Spectrum of rotational speed of output shaft (vs) Amplitude – 3rd gear



The filtered signals with isolation of gear mesh frequency harmonic amplitudes and converting them to rotational speed w.r.t time are given in the graphs below.

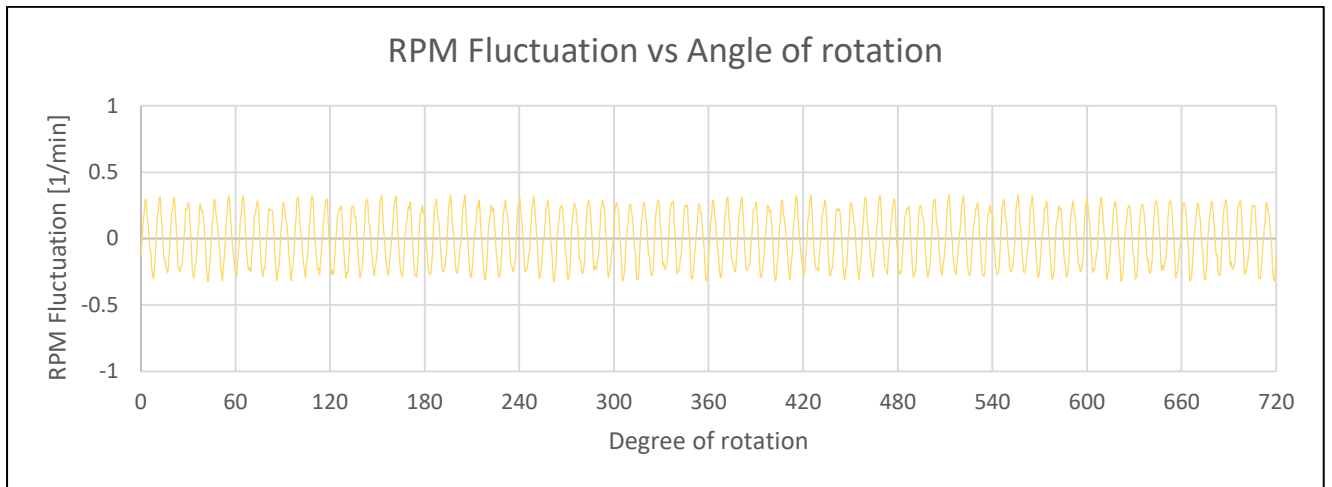


Figure 92 RPM Fluctuation of input shaft of 3rd gear by gear mesh (vs) Angle of rotation

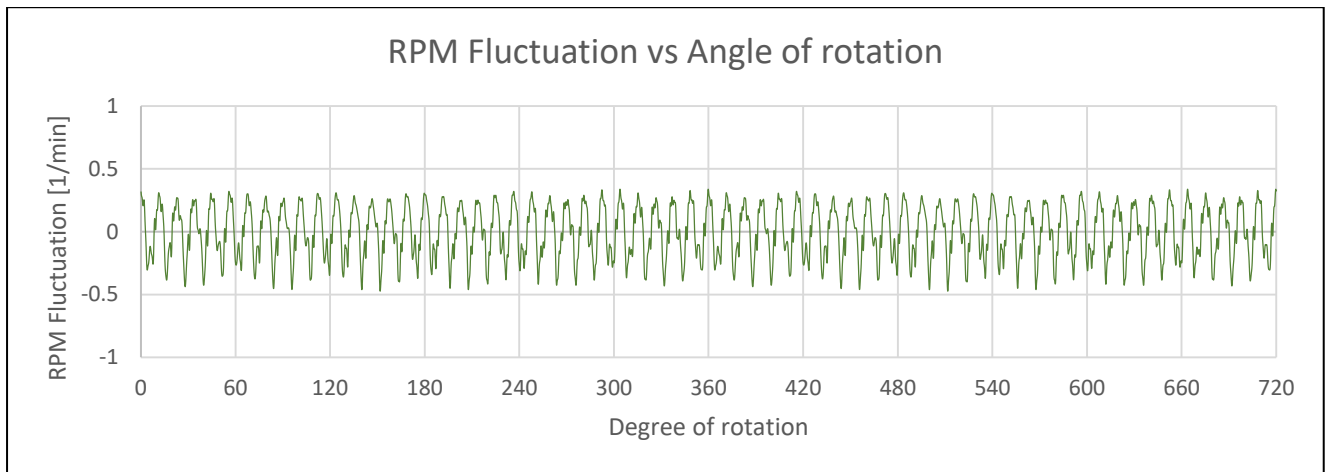


Figure 93 RPM Fluctuation of output shaft of 3rd gear by gear mesh (vs) Angle of rotation

[Attachment 2.14](#)

The graph below shows the frequency spectra of the rotational speed of 4th gear. The diagram below shows the frequency spectrum with gear mesh frequency harmonics and other noise of the 4th gear input and output.

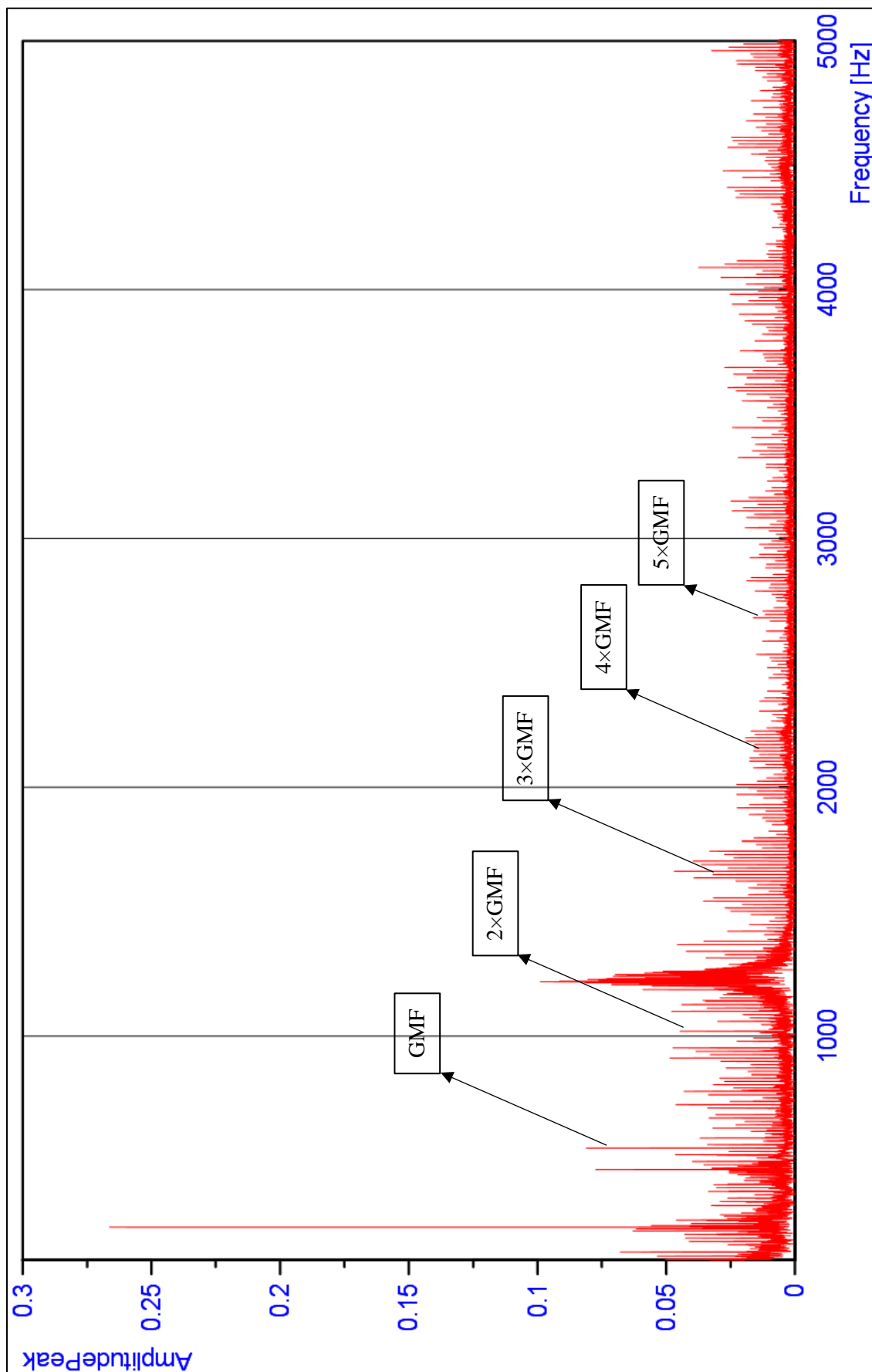


Figure 94 Frequency spectrum of rotational speed of input shaft (vs) Amplitude – 4th gear



For the output gear, the graph is given below-

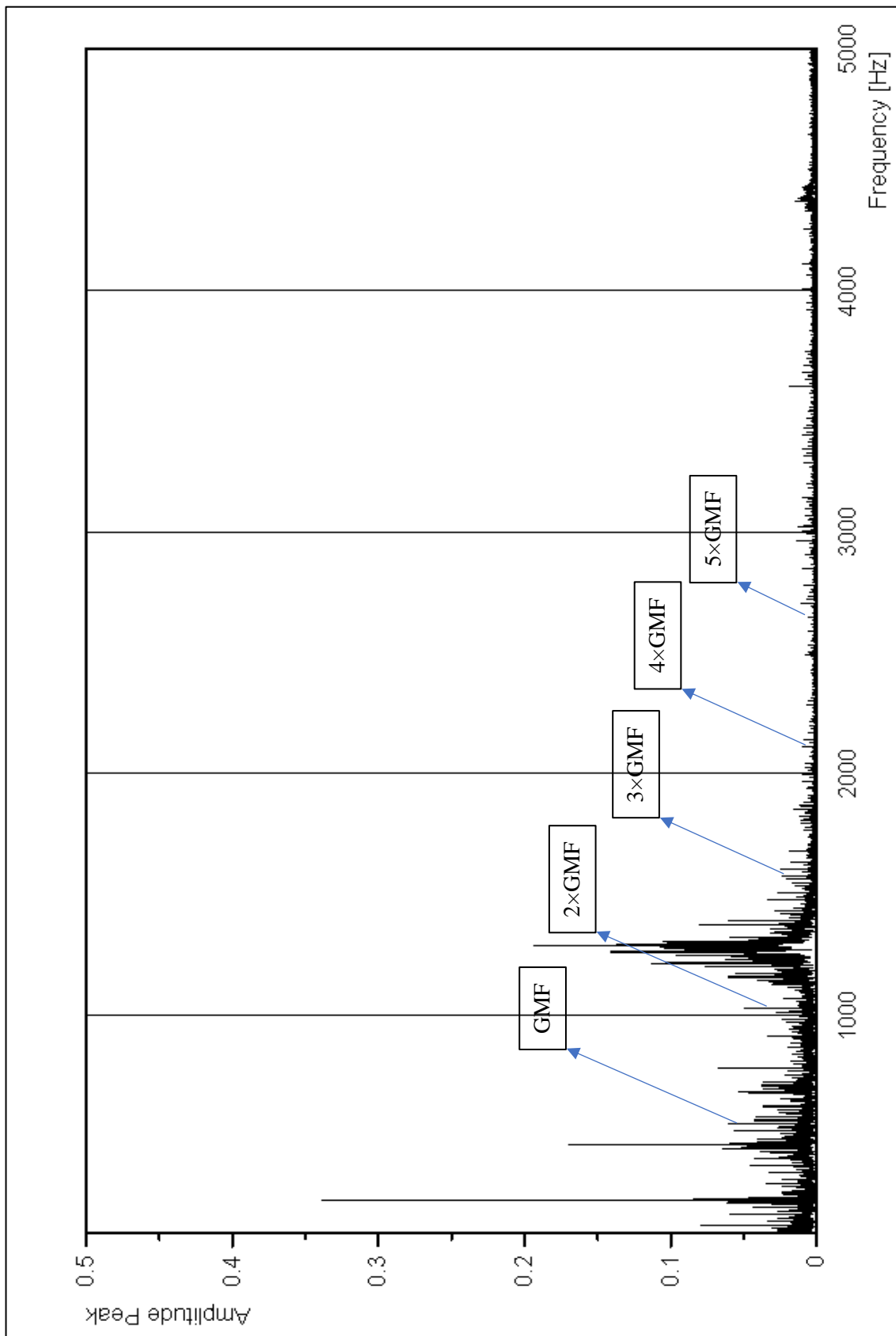


Figure 95 Frequency spectrum of rotational speed of output shaft (vs) Amplitude – 4th gear



The filtered speed of rotation signal is obtained from the analysis in DIAdem as seen in previous gears.

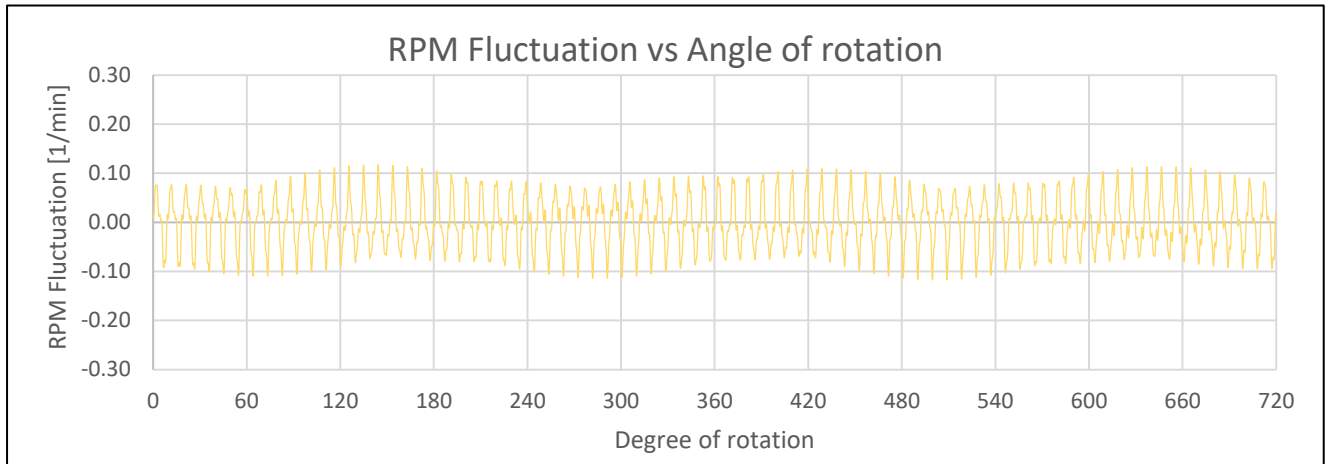


Figure 96 RPM Fluctuation of input shaft of 4th gear by gear mesh (vs) Angle of rotation

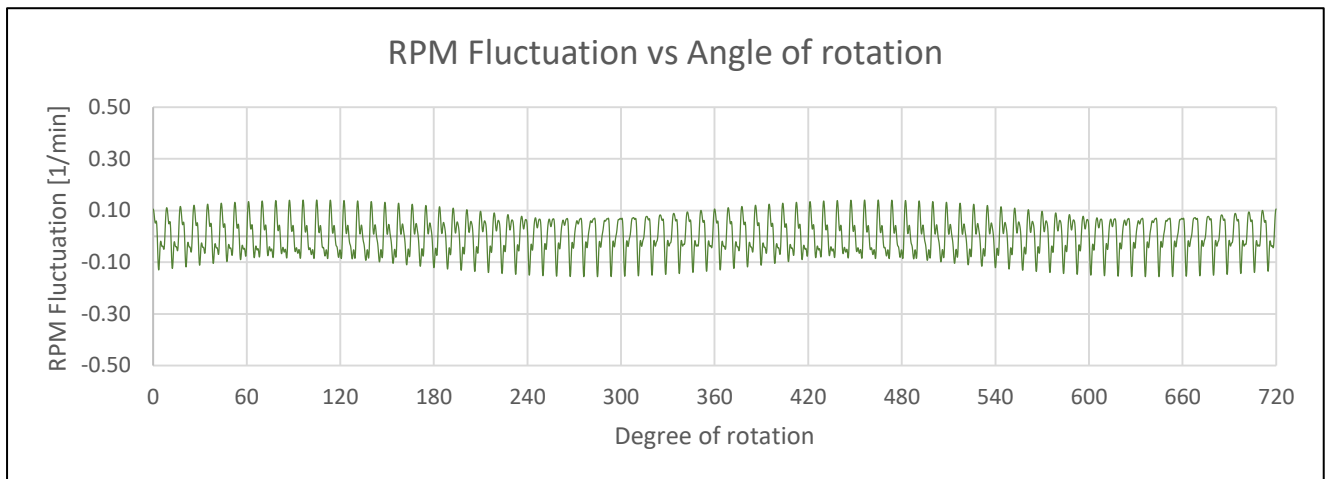


Figure 97 RPM Fluctuation of output shaft of 4th gear by gear mesh (vs) Angle of rotation

[Attachment 2.15](#)

The frequency spectra of the given signal of 5th gear is shown below. The frequency at which the gears mesh is hidden with background noise and hence is taken for processing in NI DIAdem with the procedure explained for the previous gears.

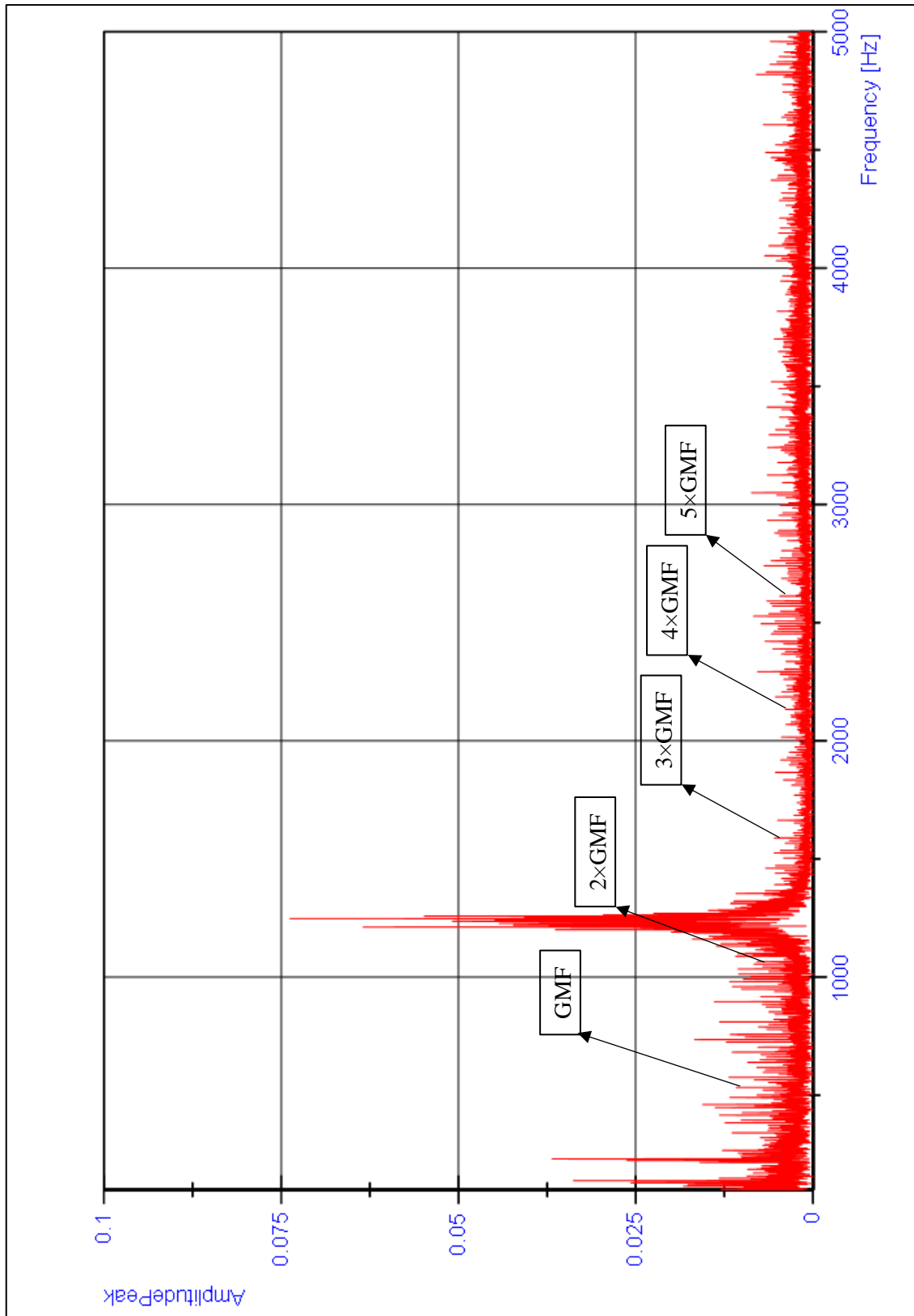


Figure 98 Frequency spectrum of rotational speed of input shaft (vs) Amplitude – 5th gear



The graphs below are for the output gear of the gearmesh.

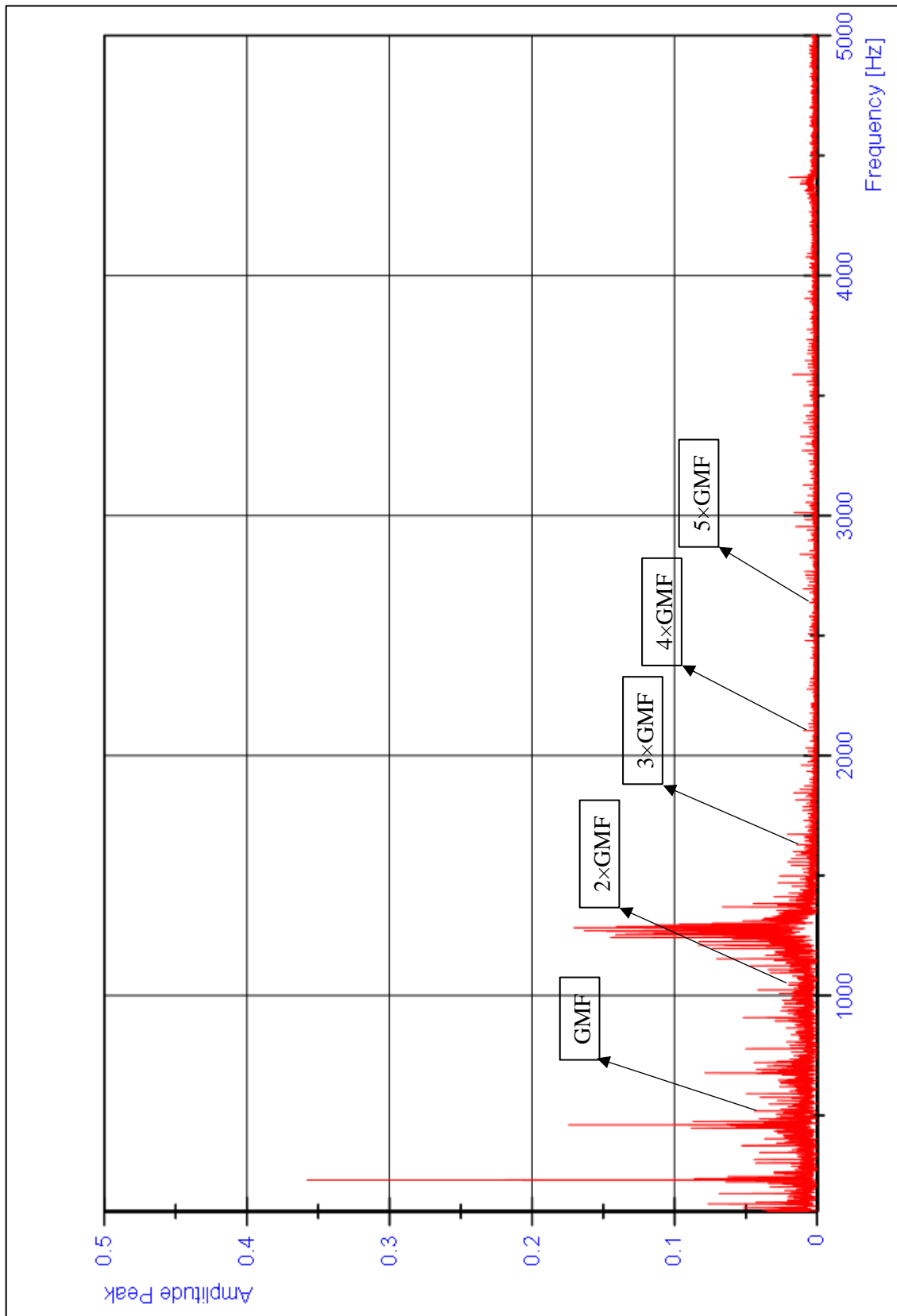


Figure 99 Frequency spectrum of rotational speed of output shaft (vs) Amplitude – 5th gear



The filtered graphs of the rotational speeds are shown below.

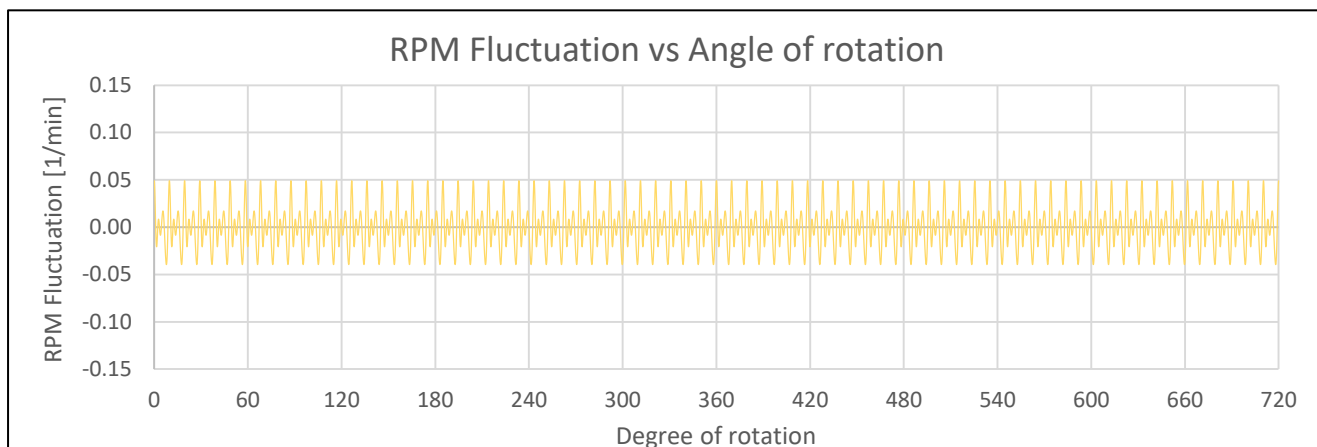


Figure 100 RPM Fluctuation of input shaft of 5th gear by gear mesh (vs) Angle of rotation

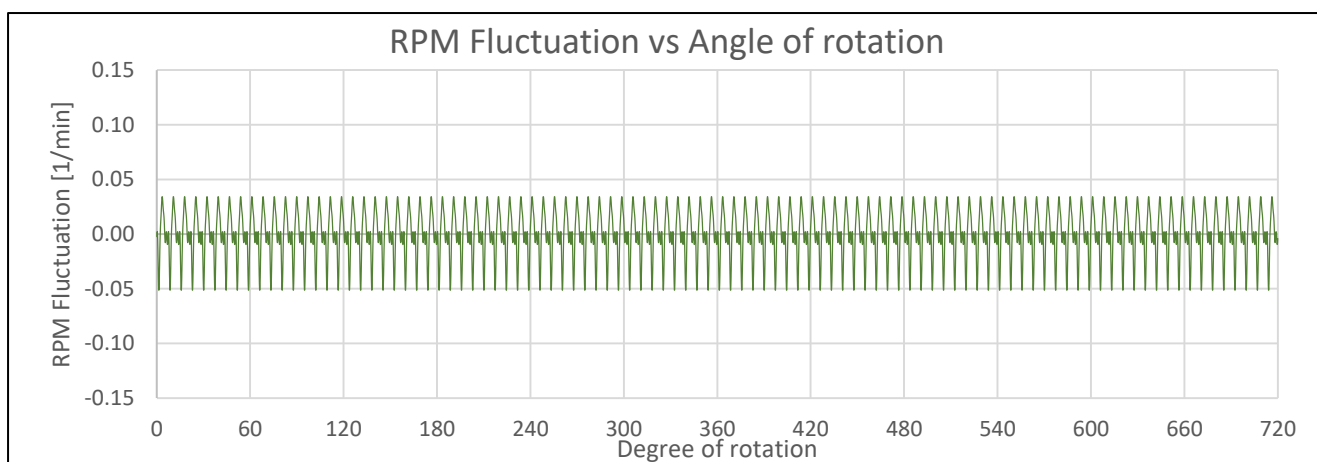


Figure 101 RPM Fluctuation of output shaft of 5th gear by gear mesh (vs) Angle of rotation

3. Actuation of disc brake

Attachment 3.1

Table G-9 Parameters of hydraulic pusher

PARAMETER	VALUE
Stroke length [mm]	60
Maximum force [N]	800
Required voltage [V]	400
Required Current [A]	0.6 A
Working condition	0.35 kW
Operating Frequency [Hz]	50
Weight with oil [kg]	19 kg



Attachment 3.2

Table G-10 Specification of UNIPRES pressure sensor

PARAMETER	VALUE
Source voltage [V]	15 – 36V; Max 100mA
Output voltage [V]	0 – 5/10V
Measurable pressure [MPa]	0 – 16 MPa
Error	0.25 – 0.4%
Dimension	Ø 38 – 80mm
Connection	M20 × 1.5/ G1/2 / G1/4

Attachment 3.3

Table G-11 Tabulation for ordering required actuator

ORDERING STEPS	
Parameters	Value
Series	ETH
Frame Size	050 (ISO 50 size)
Drive Screw	M10 (16mm)
Motor mount	B (In line with groove for initiator 6 & 12 o' clock)
Lubrication bore	1 (Integrated lubrication port)
Motor drive type	XPG BE344LJ – KPSN
Cylinder mount	G (Side flange mount)
Rod end mount	M (Male thread)
Stroke	0100
IP Rating	C (IP65 epoxy coated cylinder)



Attachment 3.4

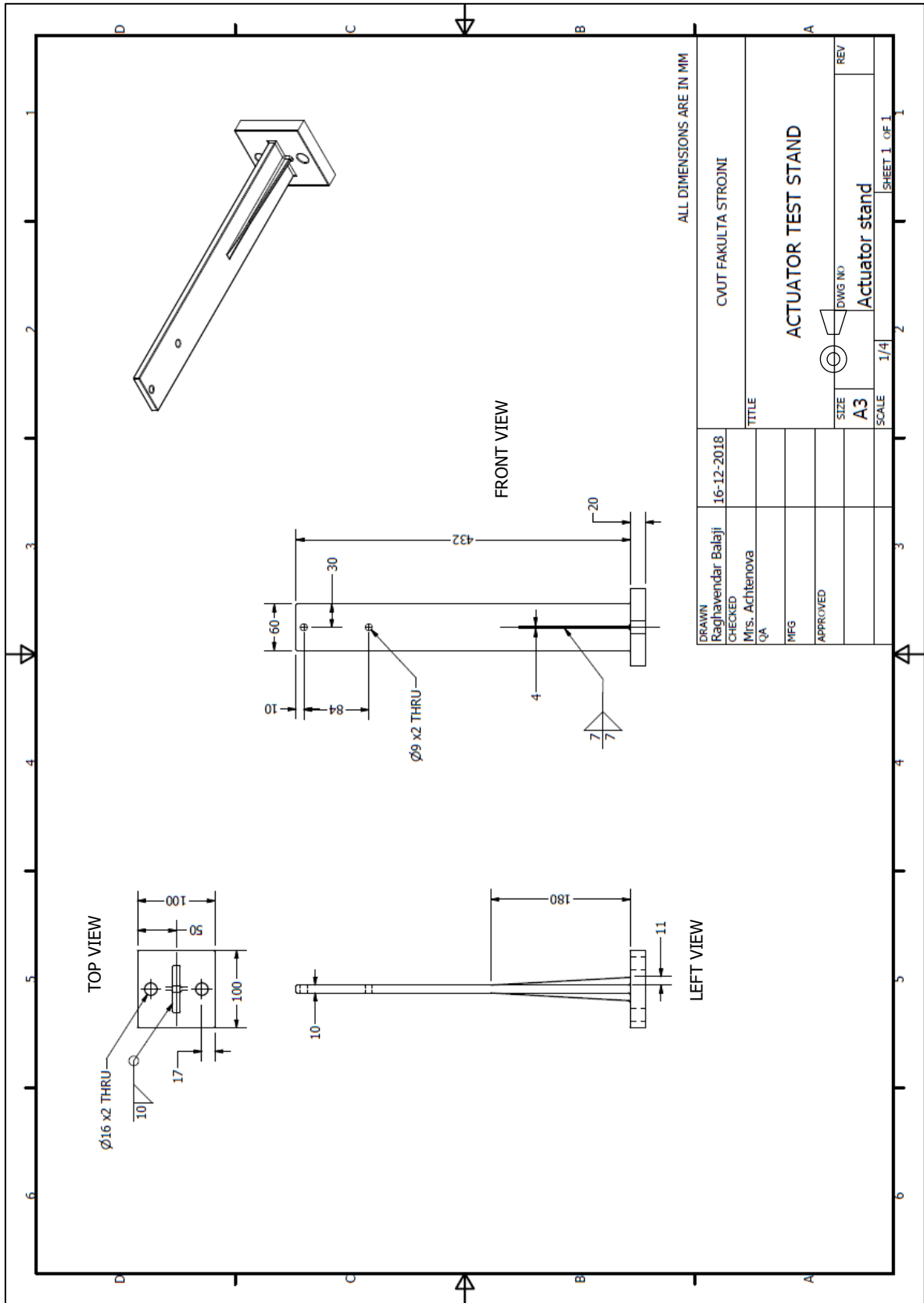


Figure 102 Actuator stand design and technical drawing



Attachment 3.5

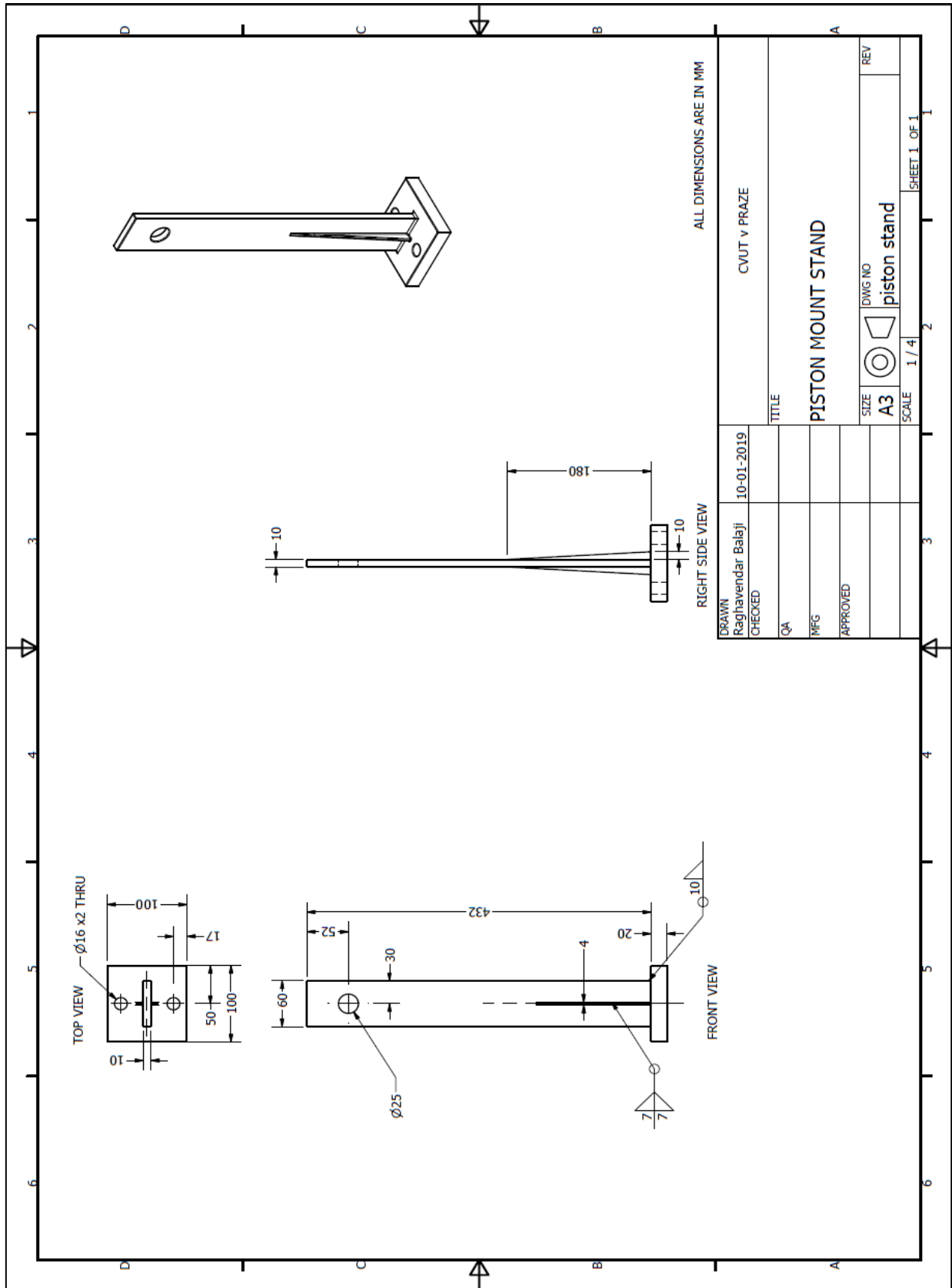


Figure 103 Proposed stand for hydraulic cylinder mounting



H. REFERENCES AND LITERATURE WORKS

[1] Mach, Ernst (1919). *The Science of Mechanics*. pp. 173–187. Chicago: The Open Court Publishing co., 1919. ISBN 1-110-30677-6.

Link: <https://archive.org/details/scienceofmechani005860mbp>

[2] Euler, Leonhard (1765). *Theoria motus corporum solidorum seu rigidorum: Ex primis nostrae cognitionis principiis stabilita et ad omnes motus, qui in huiusmodi corpora cadere possunt, accommodata* [The theory of motion of solid or rigid bodies: established from first principles of our knowledge and appropriate for all motions which can occur in such bodies] (in Latin). p. 166. A. E. Roser., 1765. ISBN 978-1-4297-4281-8.

Link: <https://archive.org/details/theoriamotuscor00eulegoog>

[3] Marion, JB; Thornton, ST (1995). *Classical dynamics of particles & systems* (4th Ed.). Thomson. ISBN 0-03-097302-3.

Link:

<https://archive.org/details/ClassicalDynamicsOfParticlesAndSystemsMarionThornton>

[4] Smith III, Julius O. (2010). *Physical Audio Signal Processing*. W3K Publishing. ISBN 978-0-9745607-2-4.

Link: <https://ccrma.stanford.edu/~jos/pasp/>

[5] H. J. Gray and A. Isaacs (Eds.). *A Dictionary of Physics*. Longman, London, 1975. ISBN 0-19-871474-2.

Link:

https://www.researchgate.net/publication/230913124_Oxford_Dictionary_of_Physics_3rd_edition

[6] Richard Boynton. (2002). *Measuring weight and all three axes of the COG of a rocket motor without having to re-position the motor*, Space Electronics, Inc.

Link:

https://www.space-electronics.com/contentAssets/Literature/Measuring_W_and_3CG_motor.pdf

[7] J. Peraire, S. Widnall (Fall 2008). *Lecture L26 – 3D Rigid Body Dynamics: The Inertia Tensor*.

Link:

<https://pdfs.semanticscholar.org/d2b5/e126c3d4bd54e39ee134b1cc28227b99a2b8.pdf>

[8] Arthur Eric Haas (1928). *Introduction to theoretical physics*. ISBN 978-0-0705809-0-9

Link: <https://pubs.acs.org/doi/abs/10.1021/ed002p719.1>

[9] Pavel Špinka (2006). *SMALL articulated vehicle: measurement of characteristics and steering of trailer – Diplomová Práce*, České Vysoké Učení Technické, Prague.



[10] Lukáš Kazda (2015). *Měření momentu setrvačnosti – Bakalářská Práce*, České Vysoké Učení Technické, Prague.

[11] Potentiometer. *Components101 – Potentiometer* [online]. 2018 [Retrieved 2018 – 05 – 09]

Link: <https://components101.com/potentiometer>

[12] Disadvantages of Hall Effect Sensors. *AZoSensors – Hall Effect Sensors*. [Online]. 2018. [Retrieved 2018 – 05 – 09]

Link: <https://www.azosensors.com/article.aspx?ArticleID=16>

[13] Murata inclinometers. *Murata MEMS Sensors and Inclinometers*. [Online] 2018. [Retrieved 2018 – 05 – 09]

Link: <https://www.murata.com/products/sensor/inclinometer>

[14] How does MEMS Inclinometer work? *Jewell Instruments*. [Online] 2018. [Retrieved 2018 – 05 – 13]

Link: <http://www.jewellinstruments.com/how-does-a-mems-sensor-work/>

[15] POSITAL inclination sensors. *POSITAL Fraba*. [Online] 2018. [Retrieved 2018 – 05 – 14]

Link: <https://www.posital.com/en/products/inclinometers/mems/MEMS-Technology.php>

[16] Hall Effect Angle sensors buy. *NCD Stores*. [Online] 2018. [Retrieved 2018 – 05 – 14]

Link: <https://store.ncd.io/product/a1332-precision-hall-effect-rotational-angle-0-to-360-sensor-i2c-mini-module/>

[17] Potentiometers for angle measurement. *Althen Mess- & Sensortechnik – Rotary Angle Sensors*. [Online] 2018. [Retrieved 2018 – 05 – 17]

Link: http://www.althensensors.com/rotary_angle_sensors_and_transducers/fcp50a/

[18] Allegro A1332 Hall Effect Angle Sensor. *Allegro Microsystems, LLC – A1332: Precision Hall Effect Angle Sensor IC with I²C Interface*. [Online] 2018. [Retrieved 2018 – 05 – 17]

Link:

<https://www.allegromicro.com/~media/Files/Datasheets/A1332-Datasheet.ashx?la=en&hash=6DD0D27FEFC284F6DD11E81B27B6BC36DF9D9635>

[19] Dvouosy inklinometr. *SITALL MEMS Analog Sensor*. [Online] 2018. [Retrieved 2018 – 05 – 31]

Link:

https://www.sitall.cz/fotky/zbozi_soubor1477.pdf

[20] DOG 2 MEMS Inclinometer. *DOG2 MEMS Series voltage inclinometer*. [Online] 2018. [Retrieved 2018 – 05 – 31]

Link:

http://www.te.com/commerce/DocumentDelivery/DDEController?Action=srchrtv&DocNm=DOG2_MEMS-Series_Inclinometer&DocType=DS&DocLang=English



[21] Jiří Tůma (2003). *Gearbox Transmission Error Measurements Based on Phase Demodulation of Encoder Signals*, Journal of Middle European Construction and Design of Cars (MECCA), January 2003 Edition.

[22] Antonio Palermo.(2018). *The measurement of Gear Transmission Error as an NVH indicator: Theoretical discussion and industrial application via low-cost digital encoders to an all-electric vehicle gearbox*. Mechanical Systems and Signal Processing, Volume 10, 15 September 2018, Pages 368-389.

Link: <https://www.sciencedirect.com/science/article/pii/S0888327018301249>

[23] Jiří Tůma. *Automotive Series: Vehicle Gearbox Noise and Vibration: Measurement, Signal Analysis, Signal Processing and Noise Reduction Measures*. ISBN: 978-1-118-35941-9.

[24] Cooley, James W.; Tukey, John W. (1965). *An algorithm for the machine calculation of complex Fourier series*, Mathematics of Computation. Volume 19 (90): 297–301. doi:10.1090/S0025-5718-1965-0178586-1. ISSN 0025-5718.

Link: <http://www.ams.org/journals/mcom/1965-19-090/S0025-5718-1965-0178586-1/S0025-5718-1965-0178586-1.pdf>

[25] Frigo M, Johnson SG (1998). *FFTW: an adaptive software architecture for the FFT*. Proceedings of the 1998 IEEE International Conference on Acoustics, Speech and Signal Processing. 3: 1381–1384. doi:10.1109/ICASSP.1998.681704

Link: <https://ieeexplore.ieee.org/document/681704>

[26] Time frequency window function. *National Instruments*. [Online] 2018. [Retrieved 2018 – 10 – 08].

Link:

<http://download.ni.com/evaluation/pxi/Understanding%20FFTs%20and%20Windowing.pdf>

[27] ABB Industrial drive ACS800 series. *ABB Industrial drives*. [Online] 2018. [Retrieved 2018 – 10 – 11].

Link:

https://library.e.abb.com/public/fcad7e1548b9e934c1257b67003616fe/EN_ACS800single_drivescatalogRevO.pdf

[28] 7AA160L04 motor catalogue. *Lonne Drive Technology*. [Online] 2018. [Retrieved 2018 – 10 – 11].

Link: https://www.schlosser-moller.no/teknisk_katalog/17/Mez_teknisk_katalog.pdf

[29] LARM IRC sensors. *LARM a.s.* [Online] 2018. [Retrieved 2018 – 10 – 11].

Link: http://www.larm.cz/templates/larm/data/82_irc300-325gb.pdf

[30] Advantech ADAM Terminal board. *Advantech Solutions Pvt., Ltd.* [Online] 2018. [Retrieved 2018 – 10 – 12].



Link: http://www.advantech.com/products/gf-5aiq/adam-3925/mod_bedc4a7c-ee23-4f25-9a9d-8837563d9f84

[31] Brake wear emissions. *Brake wear emissions*, Dekati Pvt., Ltd. [Online] 2018. [Retrieved 2018 – 11 – 19].

Link: <https://www.dekati.com/applications/emissions/engine-emissions/brake-wear-emissions>

[32] Parker ETH Linear Actuators. *Parker Hannifin Corporation*. [Online] 2018. [Retrieved 2018 – 12 – 15].

Link: https://www.parker.com/Literature/Electromechanical%20North%20America/CATALOG-S-BROCHURES/ETH%20Literature/ETH-High-Force-Electric-Cylinders_Catalog.pdf.

[33] Sara Stančín, Sašo Tomažič. (2011). *Angle Estimation of Simultaneous Orthogonal Rotations from 3D Gyroscope Measurements*, Sensors, September 2011 Volume 11 Issue 9, pp. 8536 – 8549.

Link: <https://doi.org/10.3390/s110908536>

[34] Comb filter examples. *IOP Science Journals*. [Online] 2018. [Retrieved 2018 – 1 – 9].

Link: <http://iopscience.iop.org/article/10.1088/0967-3334/36/10/2159>

[35] Aliasing examples. *Wolfcrow professor notes*. [Online] 2018. [Retrieved 2018 – 1 – 9].

Link: <https://wolfcrow.com/professor-samplers-notes-aliasing/>

[36] Frequency vs time FFT. *Myriad RF courses*. [Online] 2018. [Retrieved 2018 – 1 – 9].

Link: <https://discourse.myriardrf.org/t/understanding-construction-of-amplitude-vs-frequency-graphs-and-fft-viewers/3007>

[37] Elotechnik hydraulic cylinder HM series. *Elotechnik s.r.o.* [Online] 2018. [Retrieved 2018 – 1 – 10].

Link: <https://www.elotechnik.cz/hydraulicky-valec-dvojcinnny-hm1-2-63-32-125-121a111.html#zalozka-1>



I. LIST OF SYMBOLS AND ABBREVIATIONS

L [kg.m ² /s]	Angular momentum
ω [m/s ²]	Angular velocity
r [m]	Perpendicular distance from centre of rotation
m [kg]	Mass of body
A [m ²]	Area of body
v [m/s]	Linear velocity
<i>COG</i>	Centre of Gravity
m_{rim} [kg]	Mass of rim of wheel
m_{tot} [kg]	Total mass of experimental setup
m_{rod} [kg]	Mass of rod
a [m]	Distance of COG from front of vehicle
b [m]	Distance of COG from rear of vehicle
l [m]	Wheelbase of vehicle
h [m]	Height of COG from base (or) ground
Φ [°]	Angle of inclination of vehicle from ground
l_1 [m]	Length of principal semi-axis of ellipsoid from x – axis
l_2 [m]	Length of principal semi-axis of ellipsoid from y – axis
l_3 [m]	Length of principal semi-axis of ellipsoid from z – axis
α [°]	Rotation angle of x – axis
β [°]	Rotation angle of y – axis
γ [°]	Rotation angle of z – axis
I_o [kg.m ²]	Principal moment of inertia
x_g [m]	Distance of COG from reference x – axis
y_g [m]	Distance of COG from reference y – axis
z_g [m]	Distance of COG from reference z – axis
ϕ [°]	Angle of twist about vertical axis
k [N.m.rad ⁻¹]	Stiffness constant of wire
<i>GND</i>	Ground connection
V_{CC} [V]	Input Voltage
ϕ_1 [rad]	Angle of rotation of input gear
ϕ_2 [rad]	Angle of rotation of output gear
n_1	Number of teeth of input gear
n_2	Number of teeth of output gear
r_2 [μm]	Radius of output gear
<i>PWR</i>	Power intensity
<i>BW</i>	Bandwidth
<i>DAQ</i>	Data AcQuision
<i>GMF</i>	Gear Mesh Frequency
<i>PCD</i>	Pitch Circle Diameter
<i>IFFT</i>	Inverse Fast Fourier Transformation



J. LIST OF CONTENTS IN DVD

In the DVD enclosed are the following documents related to this thesis work

- PDF and document version of my diploma thesis.
- My LabVIEW files of all related chapters.
- All the photos and their edited copies of test benches and design files.
- CATIA and Autodesk design files of all the chapters.
- Datasheet of sensors and reference files for required experiments.
- Readings and Excel data related to Transmission Error measurement.
- NI DIAdem files containing of analysis of each gear of Transmission Error.